Lattice Boltzmann Magnetohydrodynamics

by

Andrew Maclean Wood B.Sc.

Thesis
submitted to the
University of Glasgow
for the degree of
Ph.D.

Astronomy and Astrophysics Group
Department of Physics and Astronomy,
University of Glasgow,
Glasgow G12 8QQ

September 1999

ProQuest LLC.
789 East Eisenhower Parkway
P.O. Box 1346
Ann Arbor, MI 48106 – 1346

Abstract

Understanding the dynamics of plasmas presents a formidable challenge in theoretical physics. Being governed by a complicated set of non-linear equations, analytic descriptions of their behaviour are only possible in the simplest of cases and therefore numerical methods are essential to understand any realistic situation. This thesis presents an application of the lattice Boltzmann (LB) method to the solution of the magnetohydrodynamic (MHD) equations, which model the low frequency motions of plasmas.

The lattice Boltzmann method, which has been developed over the past decade or so, is a kinetic model of fluid like systems, derived from the statistical mechanics of lattice gas cellular automata. In chapter 1, after a brief derivation of the equations to be modelled and discussion of standard numerical methods, the basic ideas of cellular automata (CA) are reviewed along with some examples. Special attention is given to lattice gas models of hydrodynamics and magnetohydrodynamics (MHD), with a discussion of the particular problem that an MHD model faces, namely the representation of the essentially non-local Lorentz force, and how this was overcome.

In chapter 2 the lattice Boltzmann method is discussed in some detail. The LB models of two dimensional hydrodynamics and magnetohydrodynamics are explained and the Navier-Stokes and MHD equations are derived from these models. The derivation is standard in the literature and bears important similarities to the theory discussed in chapter 1 despite, in the case of the MHD model, the fundamentally different means by which the interactions between the particles and magnetic field are represented. An improvement of the MHD model is proposed and a linear stability analysis is carried out. Alternative methods of discretising the lattice Boltzmann equation are also discussed.

Various tests are presented in chapter 3. The simulations of Hartmann flow confirm previously published results, although we also model the evolution of the flow towards a steady state in the case of an unmagnetised fluid. Damped Alfvén waves are also modelled. Both of these linear problems show good agreement between the numerical lattice Boltzmann solutions and the analytic solutions. Simulations of a non- linear reconnection problem are also presented, namely the coalescence of magnetic islands. The simulations reproduce correctly the qualitative features of island coalescence found in the literature.

The lattice Boltzmann method is applied to a practical problem in chapter 4, namely the shedding of vortices in the wake of an obstacle. This problem is relevant to the dynamics of solar active regions, in which the photosphere is either stirred by or drags along an erupting magnetic flux tube. The observed vorticity in such regions is greater than can be accounted for by the action of the Coriolis force on the upwelling or downwelling fluid. The effect of a magnetic field on the vortex shedding process is investigated, and it is found that if the magnetic field is strong enough, then Alfvén waves transport vorticity sufficiently fast to supress the vortex shedding process. In the case of a perpendicular magnetic field, reconnection is also observed in the wake.

Generalisations of the lattice Boltzmann MHD model are proposed in chapter 5. A thermal

MHD model and a three dimensional model are presented, and the thermal model is tested by simulating magnetosonic waves, which show good agreement with the analytic solutions.

Conclusions and suggestions for future work are discussed in chapter 6. The computer code for the numerical simulations is contained in the appendix.

The original work for this thesis is the modification of the lattice Boltzmann MHD model in section 2.4.4, the stability analysis of section 2.4.5 and the work which appears in chapters 3,4 and 5.

Acknowledgements

I would like to thank my supervisor, Dr. Declan Diver, for his guidance and encouragement during the course of my postgraduate research. My thanks are also due to Prof. John Brown and Prof. Ernest Laing for some helpful discussions and to Dr. Daniel Martinez and Dr. Xiaoyi He for clarifying a number of points.

The work for this thesis was carried out at the Department of Physics and Astronomy in the University of Glasgow, and I received financial support from the Carnegie Trust for the Universities of Scotland. I would like to express my gratitude to both these institutions. I should also acknowledge the Institute of Physics who, in addition to the Department and the Carnegie Trust, partly funded my attendance at the International Conference on Plasma Physics in Nagoya, Japan in September 1996.

I would also like to thank various members and former members of the Astronomy and Astrophysics Group for providing such a stimulating environment to work in. Firstly I should mention Dr. Shashi Kanbur for managing the computers, Dr. Andy Newsam and Dr. Norman Gray for being experts on the witchcraft that is UNIX and Miss Daphne Davidson, the group secretary. Thanks also to the other plasma theorists, Dr. Jack Ireland, Dr. Elisabeth Rooney, Dr. Saad Abdul- Rassak, Dr. David Keston and Dr. Scott McIntosh; my fellow office mates, Dr. Sarah Matthews and Dr. Andrew Conway and everyone else who made the group such a fun place to work in.

This thesis was completed after I left Glasgow to work at the British Antarctic Survey in Cambridge. I am grateful to my colleagues Dr. Keith Nicholls and Dr. Adrian Jenkins for allowing me sufficient time off from my new field of Antarctic oceanography in order to finish. Some passages were in fact drafted on board *HMS Endurance* during a scientific cruise in the Weddell Sea, which, when considered along with hand written drafts of some passages which accompanyed me on a backpacking trip through Japan and China, a trip to Italy, two trips to the United States and one to the Netherlands, could well qualify this as one of the most travelled, incomplete theses of all time. I should say that it only marginally failed to ruin my enjoyment of these excursions and I now look forward to my first thesis-free holiday in four years.

Finally, I would like to give special thanks to Mr. Nigel Gardner, my old physics teacher, who died of cancer in July, 1999. There was never a dull moment in his lessons and he taught with humour and an enthusiasm which could inspire even the most awkward teenager. It was after only a few weeks of his O-grade physics classes that I decided, at the age of 13, that I wanted to become a physicist and now I have finally achieved that ambition. I am sorry that he will never read this thesis.

Contents

List of Figures

Chapter 1

Introduction

The aim of this chapter is to provide an overview of the equations of magnetohydrodynamics and some of the numerical methods which are used to solve them. There will be particular emphasis on cellular automata and lattice gases, from which their continuum counterpart, the lattice Boltzmann method is derived. We shall also discuss briefly the derivation of the MHD equations from kinetic theory, since the derivation has many important similarities to the proof that the lattice Boltzmann method approximates the behaviour of fluid dynamics and magnetohydrodynamics in certain situations. This will set the scene for the later chapters where the lattice Boltzmann method is described in detail, and then used to model MHD flows in a number of situations and the model of Martinez et al [1] is generalised to three dimensional and thermal MHD.

1.1 Magnetohydrodynamics: Basic Theory

Magnetohydrodynamics is the theory of electrically conducting fluids in the presence of magnetic fields and can be used to describe a wide range of phenomena in liquid metals and low frequency plasma motions. The derivation of the equations of MHD can be found in many standard texts [2]. However, since analogies will later be drawn between lattice Boltzmann methods and kinetic theory, it is worthwhile to outline the arguments here.

1.1.1 Fundamental Physics

A plasma is essentially a collection of particles, a significant number of which carry electric charge. Here we consider one of the simplest cases, where the particles are categorized into two species, namely singly charged positive ions (hydrogen nuclei or protons, for the sake of argument) and negatively charged electrons. What follows can be generalised to include other particles such as positrons, neutral atoms, multiply charged ions etc.

The particles move under the influence of an electromagnetic field and hence their motion is described by the Lorentz force:

$$\mathbf{F} = q(\mathbf{E} + \mathbf{v} \times \mathbf{B}) \tag{1.1}$$

The behaviour of the electromagnetic field is determined by Maxwell's equations [3]:

$$\nabla \cdot \mathbf{E} = \frac{\rho_c}{\epsilon_0} \tag{1.2}$$

$$\nabla \times \mathbf{B} - \frac{1}{c^2}\frac{\partial \mathbf{E}}{\partial t} = \mu_0 \mathbf{j} \tag{1.3}$$

$$\nabla \cdot \mathbf{B} = 0 \tag{1.4}$$

$$\nabla \times \mathbf{E} + \frac{\partial \mathbf{B}}{\partial t} = \mathbf{0} \tag{1.5}$$

One gramme of ionized hydrogen contains 6×10^{23} protons and the same number of electrons. To consider an equation of motion for each particle, and calculate the resulting electromagnetic field is clearly unfeasible and so statistical methods must be employed.

We introduce the particle distribution function, $f_s(\mathbf{x}, \mathbf{p}, t)$. $f_s(\mathbf{x}, \mathbf{p}, t)\delta\mathbf{x}\delta\mathbf{p}$ is the number of particles of species s, which, at time t, are contained in the region of phase space $[\mathbf{x}, \mathbf{x}+\delta\mathbf{x}] \times [\mathbf{p}, \mathbf{p}+\delta\mathbf{p}]$. The evolution of each f_s is described by the Boltzmann equation [2]:

$$\frac{\partial f_s}{\partial t} + \mathbf{v} \cdot \frac{\partial f_s}{\partial \mathbf{x}} + \mathbf{F} \cdot \frac{\partial f_s}{\partial \mathbf{p}} = \left(\frac{\partial f_s}{\partial t}\right)_c, \tag{1.6}$$

where $\mathbf{p} = m_s \mathbf{v}(1 - \frac{v^2}{c^2})^{-\frac{1}{2}} \approx m_s \mathbf{v}$, since we shall only consider non-relativistic motions.

The left hand side of this equation describes the particle motion under the Lorentz force; the right hand side takes care of collisions which randomize the particle motions. If a fully ionized plasma is treated as collection of individual particles, collisions need not be considered separately as they are adequately described by the Coulomb force as two charges approach each other. However, in the kinetic treatment, f_s is generally smoothed, and so does not contain sufficient information about individual particle positions to tell when two particles are closely approaching each other. It is for this reason that the collision term must be retained.

It is straightforward to show that if $\left(\frac{\partial f_s}{\partial t}\right)_c = 0$ and f_s is a summation of delta functions, $f_s = \sum_{i=1}^{N} \delta^3(\mathbf{x} - \mathbf{x}_i(t))\delta^3(\mathbf{p} - \mathbf{p}_i(t))$, then the Boltzmann equation is equivalent to the N equations of motion for N particles:

$$\mathbf{v}_i = \dot{\mathbf{x}}_i$$

$$\mathbf{F}_i = \dot{\mathbf{p}}_i.$$

The collision term must, of course, satisfy the laws of conservation of mass, momentum, energy and charge so that:

$$\int \left(\frac{\partial f_s}{\partial t}\right)_c m_s \, \mathrm{d}^3\mathbf{p} = 0 \tag{1.7}$$

$$\sum_s \int \left(\frac{\partial f_s}{\partial t}\right)_c \mathbf{p}\, \mathrm{d}^3\mathbf{p} = 0 \tag{1.8}$$

$$\sum_s \int \left(\frac{\partial f_s}{\partial t}\right)_c \frac{p^2}{2m_s} d^3\mathbf{p} = 0 \tag{1.9}$$

$$\sum_s \int \left(\frac{\partial f_s}{\partial t}\right)_c q_s\, \mathrm{d}^3\mathbf{p} = 0 \tag{1.10}$$

If particle species are not conserved (ie. we have recombination, ionisation etc.) then equation 1.7 should be summed over s.

Several forms for the collision term are possible. If collisions can be neglected, so that $\left(\frac{\partial f_s}{\partial t}\right)_c = 0$, then the Boltzmann equation is known as the Vlasov equation. In a fully ionized plasma, the collisions are the result of many small Coulomb deflections, and the usual approach is to use the Fokker-Planck collision term. Define $\psi(\mathbf{v}, \Delta\mathbf{v})$ to be the probability that a particle with an initial velocity $\mathbf{v}$, undergoing many small deflections, acquires an increment of velocity $\Delta\mathbf{v}$ in a time Δt. Now let

$$< \Delta\mathbf{v} > = \int \psi \Delta\mathbf{v}\, \mathrm{d}^3\Delta\mathbf{v} \tag{1.11}$$

$$< \Delta\mathbf{v}\Delta\mathbf{v} > = \int \psi \Delta\mathbf{v}\Delta\mathbf{v}\, \mathrm{d}^3\Delta\mathbf{v} \tag{1.12}$$

Then the Fokker-Planck collision term is [4]

$$\left(\frac{\partial f_s}{\partial t}\right)_c = \lim_{\Delta t \to 0} \frac{1}{\Delta t}\left[-\frac{\partial}{\partial \mathbf{v}} \cdot (f_s < \Delta\mathbf{v} >) + \frac{1}{2}\frac{\partial^2}{\partial \mathbf{v}\partial \mathbf{v}} : (f_s < \Delta\mathbf{v}\Delta\mathbf{v} >)\right] \tag{1.13}$$

1.1.2 The Fluid Equations

So far, we have considered the microscopic dynamics of a plasma and stated the equations governing the evolution of the particle distribution function. For many purposes this contains more information than is necessary and further simplification can be achieved by regarding the plasma as a fluid. The macroscopic fluid quantities, namely the density and velocity are defined by taking moments of the distribution function:

$$n_s = \int f_s\, \mathrm{d}^3\mathbf{p} \tag{1.14}$$

$$n_s \mathbf{u}_s = \int f_s \mathbf{v}\, \mathrm{d}^3\mathbf{p} \tag{1.15}$$

The mass density, ρ_s for a species is simply $n_s m_s$. It is also useful to define the stress tensor:

$$\mathbf{\Pi}_s = \int f_s(\mathbf{v} - \mathbf{u}_s)(\mathbf{v} - \mathbf{u}_s)\, \mathrm{d}^3\mathbf{p} \tag{1.16}$$

By taking moments of the Fokker-Planck equation we obtain fluid equations for the different particle species:

$$\frac{\partial n_s}{\partial t} + \nabla \cdot (n_s \mathbf{u}_s) = 0 \tag{1.17}$$

$$m_s n_s \left[\frac{\partial \mathbf{u}_s}{\partial t} + (\mathbf{u}_s \cdot \nabla)\mathbf{u}_s\right] = q_s n_s(\mathbf{E} + \mathbf{u}_s \times \mathbf{B}) - \nabla \cdot \mathbf{\Pi}_s + \mathbf{P}_s \tag{1.18}$$

where $\mathbf{P}_s$ represents the rate of change of momentum of species s as a result of collisions with all other species. If the distribution function takes the form of a Maxwellian, (ie. we have local thermodynamic equilibrium) then $-\nabla \cdot \mathbf{\Pi} = -\nabla p$, a pressure gradient. If there is a small departure from a Maxwellian, then a viscous term is introduced: $\nabla \cdot (\mu \nabla \mathbf{u}) + \nabla \mu_b \nabla \cdot \mathbf{u}$, μ and μ_b begin the shear and bulk viscosities respectively.

It can be seen from these equations that taking a moment of the Fokker-Planck equation to obtain a fluid equation introduces the next highest moment of the distribution function. Continuing this approach indefinitely would result in infinitely many equations, and therefore it is necessary to postulate some approximation which closes the system of equations. The appropriate approximation will naturally depend on the problem under study. A common choice is to postulate that a particular moment of the distribution function vanishes. For example, if this moment is the heat flux vector $(\int \frac{1}{2} m f(\mathbf{v} - \mathbf{u})^2(\mathbf{v} - \mathbf{u})\, \mathrm{d}^3\mathbf{p}$, which is the trace of the third moment as measured in the local rest frame of the fluid), then the second order moment of the Boltzmann equation reduces to an adiabatic energy equation:

$$\left(\frac{\partial}{\partial t} + \mathbf{u} \cdot \nabla\right) p\rho^{-\gamma} = 0, \tag{1.19}$$

where $\gamma = 5/3$ for a monatomic gas. Other possibilities are to postulate an isothermal equation of state, if the gas is a good thermal conductor:

$$\frac{p}{\rho} = \text{constant} \tag{1.20}$$

or incompressibility, if sound waves are unimportant (among other conditions):

$$\rho = \text{constant}. \tag{1.21}$$

If the gas is strongly collisional, that is when the mean free path of a particle is small compared to the characteristic length scales of the macroscopic fields (a necessary condition for the MHD equations to be valid), then an important method for closing the system of equations is the Chapman-Enskog procedure. This essentially assumes that to lowest order the distribution function is locally in equilibrium, ie is a Maxwellian, which results in a set of inviscid equations. The first order perturbation of the distribution function is then calculated directly from a multi-scale expansion of the Boltzmann equation and the moments of this perturbation provide the dissipative terms in the fluid equations. The Chapman-Enskog procedure is the standard method used in deriving the fluid equations of a lattice Boltzmann model and will be discussed in some detail in chapter 2.

Now we take the special case of a fully ionized hydrogen plasma, and, noting that $m_i \gg m_e, n_e \approx n_i = n$, define the mass density

$$\rho = n_i m_i + n_e m_e \approx n m_i, \tag{1.22}$$

the charge density

$$\rho_c = e(n_i - n_e) \approx 0, \tag{1.23}$$

the velocity

$$\mathbf{v} = \frac{1}{\rho}(n_i m_i \mathbf{u}_i + n_e m_e \mathbf{u}_e) \approx \mathbf{u}_i \tag{1.24}$$

and the current density

$$\mathbf{j} = e(n_i \mathbf{u}_i - n_e \mathbf{u}_e) \approx ne(\mathbf{u}_i - \mathbf{u}_e). \tag{1.25}$$

It is now easy to show that the equation of mass conservation is

$$\frac{\partial \rho}{\partial t} + \nabla \cdot (\rho \mathbf{v}) = 0 \tag{1.26}$$

A simple expression for the ion-electron collision terms, $\mathbf{P}_i = -\mathbf{P}_e$ can be derived using the resistive Ohm's law, $\mathbf{E} = \eta \mathbf{j}$. This gives us

$$\mathbf{P}_e = ne\eta \mathbf{j} = n^2 e^2 \eta (\mathbf{u}_i - \mathbf{u}_e) \tag{1.27}$$

It can also be shown that

$$\mathbf{P}_e = n m_e \nu_{ei} (\mathbf{u}_i - \mathbf{u}_e) \tag{1.28}$$

where ν_{ei} is the electron-ion collision frequency, and we obtain the relationship between resistivity and collision frequency:

$$\eta = \frac{m_e \nu_{ei}}{ne^2}. \tag{1.29}$$

The first order moment equations can be combined in two different ways to give different single fluid equations. Writing them out explicitly as

$$m_i n \left(\frac{\partial \mathbf{u}_i}{\partial t} + (\mathbf{u}_i \cdot \nabla)\mathbf{u}_i \right) = en(\mathbf{E} + \mathbf{u}_i \times \mathbf{B}) - \nabla p_i \tag{1.30}$$

$$m_e n \left(\frac{\partial \mathbf{u}_e}{\partial t} + (\mathbf{u}_e \cdot \nabla)\mathbf{u}_e \right) = en(\mathbf{E} + \mathbf{u}_e \times \mathbf{B}) - \nabla p_e \tag{1.31}$$

and adding, we obtain

$$n \left(\frac{\partial}{\partial t}(m_i \mathbf{u}_i + m_e \mathbf{u}_e) + m_i (\mathbf{u}_i \cdot \nabla)\mathbf{u}_i + m_e (\mathbf{u}_e \cdot \nabla)\mathbf{u}_e \right) = en(\mathbf{u}_i - \mathbf{u}_e) \times \mathbf{B} - \nabla(p_i + p_e) \tag{1.32}$$

Since $p = p_i + p_e$, and using the above definitions for $\rho, \mathbf{v}, j$ and the approximation $m_e \ll m_i$, we get the momentum equation:

$$\rho \left(\frac{\partial \mathbf{v}}{\partial t} + (\mathbf{v} \cdot \nabla)\mathbf{v} \right) = \mathbf{j} \times \mathbf{B} - \nabla p \tag{1.33}$$

Another linear combination of the first order moment equations gives us:

$$m_i m_e n \left(\frac{\partial}{\partial t}(\mathbf{u}_i - \mathbf{u}_e) + (\mathbf{u}_i \cdot \nabla)\mathbf{u}_i - (\mathbf{u}_e \cdot \nabla)\mathbf{u}_e \right)$$

$$= en(m_i + m_e)\mathbf{E} + en(m_e\mathbf{u}_i + m_i\mathbf{u}_e) \times \mathbf{B} - m_e\nabla p_i + m_i\nabla p_e + (m_i + m_e)\mathbf{P}_i \tag{1.34}$$

This can be simplified by assuming that the convective terms are small, $m_e \ll m_i$ and using the definitions of $\rho, \mathbf{v}, j$ to give

$$\frac{m_e}{ne^2}\frac{\partial \mathbf{j}}{\partial t} = \mathbf{E} + \mathbf{v} \times \mathbf{B} - \frac{1}{ne}\mathbf{j} \times \mathbf{B} + \frac{1}{ne}\nabla p_e - \eta\mathbf{j} \tag{1.35}$$

which is a generalized Ohm's law.

1.1.3 The Magnetohydrodynamic Approximation

Magnetohydrodynamics, which underlies the problems addressed in this thesis, is an approximation of Maxwell's equations 1.2, 1.3, 1.4, 1.5, 1.26, 1.33 and 1.35 , which describes low frequency, long wavelength phenomena. Under these conditions we can neglect the displacement current, the electron mass, the Hall emf and the electron pressure gradient.

Equation 1.3 then reduces to Ampère's law:

$$\nabla \times \mathbf{B} = \mu_0\mathbf{j} \tag{1.36}$$

and equation 1.35 reduces to:

$$\mathbf{E} + \mathbf{v} \times \mathbf{B} = \eta\mathbf{j} \tag{1.37}$$

Taking the curl of equation 1.37 and applying Ampère's law and Faraday's law of induction (equation 1.5) yields:

$$\frac{\partial \mathbf{B}}{\partial t} = \nabla \times (\mathbf{v} \times \mathbf{B}) + \frac{\eta}{\mu_0}\nabla^2\mathbf{B} \tag{1.38}$$

neglecting variations in η. From now on, we shall scale the magnetic field so that $\mu_0 = 1$.

Notice that in the magnetohydrodynamic approximation, the electric field and current density can be expressed algebraically in terms of the other fields. Thus, we need only consider the evolution of $\rho, p, \mathbf{v}$ and $\mathbf{B}$ and our equations of magnetohydrodynamics are:

$$\frac{\partial \rho}{\partial t} + \nabla \cdot (\rho\mathbf{v}) = 0 \tag{1.39}$$

$$\rho\left(\frac{\partial \mathbf{v}}{\partial t} + (\mathbf{v} \cdot \nabla)\mathbf{v}\right) = -\nabla p + (\nabla \times \mathbf{B}) \times \mathbf{B} + \nabla \cdot (\mu\nabla\mathbf{v}) + \nabla(\mu_b\nabla \cdot \mathbf{v}) \tag{1.40}$$

$$\frac{\partial \mathbf{B}}{\partial t} = \nabla \times (\mathbf{v} \times \mathbf{B}) + \eta\nabla^2\mathbf{B} \tag{1.41}$$

$$\nabla \cdot \mathbf{B} = 0 \tag{1.42}$$

plus an equation of state which will depend on the particular problem which concerns us.

1.2 Numerical Methods

Having derived the MHD equations in the previous section, we now turn our attention to methods of solving these equations. The non-linear nature of the MHD equations means that for the vast majority of problems, the solutions have to be found numerically, except in the simplest problems where there is a high degree of symmetry, or the non- linear terms are negligibly small.

The basic procedure of all numerical methods is to replace the set of partial differential equations by a set of approximations, thereby reducing the system with infinitely many degrees of freedom to one with finitely many. The most common procedures for doing this are the finite difference (FD) method, the finite element method and the spectral method. The finite difference method calculates the dependent variables at a discrete set of points and replaces the partial derivatives by finite difference approximations. The finite element method tesellates the computational domain into small elements, and uses basis functions to represent the dependent variables and derivatives of the basis functions are substituted into the PDEs. The spectral method, on the other hand, transforms the equations into Fourier space (or some other orthogonal representation) and solves the equations for a truncated set of Fourier modes.

All methods have their relative advantages and disadvantages. For instance, the finite difference method is generally the simplest and results in the most efficient code. The finite element method is considered more accurate than the finite difference method, especially in problems involving complex geometries, but is more complicated and requires more computation time.

The simulations in this thesis model MHD using a lattice Boltzmann equation, which is discretised using the finite difference method and therefore we shall discuss the finite difference method in detail here. It is best to consider how the finite difference method is applies to a couple of examples, such as the one dimensional diffusion equation:

$$\frac{\partial \phi}{\partial t} = \alpha \frac{\partial^2 \phi}{\partial x^2} \tag{1.43}$$

or the convection equation:

$$\frac{\partial \phi}{\partial t} + u \frac{\partial \phi}{\partial x} = 0 \tag{1.44}$$

The dependent variable ϕ is evaluated at a set of discrete points $x_1, x_2, \ldots, x_J$ and at the times $t_1, t_2, \ldots, t_N$. The discretisation of the domain can be quite arbitrary and chosen to suit the particular initial and boundary conditions, but here we shall take it to be uniform, so that $x_{j+1} - x_j = \Delta x$, $t_{n+1} - t_n = \Delta t$. Writing $\phi_j^n = \phi(x_j, t_n)$, $\left[\frac{\partial \phi}{\partial t}\right]_j^n = \frac{\partial \phi}{\partial t}(x_j, t_n)$ etc., the approximations of the partial derivatives are calculated from Taylor series of $\phi(x,t)$, so for example:

$$\begin{aligned} \phi_{j+1}^n &= \phi(x_j + \Delta x, t_n) \\ &= \phi_j^n + \left[\frac{\partial \phi}{\partial x}\right]_j^n \Delta x + \frac{1}{2}\left[\frac{\partial^2 \phi}{\partial x^2}\right]_j^n \Delta x^2 + O(\Delta x^3) \end{aligned} \tag{1.45}$$

$$\phi_{j-1}^n = \phi_j^n - \left[\frac{\partial\phi}{\partial x}\right]_j^n \Delta x + \frac{1}{2}\left[\frac{\partial^2\phi}{\partial x^2}\right]_j^n \Delta x^2 + O(\Delta x^3) \tag{1.46}$$

so that

$$\left[\frac{\partial\phi}{\partial x}\right]_j^n = \frac{\phi_{j+1}^n - \phi_{j-1}^n}{2\Delta x} + O(\Delta x^2) \tag{1.47}$$

$$\left[\frac{\partial^2\phi}{\partial x^2}\right]_j^n = \frac{\phi_{j+1}^n - 2\phi_j^n + \phi_{j-1}^n}{\Delta x^2} + O(\Delta x^2) \tag{1.48}$$

and substituting the approximations into the diffusion equation gives

$$\frac{\phi_j^{n+1} - \phi_j^n}{\Delta t} = \alpha\frac{\phi_{j+1}^n - 2\phi_j^n + \phi_{j-1}^n}{\Delta x^2} \tag{1.49}$$

so that ϕ can now be calculated at all points (x_j, t_n), given the initial and boundary conditions, by applying the above equation recursively. This is the essence of the finite difference method. The subtleties lie in the particular choice of approximations of the partial derivatives. The key considerations are accuracy and the resulting equation should be stable, ie. small errors in the solution should not grow as the computation progresses (provided, of course, that this property is satisfied by the original PDEs). For example, consider two distinct FD approximations of the convection equation:

$$\frac{\phi_j^{n+1} - \phi_j^n}{\Delta t} + u\frac{\phi_{j+1}^n - \phi_{j-1}^n}{2\Delta x} + O(\Delta t, \Delta x^2) = 0 \tag{1.50}$$

and

$$\frac{\phi_j^{n+1} - \phi_j^n}{\Delta t} + u\frac{\phi_j^n - \phi_{j-1}^n}{\Delta x} + O(\Delta t, \Delta x) = 0 \tag{1.51}$$

The first approximation may appear to be a better choice, as ϕ_j^n should converge to the correct solution faster as $\Delta x \to 0$. However, if we take a discrete Fourier transform of the above equation (ie let $\phi_j^n = \sum_k \psi_\theta^n e^{ij\theta}$), then we get the following solutions for a particular mode:

$$\psi_\theta^{n+1} = \left[1 - i\frac{u\Delta t}{\Delta x}\sin\theta\right]\psi_\theta^n \tag{1.52}$$

for the first approximation, and

$$\psi_\theta^{n+1} = \left[1 - \frac{u\Delta t}{\Delta x}(1 - \cos\theta) - i\frac{\Delta t}{\Delta x}\sin\theta\right]\psi_\theta^n \tag{1.53}$$

for the second. Now, since the convection equation is linear, the errors in the solutions also satisfy these equations, and we can see that the errors in the first approximation grow in amplitude, whilst those in the second are damped, provided that $0 \leq u\Delta t/\Delta x \leq 1$. In particular, the fastest growing mode in equation 1.52 is that which has $\theta = \pi/2$. Thus although equation 1.50 models the long wavelength modes more accurately than equation 1.51, the numerical solutions will eventually become swamped by short wavelength modes growing without bound, and so equation 1.50

cannot be used to solve the convection equation. Equation 1.51 does not suffer from this problem; accuracy is sacrificed in favour of stability. The stability constraint that $0 \leq u\Delta t/\Delta x \leq 1$ is called the Courant-Friedrichs- Lewy condition (or CFL condition) and is frequently encountered in explicit FD approximations of hyperbolic PDEs. For instance, another FD approximation of the convection equation is the Lax-Wendroff approximation:

$$\frac{\phi_j^{n+1} - \phi_j^n}{\Delta t} + u\frac{\phi_{j+1}^n - \phi_{j-1}^n}{2\Delta x} - \frac{1}{2}u^2\Delta t\frac{\phi_{j+1}^n - 2\phi_j^n + \phi_{j-1}^n}{\Delta x^2} = 0 \tag{1.54}$$

The truncation error for the $\frac{\partial\phi}{\partial t}$ term is $\frac{\partial^2\phi}{\partial t^2}\frac{\Delta t}{2}$, and applying $\frac{\partial\phi}{\partial t} = -u\frac{\partial\phi}{\partial x} \Longrightarrow \frac{\partial^2\phi}{\partial t^2} = u^2\frac{\partial^2\phi}{\partial x^2}$, we can see that it cancels the diffusive term which has been introduced. Thus this is an order $O(\Delta t^2, \Delta x^2)$ approximation. A Fourier analysis shows that numerical stability requires that the CFL condition $\mid u\Delta t/\Delta x \mid \leq 1$ be satisfied.

The stability constraints on equation 1.49 are more restrictive. Analysis shows that $0 \leq \frac{\alpha\Delta t}{\Delta x^2} \leq \frac{1}{2}$. Note that unconditional stability cannot be achieved by an explicit method; to do so requires an implicit method where $\frac{\partial^2\phi}{\partial x^2}$ etc. are evaluated at t_{n+1}, ie

$$\frac{\phi_j^{n+1} - \phi_j^n}{\Delta t} = \alpha\frac{\phi_{j+1}^{n+1} - 2\phi_j^{n+1} + \phi_{j-1}^{n+1}}{\Delta x^2} \tag{1.55}$$

This approximation is unconditionally stable. The main advantage of implicit methods is that they allow a larger Δt. However, they also require more computational work, and since accuracy considerations often demand Δt be small anyway, they are more advantageous for equations such as the diffusion equation, for which the stability constraints on explicit methods can be particularly severe [5].

1.2.1 Cellular Automata and Lattice Gases

A relatively new approach to the modelling of fluid equations is the cellular automaton (CA) [6, 7, 8, 9]. This concept was originally conceived by John von Neumann as an environment for the simulation of von Neumann machines [10, 11, 12] - machines which are capable of self-replication in a manner analogous to the DNA molecule. Since then numerous CA have been found for modelling a wide variety of complex systems from fluids to artificial life, for example, John Conway's *Game of Life* [13], which, despite its apparent simplicity, can exhibit some startlingly complex behaviour.

Formally, a cellular automaton is an array of cells, each of which can be in a one of a finite number of states. The state of each cell evolves in discrete time steps, the new state of a cell being entirely determined by the previous states of a small neighbourhood of cells. The local nature of a cellular automaton, where the neighbourhood of a cell generally consists of its nearest and next to nearest neighbours, is one of its most powerful features, allowing it to be modelled highly efficiently on a parallel computer.

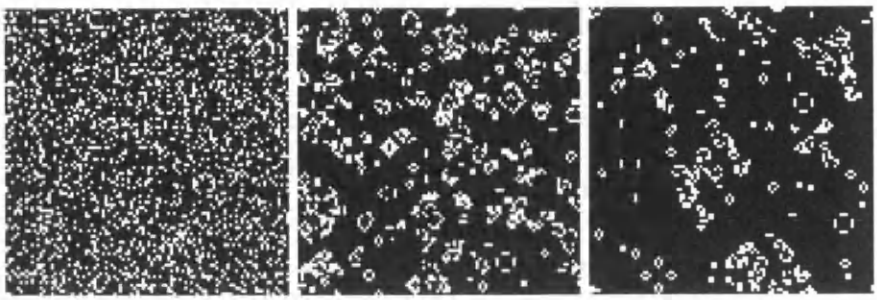

Figure 1.1: Evolution of the *Game of Life* from a random configuration, with one fifth of the cells initially switched on. On-cells are represented in white, off-cells in black. The array shown is 100 cells square. Boundary conditions are periodic, ie the neighbourhoud of a cell at an edge includes cells at the opposite edge. The figures show from left to right the initial state of the *Life Universe*, the state after 30 time steps and the state after 300 time steps.

The Game of Life

This is probably the most famous example of a CA, and is the one most often quoted in texts [14, 15, 6, 13]. The cells are arranged in a 2-dimensional, square lattice, the neighbourhood of a cell consisting of the cell itself and its eight closest neighbours. The set of cellular states is $\{0, 1\}$, so that a cell is either 'on' or 'off' depending on whether it is in state 1 or 0. The updating rules are such that if exactly two neighbours of a cell (excluding itself) are on, the cell will remain unchanged; if three are on the cell will be turned on; any other number and the cell will be turned off.

To appreciate the remarkable complexity arising from these simple rules, it is best to watch the *Game of Life* evolving in real time on a fast computer. An initially random state will begin with frenzied activity, eventually settling down to a quiescent state with bursts of new activity arising occasionally. A typical example of this is shown in figure 1.1

Close examination of a number of such cases reveals that similar features occur repeatedly from almost any initial state [14]. Typical examples are gliders (figure 1.2), eaters and blinkers. A particularly interesting configuration is one known as the r-pentomino (figure 1.3). This starts from five on-cells arranged in an r-shape, and after several hundred time steps evolves into a complicated pattern from which many gliders emerge.

More interesting examples are discussed at length in several texts [14, 13]. For instance, it has been discovered that a particular 'collision' of thirteen gliders results in a 'glider gun' which produces new gliders indefinitely. It has also been shown that there are configurations that behave like logical AND, OR and NOT gates when gliders collide with them in a particular way. Thus, if we regard gliders as being analogous to electrical signals which can be produced by a glider gun, we have all the necessary ingredients to embed a computer in the life 'universe'. This, together with the ability of gliders to collide and produce more gliders can be shown to allow the existence of von

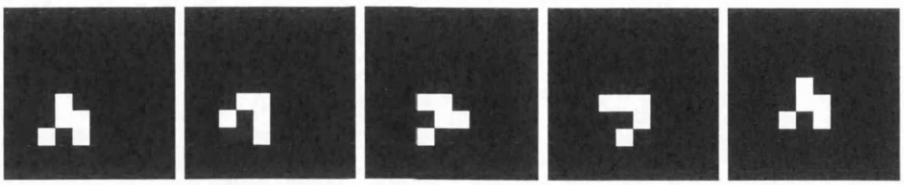

Figure 1.2: Motion of a glider

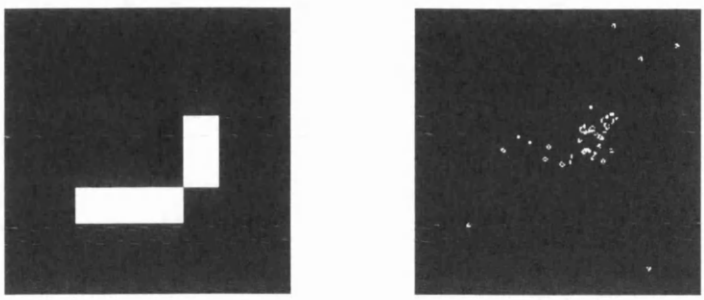

Figure 1.3: The r-pentomino. From the initial configuration of five on-cells (left), this evolves into a complicated pattern, producing many gliders (right - after 400 time steps).

Neumann machines [10]

Lattice Gases

Of more interest to physicists is a class of cellular automata known as lattice gases. As the name suggests these are used to model fluid like systems. The first lattice gas model originally proposed by Hardy eta al [16] (the HPP lattice gas) is modelled on a square lattice, with a cell's neighbourhood consisting of the cells immediately to the north, south, east and west. The cellular states are characterised by a set of four occupation numbers, representing particles moving in each of the four directions. Each occupation number can only take on the value zero or one.

The updating rule is a two step process. Firstly the particles are streamed, so that a particle moving north will be located in the next cell to the north at the subsequent time step. Secondly the particles are scattered in such a way to preserve particle number and momentum. It is easily seen that there are only two configurations which will be changed by scattering, namely when a cell contains exactly two particles which are moving in opposite directions. After scattering, their momenta will have rotated by ninety degrees, so that, for example, two particles moving north and south will emerge moving east and west.

This simple scheme models the particle nature of a gas in a very intuitive way. An example of the model in action is shown in figure 1.4. This begins with an initial uniform density of 2

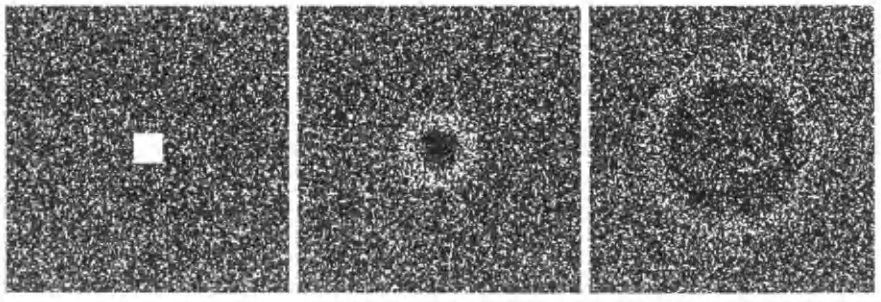

Figure 1.4: A Sound Wave Progpagating in a Lattice Gas. From the initial configuration (left), with a density enhancement on a uniform background, the wavefront propagates isotropically through the gas despite the anisotropy of the lattice. Cells containing more than two particles are white, others are black. The above lattice is 200 cells square, and periodic boundary conditions are applied.

particles per cell, except in the center of the lattice where we have 4 particles per cell. This density enhancement gives rise to a sound wave which propagates through the gas. Notice that despite the anisotropy of the lattice and particle velocities, the wavefront propagates isotropically.

Despite the isotropy of the pressure in the lattice gas described above, it can be shown that the viscosity is not isotropic [16]. This problem was solved by Frisch et al [17], using a hexagonal lattice each cell being linked to its six neighbours (the FHP lattice gas). A detailed analysis of the statistical mechanics of lattice gases forms the basis of the lattice Boltzmann method and will be discussed at length in chapter 2.

Lattice Gas Magnetohydrodynamics

If the lattice gas model is to be extended to model MHD, there is a apparent problem to be overcome, namely the non-local nature of the Lorentz force. Recall that

$$\nabla \times \mathbf{B} = \mathbf{j} \tag{1.56}$$

Since $\nabla \cdot \mathbf{B} = 0$, we can write $\mathbf{B}$ in terms of a vector potential:

$$\mathbf{B} = \nabla \times \mathbf{A} \tag{1.57}$$

On choosing a particular guage for $\mathbf{A}$, for instance the Coulomb guage where $\nabla \cdot \mathbf{A} = 0$, equation 1.56 becomes

$$\nabla^2 \mathbf{A} + \mathbf{j} = 0 \tag{1.58}$$

Explicit solutions of equation 1.58 can be found [3] and are given by

$$\mathbf{A}(\mathbf{x}, t) = \frac{1}{4\pi} \int \frac{\mathbf{j}(\mathbf{x}', t)}{|\mathbf{x} - \mathbf{x}'|} \mathrm{d}^3\mathbf{x}' \tag{1.59}$$

It should be apparent from inspection of equation 1.59 that the magnetic field is non-locally dependent on the current density, thus threatening the potential of a lattice gas to model MHD. Even if the displacement current is retained in Ampère's law, thus technically restoring locality in a physical sense, the behaviour is still effectively non-local for our purposes since the velocity at which information propagates (ie c) is several orders of magnitude greater than the fluid velocity.

This problem is only an apparent one, however, because the above argument has naively neglected the effect of the magnetic field on the current density. Examination of the full MHD equations reveals that when the resistivity is negligible, the magnetic field lines move as if they are frozen into the fluid, and disturbances in the magnetic field propagate at the Alfvén speed. Therefore, provided that the Alfvén speed is not greater than the lattice speed, locality can potentially be restored. The apparent contradiction with the previous paragraph can be resolved by noting that a change in current density at one point in space, instantaneously affects the magnetic field at all other points in space. This change in the magnetic field then, by Faraday's law, induces an electric field which causes a change in the current density, since the plasma is a conducting medium. Thus the current density at one point cannot change without instantaneously affecting the current density everywhere. It is this feedback between $\mathbf{B}$ and $\mathbf{j}$ which renders the dynamics effectively local.

Montgomery and Doolen [18, 19] made first attempt to formulate an MHD lattice gas scheme by introducing additional degrees of freedom to account for the vector potential. The updating rule for the vector potential required the evaluation of some space averaged quantities, thus destroying the essential feature of locality. Furthermore, the model is intrinsically two dimenional, due to the method of representing the magnetic field.

Chen and Matthaes [20] and Chen et al [21] later developed a model which did not suffer from the pitfalls of the Montgomery and Doolen scheme. We shall discuss the scheme here in some detail, since modified versions of its lattice Boltzmann generalization [22, 1] are used in this thesis.

Firstly, we introduce the Elsässer variables [23], defined by

$$\mathbf{z}^{\pm} = \mathbf{v} \pm \mathbf{B} \tag{1.60}$$

in units where $\rho = 1$. Then, neglecting the pressure terms

$$\begin{aligned}
\frac{\partial \mathbf{z}^{\pm}}{\partial t} &= \frac{\partial \mathbf{v}}{\partial t} \pm \frac{\partial \mathbf{B}}{\partial t} \\
&\approx -\mathbf{v}\cdot\nabla\mathbf{v} + \mathbf{B}\cdot\nabla\mathbf{B} \pm \mathbf{B}\cdot\nabla\mathbf{v} \mp \mathbf{v}\cdot\nabla\mathbf{B} \\
&= -\mathbf{v}\cdot\nabla(\mathbf{v}\pm\mathbf{B}) \pm \mathbf{B}\cdot\nabla(\mathbf{v}\pm\mathbf{B}) \\
&= -(\mathbf{v}\mp\mathbf{B})\cdot\nabla(\mathbf{v}\pm\mathbf{B}) \\
&= -\mathbf{z}^{\mp}\cdot\nabla\mathbf{z}^{\pm}
\end{aligned} \tag{1.61}$$

Equation 1.61 suggests that each Elsässer variable is advected by the other, implying that the $\mathbf{v}$ and $\mathbf{B}$ fields should be treated on a more equal footing. The model of Chen and Matthaeus [20] uses this concept and assigns to each particle two vectors, $\mathbf{e}_a, \mathbf{e}_b$, where $\mathbf{e}_a = (\cos 2\pi a/6, \sin 2\pi a/6), \mathbf{e}_b =$

$(\cos 2\pi b/6, \sin 2\pi b/6)$ and $a, b = 1, \ldots, 6$ on a 2D hexagonal lattice. The particle now does not have a well defined velocity, but executes a random walk across the lattice, at each time step having a probability $1 - |P_{ab}|$ of moving in the direction $\mathbf{e}_a$ and a probablity of $|P_{ab}|$ of moving in the direction $\mathbf{e}_b P_{ab}/|P_{ab}|$. The collision rules are chosen so as to conserve particle number, momentum and magnetic field which are defined as follows. If N_{ab} is the occupation number of a particle state $\{\mathbf{e}_a, \mathbf{e}_b\}$, then the fluid density at a lattice point is the sum of the N_{ab} at that point:

$$\rho = \sum_{a,b} N_{ab} \tag{1.62}$$

The fluid velocity is defined by

$$\rho \mathbf{v} = \sum_{a,b} \{(1 - |P_{ab}|)\mathbf{e}_a + P_{ab}\mathbf{e}_b\} N_{ab} \tag{1.63}$$

where $(1 - |P_{ab}|)\mathbf{e}_a + P_{ab}\mathbf{e}_b$ is the expectation value of the velocity of the state $\{\mathbf{e}_a, \mathbf{e}_b\}$. Since the vectors $\mathbf{e}_a, \mathbf{e}_b$ are analogous to the Elsässer variables, a linear combination of them is used to construct the magnetic field:

$$\rho \mathbf{B} = \sum_{a,b} \{Q_{ab}\mathbf{e}_b + R_{ab}\mathbf{e}_a\} N_{ab} \tag{1.64}$$

The 6×6 tensors P_{ab}, Q_{ab} and R_{ab} are constrained by demanding that the fields $n, \mathbf{v}$ and $\mathbf{B}$ obey, as closely as possible, the equations of MHD. Derivation of suitable P_{ab}, Q_{ab}, R_{ab} and the MHD equations from the updating rules is rather complicated [21], and the analytic theory is considerably simplified anyway by generalising the lattice gas CA to the lattice Boltzmann method which will be discussed in chapter 2.

1.3 Applications

1.3.1 Controlled Fusion

The understanding of MHD instabilities is crucial to the problem of magnetically confining fusion plasmas. There are many experiments experiments around the world exploring various approaches to this problem, eg JET at Culham, Oxfordshire, TFTR at Princeton, JT-60U in Japan. Strictly speaking the plasma parameters of a tokamak plasma are outwith the ranges required to satisfy the MHD approximation. However, it can be shown that low frequency motions perpendicular to the toroidal field are well approximated by 2D incompressible MHD.

An important example of an MHD application in tokamaks is the modelling of disruptions, where resistive instabilities give rise to reconnection events which release large amounts of energy. Disruptions are a serious problem in tokamaks because they can limit the central temperature of the plasma, thus limiting the potential for fusion to take place; they can lead to the termination of the discharge and they can even cause damage to the experimental apparatus. In fact, if viewed

in terms of the power output per unit volume, major tokamak disruptions can be the most violent events in the solar system.

The other approach to controlled nuclear fusion, namely inertial confinement, is to compress a small pellet of fuel by bombarding it with high intensity laser light. MHD is of little relevance in this case, since the main processes of interest are the interactions of electromagnetic waves with the plasma and the short time scale evolution of the plasma. Such phenomena cannot be modelled in the MHD approximation.

1.3.2 Astrophysical and Geophysical Plasmas

Naturally occurring plasmas are widespread, and magnetohydrodynamics is used to describe them in many situations, from the earth's magnetosphere to galactic jets.

Close to home, MHD dynamo theory is used to explain the origin of the earth's magnetic field as a result of currents within the molten iron core. Studies of the interaction between the earth's magnetosphere and the solar wind provide clues to the general model of a planetary magnetosphere.

The sun perhaps provides the richest source of MHD phenomena to study. As for the earth, dynamo theory is applied to explain its magnetic field. The most fascinating processes, however, appear at the surface. (Perhaps they are selected as such by our inability to peer at more fascinating processes occurring inside.) Here we can observe arcs of plasma, projecting out of the surface and supported against their own weight by a magnetic field. Such structures, which are probably formed by turbulent processes beneath the surface, can persist for months before suddenly releasing huge amounts of energy in a dramatic flare.

Outside the solar system nearly all the matter which we can see in visible light is in the plasma state. As well as the obvious generalisations of solar MHD to other types of stars, MHD turbulence has been invoked to explain the anomalous viscosities in accretion disks and the jets of active galactic nuclei have been modelled using the relativistic generalisation of MHD.

Chapter 2

Lattice Boltzmann Statistics

2.1 Problems with the Lattice Gas Approach

In Section 1.2.1, we presented the HPP lattice gas [16], which is a simple CA model for a fluid in two dimensions and demonstrated qualitative similarities between the model and real fluid behaviour. This model, however, suffers from some deficiencies which can be overcome by more sophisticated approaches.

Firstly, it can be shown that the HPP gas only obeys the Navier-Stokes equations approximately [16]. Although the fluid pressure is isotropic, it can be shown that the viscosity is not, so that transport is preferred parallel to the lattice vectors. This problem is solved by the FHP gas [17], which uses a hexagonal lattice, as opposed to a square one, with six directions rather than four. Wolfram [24] discusses this model in considerable detail. The macroscopic equations which this gas obeys are, to second order [24]:

$$\frac{\partial \rho}{\partial t} + \nabla \cdot (\rho \mathbf{v}) = 0 \tag{2.1}$$

$$\frac{\partial \rho \mathbf{v}}{\partial t} + \frac{1}{4}\rho c^{(2)} \left[(\mathbf{v} \cdot \nabla)\mathbf{v} + \mathbf{v}(\nabla \cdot \mathbf{v}) - \frac{1}{2}\nabla v^2 \right] = -\frac{1}{2}\nabla \rho - \frac{1}{8}\rho c_{\nabla}^{(2)} \nabla^2 \mathbf{v} - \frac{1}{4}\Xi \tag{2.2}$$

where

$$\Xi = \mathbf{v}(\mathbf{v} \cdot \nabla)(\rho c^{(2)}) - \frac{1}{2}v^2 \nabla(\rho c^{(2)}) + (\mathbf{v} \cdot \nabla)(\rho c_{\nabla}^{(2)}) - \frac{1}{2}(\nabla \cdot \mathbf{v})\nabla(\rho c_{\nabla}^{(2)}) \tag{2.3}$$

and $c^{(2)}, c_{\nabla}^{(2)}$ are determined from the statistical mechanics of the lattice gas.

The equation of mass continuity is thus obeyed to second order. The momentum equation is similar in structure to the Navier-Stokes momentum equation, with a number of unphysical features: there is a pressure like term $-\frac{1}{2}\nabla v^2$ giving a velocity dependent equation of state; the coefficient of the non-linear terms $\rho[(\mathbf{v} \cdot \nabla)\mathbf{v} + \mathbf{v}(\nabla \cdot \mathbf{v})]$ is not unity and the expression Ξ does not appear in the Navier-Stokes equations.

In addition to these unphysical effects, lattice gases also suffer from numerical noise and in order to obtain smooth macroscopic fields, spatial averaging over a large lattice is required.

2.2 The Lattice Boltzmann Method

All the problems mentioned in the previous section can be overcome by the lattice Boltzmann (LB) method [25, 26]. The formalism is identical to cellular automata, but where traditionally CA have used discrete, integral states, the LB method uses the continuum of real numbers to define the cellular states. Thus, in our gas model, instead of dealing with particle numbers which can assume non-negative, integral values, we use a distribution function which can have any non-negative real value.

This method retains the essential advantages of CA, namely the simplicity of the microscopic dynamics and the local nature of the iteration scheme allowing parallel implementation of the computer code. There are also number of additional advantages over finite state CA [26, 27]: numerical noise is eliminated since the distribution function, unlike particle number, is not prone to statistical fluctuations; there is no need to impose an exclusion rule, thus allowing greater freedom of choice in the collision operator and more control over the transport co-efficients; the form of the collision operator can be expicitly specified, allowing the transport co-efficients to be calculated more easily; all the unphysical features of the CA fluid can be eliminated to second order.

2.3 Lattice Boltzmann Hydrodynamics

Since the microscopic dynamics are more intuitive, we shall dicuss the lattice Boltzmann method for hydrodynamics [28, 29, 26, 30], before the MHD model, and demonstrate that it obeys the Navier-Stokes equations:

$$\frac{\partial \rho}{\partial t} + \nabla \cdot (\rho \mathbf{v}) = 0 \tag{2.4}$$

$$\rho \left(\frac{\partial \mathbf{v}}{\partial t} + (\mathbf{v} \cdot \nabla)\mathbf{v} \right) = -\nabla p + \mu \nabla^2 \rho \mathbf{v} + \mu_b \nabla \nabla \cdot (\rho \mathbf{v}) \tag{2.5}$$

2.3.1 Microscopic Dynamics

The fluid is modelled on a hexagonal lattice. The cellular states are specified by seven non-negative real numbers $f_0, \ldots, f_6$, which specify the expectation values of the number of particles of given momenta; f_0 is the mean number of particles at rest in a lattice site, f_a is the mean number moving in the direction $\mathbf{e}_a = (\cos \frac{\pi a}{3}, \sin \frac{\pi a}{3}), a = 1, \ldots, 6, \mathbf{e}_0 = (0, 0)$.

The macroscopic variables are defined as moments of the distribution function f:

$$\rho = \sum_{a=0}^{6} f_a \tag{2.6}$$

$$\rho \mathbf{v} = \sum_{a=1}^{6} f_a \mathbf{e}_a \tag{2.7}$$

Another useful quantity to define is the momentum flux tensor:

$$\mathbf{\Pi} = \sum_{a=1}^{6} f_a \mathbf{e}_a \mathbf{e}_a \tag{2.8}$$

As for a CA gas, the updating rule is a two step process: particles are streamed to the neighbouring sites and are then subjected to collisions which conserve particle number (and therefore mass) and momentum. This is described by the following equations:

$$f_a(\mathbf{x}, t) = f_a(\mathbf{x} - \mathbf{e}_a, t-1) + \Omega_a(\mathbf{x} - \mathbf{e}_a, t-1), \qquad a = 0, \ldots, 6 \tag{2.9}$$

The conservation laws impose the following constraints on the collision operator Ω:

$$\sum_{a=0}^{6} \Omega_a = 0 \tag{2.10}$$

$$\sum_{a=1}^{6} \Omega_a \mathbf{e}_a = 0 \tag{2.11}$$

In order that the second law of thermodynamics be obeyed, the collisions must cause the distribution function to relax to an equilibrium, $f^{(\mathrm{eq})}$, at which point the collision operator, Ω must vanish. Since fluid approximations usually depend on the gas being close to thermal equilibrium, Ω can be Taylor expanded to first order about $f^{(\mathrm{eq})}$, so that [31, 32]:

$$\Omega_a = \sum_b M_{ab}(f_b - f_b^{(\mathrm{eq})}) + O\left((f - f^{(\mathrm{eq})})^2\right) \tag{2.12}$$

This is usually the most general collision operator which is of interest in the lattice Boltzmann method. The full non-linear collision operator can, in principle improve the stability of the lattice Boltzmann method, but requires much more computational work. Furthermore, the higher order terms are negligible in a collision dominated fluid, so do not affect the derivation of the Navier-Stokes equations. Since the microscopic dynamics of a lattice gas are a considerably simplified version of those of a real gas, we would expect the higher order contributions to be unphysical in any case. The collision operator can be simplified still further by assuming a single time scale, $M_{ab} = -\frac{1}{\tau}\delta_{ab}$, so that

$$\Omega = -\frac{1}{\tau}\left(f - f^{(\mathrm{eq})}\right) \tag{2.13}$$

which is known as the Bathnagar-Gross-Krook (BGK) collision operator. It is easy to show that numerical stability requires that $\tau > \frac{1}{2}$.

The choice of $f^{(\mathrm{eq})}$ can also be quite arbitrary and we shall it take to be quadratic in $\mathbf{e}_a$. The most general form satisfying equations 2.10 and 2.11 is

$$f_0^{(\mathrm{eq})} = \rho\left(1 - c^{(1)} - \frac{1}{2}\,\mathrm{tr}c^{(2)}\right) \tag{2.14}$$

$$f_a^{(\mathrm{eq})} = \frac{\rho}{6}\left[c^{(1)} + 2\mathbf{v}\cdot\mathbf{e}_a + \mathbf{c}^{(2)} : \mathbf{e}_a\mathbf{e}_a\right] \tag{2.15}$$

where the scalar $c^{(1)}$ and symmetric second rank tensor $\mathbf{c}^{(2)}$ can be chosen later, in order that $\rho, \mathbf{v}$ satisfy the Navier-Stokes equations.

2.3.2 The Continuum Limit and Macroscopic Equations

Having defined the microscopic dynamics, we now demonstrate that equations 2.9 give rise to the Navier-Stokes equations. If f varies sufficiently slowly over the lattice, then we can take a Taylor expansion of equations 2.9, truncated after first order [24]:

$$\frac{\partial f_a}{\partial t} + \mathbf{e}_a \cdot \nabla f_a = \Omega_a \tag{2.16}$$

which is called the lattice Boltzmann equation. Notice the similarity in structure to the Boltzmann equation 1.6 with $\mathbf{F} = 0$, the most important difference being that we have a continuum of velocities in equation 1.6, but only seven discrete velocities in equation 2.16.

In an analogous fashion to section 1.1.2, macroscopic equations are obtained by taking moments of equation 2.16. The zeroth order moment immediately gives the continuity equation:

$$\frac{\partial \rho}{\partial t} + \nabla \cdot (\rho \mathbf{v}) = 0, \tag{2.17}$$

and the first order moment gives a momentum equation:

$$\frac{\partial (\rho \mathbf{v})}{\partial t} + \nabla \cdot \mathbf{\Pi} = 0 \tag{2.18}$$

It is straightforward to show that for equation 2.18 to be equivalent to equation 2.5, in the ideal limit, we must have

$$\mathbf{\Pi} = p\mathbf{I} + \rho\mathbf{v}\mathbf{v}. \tag{2.19}$$

If f is a slowly varying function of space and time (a condition for equation 2.16 to be valid), we can say that $f \approx f^{(\mathrm{eq})}$, and so equation 2.19 imposes further constraints on $f^{(\mathrm{eq})}$ so that

$$\frac{\rho}{2}\left(c^{(1)} + \frac{1}{4}\,\mathrm{tr}\mathbf{c}^{(2)}\right) = p, \tag{2.20}$$

$$\frac{\rho}{4}\mathbf{c}^{(2)} = \rho\mathbf{v}\mathbf{v} \tag{2.21}$$

If we have an equation of state for an isothermal, ideal gas, so that

$$p = c_s^2 \rho \tag{2.22}$$

where the isothermal sound speed, c_s, must be chosen so that $f > 0$ over a sufficiently wide range of v, then

$$f_0^{(\mathrm{eq})} = \rho(1 - 2c_s^2 - v^2) \tag{2.23}$$

$$f_a^{(\mathrm{eq})} = \frac{\rho}{6}\left[2c_s^2 - v^2 + 2\mathbf{v}\cdot\mathbf{e}_a + 4(\mathbf{v}\cdot\mathbf{e}_a)^2\right] \tag{2.24}$$

Thus we have a scheme, which models an ideal, isothermal gas to first order.

2.3.3 The Chapman-Enskog Expansion and Transport Coefficients

In order to derive the coefficients of viscosity, we must include higher order terms in our macroscopic equations, by employing a Chapman-Enskog procedure.

Firstly, we Taylor expand equation 2.9 to second order:

$$\frac{\partial f_a}{\partial t} + \mathbf{e}_a \cdot \nabla(f_a + \Omega_a) - \mathbf{e}_a \cdot \nabla \frac{\partial (f_a + \Omega_a)}{\partial t} - \Omega_a$$
$$-\frac{1}{2}\frac{\partial^2 \Omega_a}{\partial t^2} - \frac{1}{2}\mathbf{e}_a\mathbf{e}_a : \nabla\nabla(f_a + \Omega_a) + \frac{\partial \Omega_a}{\partial t} - \frac{1}{2}\frac{\partial^2 f_a}{\partial t^2} = 0 \tag{2.25}$$

The essence of the Chapman-Enskog procedure is to assume that the dependant variables can be written as functions of multiple time scales, $t_1 = \epsilon t$, $t_2 = \epsilon^2 t$ and $x_1 = \epsilon x$, so that $f(x,t) = f(x_1, t_1, t_2) = f(\epsilon x, \epsilon t, \epsilon^2 t)$. This means that we write the differential operators in the following way [1, 33, 34]:

$$\frac{\partial}{\partial t} = \epsilon \frac{\partial}{\partial t_1} + \epsilon^2 \frac{\partial}{\partial t_2}, \tag{2.26}$$

$$\nabla = \epsilon \nabla_1, \tag{2.27}$$

where ϵ is the expansion parameter assumed to be small, implying that t_2 is a slower time sale than t_1, and will be associated with diffusion effects. Since ∇ is only being expanded to first order, we can drop the subscript from ∇_1 without confusion. The distribution function is expanded, assuming small departures from equilibrium:

$$f_a = f_a^{(0)} + \epsilon f_a^{(1)} + \epsilon^2 f_a^{(2)} + \ldots, \tag{2.28}$$

where $f_a^{(0)} = f_a{}^{(\mathrm{eq})}$, so that the collision operator is

$$\Omega_a = -\frac{1}{\tau}(\epsilon f_a^{(1)} + \epsilon^2 f_a^{(2)} + \ldots) \tag{2.29}$$

Replacing these expansions into equation 2.25, we get to order ϵ:

$$\frac{\partial f_a^{(0)}}{\partial t_1} + \mathbf{e}_a \cdot \nabla f_a^{(0)} = -\frac{1}{\tau} f_a^{(1)} \tag{2.30}$$

and to order ϵ^2:

$$\frac{\partial f_a^{(1)}}{\partial t_1} + \frac{\partial f_a^{(0)}}{\partial t_2} - \frac{1}{\tau}\frac{\partial f_a^{(1)}}{\partial t_1} + \mathbf{e}_a \cdot \nabla f_a^{(1)} - \frac{1}{\tau}\mathbf{e}_a \cdot \nabla f_a^{(1)}$$
$$+\frac{1}{\tau} f_a^{(2)} - \frac{1}{2}(\mathbf{e} \cdot \nabla)^2 f_a^{(0)} - \mathbf{e}_a \cdot \nabla \frac{\partial f_a^{(0)}}{\partial t_1} - \frac{1}{2}\frac{\partial^2 f_a^{(0)}}{\partial t_1^2} = 0 \tag{2.31}$$

From equation 2.30 we also get

$$\frac{1}{2\tau}\left(\frac{\partial}{\partial t_1} + \mathbf{e}_a \cdot \nabla\right) f_a^{(1)} = -\frac{1}{2}\left(\frac{\partial^2 f_a^{(0)}}{\partial t_1^2} + 2\mathbf{e}_a \cdot \nabla \frac{\partial f_a^{(0)}}{\partial t_1} + (\mathbf{e}_a \cdot \nabla)^2 f_a^{(0)}\right) \tag{2.32}$$

Substituting equation 2.32 into equation 2.31 then gives us

$$\frac{\partial f_a^{(0)}}{\partial t_2} + \left(1 - \frac{1}{2\tau}\right)\left(\frac{\partial f_a^{(1)}}{\partial t_1} + \mathbf{e}_a \cdot \nabla f_a^{(1)}\right) = -\frac{1}{\tau} f_a^{(2)} \tag{2.33}$$

Summing equations 2.30 and 2.33 over a, and using $\sum_a f_a^{(1)} = \sum_a f_a^{(2)} = 0$, we recover the continuity equation:

$$\frac{\partial \rho}{\partial t} + \nabla \cdot (\rho \mathbf{v}) = 0 \tag{2.34}$$

Similarly, taking the first moment of 2.30 and 2.31, and using $\sum_a f_a^{(1)} \mathbf{e}_a = \sum_a f_a^{(2)} \mathbf{e}_a = 0$, we get

$$\frac{\partial (\rho \mathbf{v})}{\partial t} + \nabla \cdot \mathbf{\Pi} = 0, \tag{2.35}$$

where

$$\mathbf{\Pi} = \sum_{a=1}^{6} \mathbf{e}_a \mathbf{e}_a \left[f_a^{(0)} + \epsilon \left(1 - \frac{1}{2\tau}\right) f_a^{(1)} \right] \tag{2.36}$$

Since $f_a^{(0)} = f_a{}^{(\mathrm{eq})}$ has already been chosen to satisfy, to lowest order, the ideal Navier-Stokes equations, we can write equation 2.35 as

$$\rho \left(\frac{\partial \mathbf{v}}{\partial t} + \mathbf{v} \cdot \nabla \mathbf{v}\right) = -\nabla p - \nabla \cdot \mathbf{\Pi}^{(1)} \tag{2.37}$$

where $\mathbf{\Pi}^{(1)}$ is the first order correction to the momentum flux tensor. Using equation 2.30, we have

$$\mathbf{\Pi}^{(1)} = -\tau \sum_{a=1}^{6} \left(\frac{\partial}{\partial t_1} + \mathbf{e}_a \cdot \nabla_1\right) f_a^{(0)} \mathbf{e}_a \mathbf{e}_a \tag{2.38}$$

and inserting expression 2.24 for $f_a^{(0)}$ we get

$$\mathbf{\Pi}^{(1)} = \tau \left\{ c_s^2 \nabla \cdot (\rho \mathbf{v}) + c_s^2 \mathbf{v} \nabla \rho + c_s^2 (\nabla \rho) \mathbf{v} - \nabla \cdot (\rho \mathbf{v} \mathbf{v} \mathbf{v}) \right\} - \frac{\tau}{4} \left\{ \nabla_1 \cdot (\rho \mathbf{v}) \mathbf{I} + \nabla_1 (\rho \mathbf{v}) + [\nabla_1 (\rho \mathbf{v}]^T \right\} \tag{2.39}$$

which, on choosing $c_s^2 = \frac{1}{4}$, gives us the following momentum equation:

$$\begin{aligned} \rho \left(\frac{\partial \mathbf{v}}{\partial t} + \mathbf{v} \cdot \nabla \mathbf{v}\right) &= -\nabla c_s^2 \rho \\ &+ \frac{1}{4}\left(\tau - \frac{1}{2}\right) \nabla \cdot (\rho \nabla \mathbf{v}) + \left(\tau - \frac{1}{2}\right) \nabla \cdot (\rho \mathbf{v} \mathbf{v} \mathbf{v}) \end{aligned} \tag{2.40}$$

Comparing this with equation 2.5, we can see that the viscosity is given by:

$$\nu = \frac{1}{4}\left(\tau - \frac{1}{2}\right), \tag{2.41}$$

Thus, the condition for positive viscosity is the same as the condition for numerical stability, namely $\tau > \frac{1}{2}$, so that the ν can be made arbitrarily small by choosing τ sufficiently close to $\frac{1}{2}$. The non-linear term $\nabla \cdot (\rho \mathbf{v} \mathbf{v} \mathbf{v})$ was considered in detail by Qian and Orszag [35], who showed that it scaled as the second power of the Mach number, thus limiting the lattice Boltzmann method to the low Mach number regime.

2.3.4 Further Extension of Lattice Boltzmann Hydrodynamics

Hydrodynamics in Higher Dimensions

There also exist lattice Boltzmann schemes for modelling three dimensional hydrodynamics. One problem however, is that there does not exist a 3D lattice which will allow a single speed model with isotropic transport coefficients. There are a couple of ways round this. One is to extend the method to four dimensions and use a face-centred, hypercubic lattice [36], the particle velocities being permutations of $(\pm 1, \pm 1, 0, 0)$ which gives 24 moving states. Using the same procedure detailed above, it can be shown that this method yields the Navier-Stokes equations in four dimensions, and three dimensional hydrodynamics can be modelled as a projection onto a 3D hypersurface.

The other way of getting isotropic transport, is to allow links beyond nearest neighbours on a 3D body-centred cubic lattice [37]. The particle velocities are $(\pm 1, \pm 1, \pm 1)$ and permutations of $(\pm 2, 0, 0)$, giving 14 moving states. The advantages over the 4D method are that there is no redundant, unphysical dimension and there are fewer particle states per cell, thus making less demand on computer memory and time.

Thermohydrodynamics

The models discussed so far have been restricted to an isothermal equation of state, and have ignored energy conservation. This is because the moving particles can only have a single speed.

To include an energy equation, multi-speed models must be used [38, 34]. On a 2D, hexagonal lattice, the particle velocities are $\mathbf{e}_{\sigma a} = \sigma(\cos\frac{\pi a}{3}, \sin\frac{\pi a}{3})$, $a = 1, \ldots, 6$, $\sigma = 0, \ldots, N$. Collisions conserve mass, momentum and energy, which are defined by:

$$\rho = \sum_{\sigma,a} f_{\sigma a} \tag{2.42}$$

$$\rho \mathbf{v} = \sum_{\sigma,a} f_{\sigma a} \mathbf{e}_{\sigma a} \tag{2.43}$$

$$E = \sum_{\sigma,a} f_{\sigma a} \frac{1}{2} e_{\sigma a}^2 \tag{2.44}$$

The Chapman-Enskog procedure then gives, with appropriate choice of $f^{(\mathrm{eq})}$, the equations of thermohydrodynamics, with an ideal equation of state.

2.4 Lattice Boltzmann Magnetohydrodynamics

Modelling of magnetohydrodynamics by a lattice Boltzmann scheme is a harder problem than ordinary hydrodynamics. The major problem is the non-local nature of the Lorentz force, $\mathbf{j} \times \mathbf{B}$. Any changes in the magnetic field, which result from changes in the current density, propagate through

the plasma at the speed of light, which is infinite in the MHD approximation. However, as we discussed in section 1.2.1 and was originally demonstrated by Chen and Matthaeus [20], this problem is illusory.

Early lattice gas and lattice Boltzmann methods [18, 19, 39] incorporated additional degrees of freedom into the basic hydrodynamic scheme, to account for the vector potential. To update the dynamics, some space average quantities need to be evaluated, which destroys the local nature of the algorithm.

In section 1.2.1, we described a purely local MHD lattice gas model [20, 21] which uses 36 pairs of lattice vectors $(\mathbf{e}_a, \mathbf{e}_b)$ to specify the particle states, and in which the streaming rule makes the particles undergo a random walk across the lattice, with a specified probability of moving in either the direction of $\mathbf{e}_a$ or $\mathbf{e}_b$. This method has been extended to the lattice Boltzmann scheme by Chen et al [22] and further simplified to reduce the number of particle states by Matinez et al [1]. This is the model which we shall describe here.

2.4.1 Microscopic Dynamics and Moments of the Distribution Function

As with the pure hydro model, we use a 2D hexagonal lattice, with the nearest neighbour links being the vectors $\mathbf{e}_a = (\cos\frac{\pi a}{3}, \sin\frac{\pi a}{3})$, $a = 1, \ldots, 6$. The moving particle states are specified by pairs of lattice vectors, $(\mathbf{e}_a, \mathbf{e}_b)$, where $a = 1, \ldots, 6$, $b = a \pm 1$.

Macroscopic variables are defined as moments of the distribution function:

$$\rho = f_0 + \sum_{a,b} f_{ab} \tag{2.45}$$

$$\rho\mathbf{v} = \sum_{a,b} f_{ab}\left[(1-p)\mathbf{e}_a + p\mathbf{e}_b\right] = \sum_{a,b} f_{ab}\mathbf{v}_{ab} \tag{2.46}$$

$$\rho\mathbf{B} = \sum_{a,b} f_{ab}\left[q\mathbf{e}_b + r\mathbf{e}_a\right] = \sum_{a,b} f_{ab}\mathbf{B}_{ab} \tag{2.47}$$

Where p, q, r are parameters to be chosen later. Also useful to define are the momentum flux tensor and the magnetic momentum flux tensor:

$$\mathbf{\Pi} = \sum_{a,b} f_{ab}\mathbf{v}_{ab}\mathbf{v}_{ab} \tag{2.48}$$

$$\mathbf{\Lambda} = \sum_{a,b} f_{ab}\mathbf{B}_{ab}\mathbf{v}_{ab} \tag{2.49}$$

In one time step, a particle has a probability $1-p$ of moving in the direction $\mathbf{e}_a$, and p of moving in the direction $\mathbf{e}_b$. So the updating rules, with collisions are:

$$f_0(\mathbf{x}, t) = f_0(\mathbf{x}, t-1) + \Omega_0(\mathbf{x}, t-1) \tag{2.50}$$

$$f_{ab}(\mathbf{x},t) = (1-p)\left[f_{ab}(\mathbf{x}-\mathbf{e}_a,t-1)+\Omega_{ab}(\mathbf{x}-\mathbf{e}_a,t-1)\right]$$
$$+p\left[f_{ab}(\mathbf{x}-\mathbf{e}_b,t-1)+\Omega_{ab}(\mathbf{x}-\mathbf{e}_b,t-1)\right] \tag{2.51}$$

The collision operator, Ω is chosen to conserve mass, momentum and magnetic field:

$$\sum_{a,b}\Omega_{ab} = 0 \tag{2.52}$$

$$\sum_{a,b}\Omega_{ab}\mathbf{v}_{ab} = 0 \tag{2.53}$$

$$\sum_{a,b}\Omega_{ab}\mathbf{B}_{ab} = 0 \tag{2.54}$$

As usual Ω will represent a linear relaxation to equilibrium:

$$\Omega = -\frac{1}{\tau}(f - f^{(\mathrm{eq})}) \tag{2.55}$$

If we choose $f^{(\mathrm{eq})}$ to be quadratic in $(\mathbf{e}_a, \mathbf{e}_b)$, so that it is of the form:

$$f_{ab}^{(\mathrm{eq})} = c^{(1)} + \mathbf{c}^{(2)}\cdot\mathbf{e}_a + \mathbf{c}^{(3)}\cdot\mathbf{e}_b + \mathbf{c}^{(4)} : \mathbf{e}_a\mathbf{e}_a + \mathbf{c}^{(5)} : \mathbf{e}_a\mathbf{e}_b + \mathbf{c}^{(6)} : \mathbf{e}_b\mathbf{e}_b \tag{2.56}$$

where $c^{(1)}$ is a scalar, $\mathbf{c}^{(2)}$, $\mathbf{c}^{(3)}$ are vectors, $\mathbf{c}^{(4)}$, $\mathbf{c}^{(5)}$, $\mathbf{c}^{(6)}$ are tensors and $\mathbf{c}^{(4)}$ and $\mathbf{c}^{(6)}$ are symmetric, then, in order that equation 2.52, 2.53 and 2.54 be satisfied, we must have:

$$\rho = f_0^{(eq)} + 12c^{(1)} + 6\ \mathrm{tr}\mathbf{c}^{(4)} + 3\ \mathrm{tr}\mathbf{c}^{(5)} + 6\ \mathrm{tr}\mathbf{c}^{(6)} \tag{2.57}$$

$$\rho\mathbf{v} = (6-3p)\mathbf{c}^{(2)} + (3+3p)\mathbf{c}^{(3)} \tag{2.58}$$

$$\rho\mathbf{B} = (3q+6r)\mathbf{c}^{(2)} + (6q+3r)\mathbf{c}^{(3)} \tag{2.59}$$

2.4.2 Macroscopic Equations

Following the same procedure has section 2.3.2, the first order Taylor expansion of equations 2.50 and 2.51, gives the lattice Boltzmann equations:

$$\frac{\partial f_0}{\partial t} = \Omega_0 \tag{2.60}$$

$$\frac{\partial f_{ab}}{\partial t} + \mathbf{v}_{ab}\cdot\nabla f_{ab} = \Omega_{ab} \tag{2.61}$$

The zeroth order moment of equations 2.60 and 2.61 gives us the continuity equation:

$$\frac{\partial\rho}{\partial t} + \nabla\cdot(\rho\mathbf{v}) = 0 \tag{2.62}$$

There are two first order moment equations, got by multiplying equation 2.61 by either $\mathbf{v}_{ab}$ or $\mathbf{B}_{ab}$ and summing over a and b. These are

$$\frac{\partial(\rho\mathbf{v})}{\partial t} + \nabla\cdot\mathbf{\Pi} = 0 \tag{2.63}$$

$$\frac{\partial(\rho \mathbf{B})}{\partial t} + \nabla \cdot \mathbf{\Lambda} = 0 \tag{2.64}$$

In order for these to be equivalent to equations 1.40 and 1.41, in the limit constant ρ and negligible ν and η we must have

$$\mathbf{\Pi}^{(0)} = (P + \frac{1}{2}B^2)\mathbf{I} + \rho(\mathbf{vv} - \mathbf{BB}) \tag{2.65}$$

$$\mathbf{\Lambda}^{(0)} = \rho(\mathbf{Bv} - \mathbf{vB}) \tag{2.66}$$

Inserting expression 2.57 into the above equations, we get the conditions

$$\begin{aligned}\mathbf{\Pi} = &\left[(6 - 6p + 6p^2)\, c^{(1)} + \left(\frac{3}{2} - \frac{3p}{2} + \frac{15p^2}{4}\right) \mathrm{tr}c^{(4)}\right.\\ &\left. + \left(\frac{3}{4} + 3p + 3p^2\right) \mathrm{tr}c^{(5)} + \left(\frac{15}{4} - 6p + \frac{15p^2}{4}\right) \mathrm{tr}c^{(6)}\right] \mathbf{I} + \left(3 - 3p - \frac{3p^2}{2}\right) \mathbf{c}^{(4)}\\ &+ \left(\frac{3}{4} - 3p + 3p^2\right) \left(\mathbf{c}^{(5)} + (\mathbf{c}^{(5)})^T\right) + \left(\frac{-3}{2} + 6p - \frac{3p^2}{2}\right) \mathbf{c}^{(6)}\end{aligned} \tag{2.67}$$

$$\begin{aligned}\mathbf{\Lambda} = &\left[(3q + 3pq + 6r - 3pr)\, c^{(1)} + \left(\frac{3q}{4} + 3pq + \frac{3r}{2} - \frac{3pr}{4}\right) \mathrm{tr}c^{(4)}\right.\\ &\left. + \left(-\frac{3q}{4} + \frac{3pq}{2} + \frac{3r}{4} - \frac{3pr}{2}\right) \mathrm{tr}c^{(5)} + \left(\frac{3q}{4} + \frac{3pq}{4} + \frac{15r}{4} - 3pr\right) \mathrm{tr}c^{(6)}\right] \mathbf{I}\\ &+ \left(\frac{3q}{2} - 3pq + 3r - \frac{3pr}{2}\right) \mathbf{c}^{(4)} + \left(\frac{-3q}{4} + \frac{3pq}{2} + \frac{3r}{4} + 3pr\right) \mathbf{c}^{(5)}\\ &+ \left(\frac{15q}{4} - 3pq + \frac{3r}{4} - \frac{3pr}{2}\right) (\mathbf{c}^{(5)})^T + \left(\frac{3q}{2} + \frac{3pq}{2} - \frac{3r}{2} + 3pr\right) \mathbf{c}^{(6)}\end{aligned} \tag{2.68}$$

The required form of $c^{(1)}, \ldots, c^{(6)}$ can now be found on equating expressions 2.67, 2.68 with 2.65 and 2.66. Firstly we note that the term involving $c^{(1)}$ in equation 2.68 would give rise to an unphysical pressure like term in the induction equation. Demanding that this term disappear gives us the constraint

$$r = -q\frac{1+p}{2-p} \tag{2.69}$$

In order to obtain a correctly structured induction equation, it is necessary that the symmetric component of 2.68 vanish. Denoting the symmetric part of $\mathbf{c}^{(5)}$ by $S(\mathbf{c}^{(5)})$, after substituting expression 2.69 and simplifying, we are left with

$$(2p - p^2)\mathbf{c}^{(4)} + (2p - 1)S(\mathbf{c}^{(5)}) + (p^2 - 1)\mathbf{c}^{(6)} = 0 \tag{2.70}$$

The pressure like term in 2.68 involving $\mathrm{tr}c^{(4)}, \mathrm{tr}c^{(5)}, \mathrm{tr}c^{(6)}$ should also vanish. This constraint turns out to be equivalent to the trace of equation 2.70. The last condition arising from equation 2.68 is that the anti-symmetric component should equal $\rho(\mathbf{Bv} - \mathbf{vB})$ which gives us

$$A(\mathbf{c}^{(5)}) = \frac{2(2-p)}{9qC}\rho\,(\mathbf{Bv} - \mathbf{vB}) \tag{2.71}$$

where $A(\mathbf{c}^{(5)})$ is the anti-symmetric component of $\mathbf{c}^{(5)}$ and $C = 2(p^2 - p + 1)$.

From equation 2.67 we can see that

$$\left(3 - 3p - \frac{3p^2}{2}\right)\mathbf{c}^{(4)} + \left(\frac{3}{2} + 3p - 3p^2\right)\mathbf{c}^{(5)} + \left(-\frac{3}{2} + 6p - \frac{3p^2}{2}\right)\mathbf{c}^{(6)} = \rho\left(\mathbf{vv} - \mathbf{BB}\right) \tag{2.72}$$

$$\begin{aligned}&\left(6 - 6p + 6p^2\right)c^{(1)} + \left(\frac{3}{2} - \frac{3p}{2} + \frac{15p^2}{4}\right)\mathrm{tr}c^{(4)} \\ &+ \left(\frac{3}{4} - 3p + 3p^2\right)\mathrm{tr}c^{(5)} + \left(\frac{15}{4} - 6p + \frac{15p^2}{4}\right)\mathrm{tr}c^{(6)} = P + \frac{1}{2}\rho B^2\end{aligned} \tag{2.73}$$

We now have all the equations we need to choose $f_0^{(\mathrm{eq})}, c^{(1)}, \ldots, c^{(6)}$ in order to satisfy the MHD equations. Arbitrarily choosing $\mathbf{c}^{(4)} = 0$, we get the following form for the equilibrium distribution:

$$\begin{aligned}f_{ab}^{(\mathrm{eq})} = \frac{\rho}{12}\Bigg[&\frac{12}{\alpha + 12} + \frac{4}{C}\Bigg(\mathbf{v}_{ab}\cdot\mathbf{v} + \frac{(2-p)^2}{3q^2}\mathbf{B}_{ab}\cdot\mathbf{B} \\ &+ \frac{4(2p-1)}{C}\left[(\mathbf{e}_b\cdot\mathbf{v})^2 - (\mathbf{e}_b\cdot\mathbf{B})^2\right] \\ &+ \frac{4(1-p^2)}{C}\left[(\mathbf{e}_a\cdot\mathbf{v})(\mathbf{e}_b\cdot\mathbf{v}) - (\mathbf{e}_a\cdot\mathbf{B})(\mathbf{e}_b\cdot\mathbf{B})\right] \\ &+ \frac{2(2-p)}{3q}\left[(\mathbf{e}_a\cdot\mathbf{v})(\mathbf{e}_b\cdot\mathbf{B}) - (\mathbf{e}_a\cdot\mathbf{B})(\mathbf{e}_b\cdot\mathbf{v})\right] \\ &- \frac{(2p-1)(2-p)}{C}v^2 - \frac{p^2 - 4p + 1}{C}B^2\Bigg)\Bigg]\end{aligned} \tag{2.74}$$

$$f_0^{(\mathrm{eq})} = \rho\left[\frac{\alpha}{\alpha + 12} - \frac{2}{C}v^2\right] \tag{2.75}$$

It will be shown later that in order to eliminate certain unphysical second order terms, it is necessary to have $p = 0, 1$ or $\frac{1}{2}$. Martinez et al [1] choose $p = \frac{1}{2}$, (although $p = 0$ is probably a better choice). This simplifies the distribution function to the following form:

$$\begin{aligned}f_{ab}^{(\mathrm{eq})} = \frac{\rho}{12}\Bigg[&\frac{12}{\alpha + 12} + \frac{8}{3}\Big(\mathbf{v}_{ab}\cdot\mathbf{v} + \mathbf{B}_{ab}\cdot\mathbf{B} \\ &+ 2\left[(\mathbf{e}_a\cdot\mathbf{v})(\mathbf{e}_b\cdot\mathbf{v}) - (\mathbf{e}_a\cdot\mathbf{B})(\mathbf{e}_b\cdot\mathbf{B})\right] \\ &+ \frac{2}{\sqrt{3}}\left[(\mathbf{e}_a\cdot\mathbf{v})(\mathbf{e}_b\cdot\mathbf{B}) - (\mathbf{e}_a\cdot\mathbf{B})(\mathbf{e}_b\cdot\mathbf{v})\right] + \frac{B^2}{2}\Big)\Bigg]\end{aligned} \tag{2.76}$$

$$f_0^{(\mathrm{eq})} = \rho\left(\frac{\alpha}{\alpha + 12} - \frac{4}{3}v^2\right) \tag{2.77}$$

2.4.3 Transport Coefficients

The procedure for finding the transport coefficients is identical to that of section 2.3.3. The second order Taylor expansion of equation 2.51 is:

$$\begin{aligned}&\frac{\partial f_{ab}}{\partial t} + \mathbf{v}_{ab}\cdot\nabla(f_{ab} + \Omega_{ab}) - \mathbf{v}_{ab}\cdot\nabla\frac{\partial(f_{ab} + \Omega_{ab})}{\partial t} - \Omega_{ab} - \frac{1}{2}\frac{\partial^2\Omega_{ab}}{\partial t^2} \\ &- \frac{1}{2}\left[(1-p)\mathbf{e}_a\mathbf{e}_a + p\mathbf{e}_b\mathbf{e}_b\right] : \nabla\nabla(f_{ab} + \Omega_{ab}) + \frac{\partial\Omega_{ab}}{\partial t} - \frac{1}{2}\frac{\partial^2 f_{ab}}{\partial t^2} = 0\end{aligned} \tag{2.78}$$

The differential operators are expanded in the same way as equations 2.26, 2.27, 2.28 and 2.29, which gives us the following equations to order ϵ and ϵ^2:

$$\frac{\partial f_{ab}^{(0)}}{\partial t_1} + \mathbf{v}_{ab} \cdot \nabla f_{ab}^{(0)} = -\frac{1}{\tau} f_{ab}^{(1)} \tag{2.79}$$

$$\frac{\partial f_{ab}^{(1)}}{\partial t_1} + \frac{\partial f_{ab}^{(0)}}{\partial t_2} + \mathbf{v}_{ab} \cdot \nabla \frac{\partial f_{ab}^{(0)}}{\partial t_1} - \frac{1}{\tau} \mathbf{v}_{ab} \cdot \nabla f_{ab}^{(1)} - \frac{1}{2} \left[(1-p) \mathbf{e}_a \mathbf{e}_a + p \mathbf{e}_b \mathbf{e}_b \right] : \nabla \nabla f_{ab}^{(0)} - \frac{1}{\tau} \frac{\partial f_{ab}^{(1)}}{\partial t_1} - \frac{1}{2} \frac{\partial^2 f_{ab}^{(0)}}{\partial {t_1}^2} = -\frac{1}{\tau} f_{ab}^{(2)} \tag{2.80}$$

Operating on equation 2.79 with $\frac{\partial}{\partial t_1} + \mathbf{v}_{ab} \cdot \nabla$ we obtain:

$$\frac{1}{2\tau} \left(\frac{\partial}{\partial t_1} + \mathbf{v}_{ab} \cdot \nabla \right) f_{ab}^{(1)} = -\frac{1}{2} \left(\frac{\partial^2 f_{ab}^{(0)}}{\partial {t_1}^2} + 2 \mathbf{v}_{ab} \cdot \nabla \frac{\partial f_{ab}^{(0)}}{\partial t_1} + \mathbf{v}_{ab} \mathbf{v}_{ab} : \nabla \nabla f_{ab}^{(0)} \right) \tag{2.81}$$

which can be combined with equation 2.80 to get

$$\frac{\partial f_{ab}^{(0)}}{\partial t_2} + \left(1 - \frac{1}{2\tau} \right) \left(\frac{\partial f_{ab}^{(1)}}{\partial t_1} + \mathbf{v}_{ab} \cdot \nabla f_{ab}^{(1)} \right) - \frac{p(1-p)}{2} (\mathbf{e}_a - \mathbf{e}_b)(\mathbf{e}_a - \mathbf{e}_b) : \nabla \nabla f_{ab}^{(0)} = -\frac{1}{2} f_{ab}^{(2)} \tag{2.82}$$

Taking the various moments of equations 2.79, 2.82 and using

$$\sum_{a,b} f_{ab}^{(1)} = \sum_{a,b} f_{ab}^{(2)} = 0$$

we obtain the following macroscopic equations:

$$\frac{\partial \rho}{\partial t} + \nabla \cdot (\rho \mathbf{v}) = \frac{p(1-p)}{2} \sum_{a,b} (\mathbf{e}_a - \mathbf{e}_b)(\mathbf{e}_a - \mathbf{e}_b) : \nabla \nabla f_{ab}^{(0)} \tag{2.83}$$

$$\frac{\partial (\rho \mathbf{v})}{\partial t} + \nabla \cdot \mathbf{\Pi} = \frac{p(1-p)}{2} \sum_{a,b} \mathbf{v}_{ab} (\mathbf{e}_a - \mathbf{e}_b)(\mathbf{e}_a - \mathbf{e}_b) : \nabla \nabla f_{ab}^{(0)} \tag{2.84}$$

$$\frac{\partial (\rho \mathbf{B})}{\partial t} + \nabla \cdot \mathbf{\Lambda} = \frac{p(1-p)}{2} \sum_{a,b} \mathbf{B}_{ab} (\mathbf{e}_a - \mathbf{e}_b)(\mathbf{e}_a - \mathbf{e}_b) : \nabla \nabla f_{ab}^{(0)} \tag{2.85}$$

where

$$\mathbf{\Pi} = \sum_{a,b} \mathbf{v}_{ab} \mathbf{v}_{ab} \left[f_{ab}^{(0)} + \epsilon \left(1 - \frac{1}{2\tau} \right) f_{ab}^{(1)} \right] \tag{2.86}$$

$$\mathbf{\Lambda} = \sum_{a,b} \mathbf{B}_{ab} \mathbf{v}_{ab} \left[f_{ab}^{(0)} + \epsilon \left(1 - \frac{1}{2\tau} \right) f_{ab}^{(1)} \right] \tag{2.87}$$

Inserting the expression for $f_{ab}^{(0)}$ (equation 2.76) into equation 2.83, we get the following continuity equation:

$$\frac{\partial \rho}{\partial t} + \nabla \cdot (\rho \mathbf{v}) = \epsilon^2 \frac{p(1-p)}{2} \nabla \cdot \left[\frac{6}{\alpha + 12} \nabla \rho + \frac{3}{C^2} \nabla (\rho v^2) + \right.$$
$$\left. \frac{2p^2 - 2p - 1}{C^2} \left(2\nabla \cdot (\rho \mathbf{v}\mathbf{v}) + \nabla (\rho B^2) - 2\nabla \cdot (\rho \mathbf{B}\mathbf{B}) \right) \right] \tag{2.88}$$

Any non-zero value of p, therefore, gives rise to unphysical terms in the mass continuity equation.

There are several contributions to the viscous and resistive terms in the momentum and induction equations. Again, using equation 2.76, we find that

$$\frac{p(1-p)}{2} \sum_{a,b} \mathbf{v}_{ab} (\mathbf{e}_a - \mathbf{e}_b)(\mathbf{e}_a - \mathbf{e}_b) : \nabla \nabla f_{ab}^{(0)} =$$
$$\frac{p(1-p)}{2} \left\{ 2(C-3) \nabla \left[\nabla \cdot (\rho \mathbf{v}) \right] + (C+3) \nabla^2 (\rho \mathbf{v}) \right\}$$
$$+ \sqrt{3}(2p-1) \left\{ 2\nabla \left[\nabla \cdot (\rho \mathbf{B}) \right] - \nabla^2 (\rho \mathbf{B}) \right\} \tag{2.89}$$

$$\frac{p(1-p)}{2} \sum_{a,b} \mathbf{B}_{ab} (\mathbf{e}_a - \mathbf{e}_b)(\mathbf{e}_a - \mathbf{e}_b) : \nabla \nabla f_{ab}^{(0)} =$$
$$\frac{\sqrt{3} p(1-p)}{8C} (2p-1) \left\{ 2\nabla \left[\nabla \cdot (\rho \mathbf{v}) \right] - \nabla^2 (\rho \mathbf{v}) \right\}$$
$$+ \frac{1}{\sqrt{3}} \left\{ -2(C-3) \nabla \left[\nabla \cdot (\rho \mathbf{B}) \right] + +3(C-1) \nabla^2 (\rho \mathbf{B}) \right\} \tag{2.90}$$

The other contributions, which are controllable through τ, come from

$$\mathbf{\Pi}^{(1)} = \left(1 - \frac{1}{2\tau} \right) \sum_{a,b} \mathbf{v}_{ab} \mathbf{v}_{ab} f_{ab}^{(1)} \tag{2.91}$$

$$\mathbf{\Lambda}^{(1)} = \left(1 - \frac{1}{2\tau} \right) \sum_{a,b} \mathbf{B}_{ab} \mathbf{v}_{ab} f_{ab}^{(1)} \tag{2.92}$$

with $f_{ab}^{(1)} = -\tau \left(\frac{\partial}{\partial t} + \mathbf{v}_{ab} \cdot \nabla \right) f_{ab}^{(0)}$. We obtain

$$\nabla \cdot \mathbf{\Pi}^{(1)} = \left(\tau - \frac{1}{2} \right) \left[\left(\frac{C}{4} - c_s^2 \right) \nabla \left[\nabla \cdot (\rho \mathbf{v}) \right] + \frac{C}{8} \nabla^2 (\rho \mathbf{v}) \right] - c_s^2 \nabla \cdot \mathbf{v} \nabla \rho] \tag{2.93}$$

$$\nabla \cdot \mathbf{\Lambda}^{(1)} = \left(\tau - \frac{1}{2} \right) \frac{C}{4} \left(-\nabla \left[\nabla \cdot (\rho \mathbf{B}) \right] + \frac{3}{2} \nabla^2 (\rho \mathbf{B}) \right) \tag{2.94}$$

The macroscopic equations can now be written:

$$\rho \left(\frac{\partial \mathbf{v}}{\partial t} + \mathbf{v} \cdot \nabla \mathbf{v} \right) = -\nabla \left(P + \frac{\rho B^2}{2} \right) + \rho \mathbf{B} \cdot \nabla \mathbf{B} + \mathbf{B} \nabla \cdot (\rho \mathbf{B})$$
$$+ \left[\left(\tau - \frac{1}{2} \right) \frac{C}{8} + \frac{p(1-p)}{8C} (C+3) \right] \nabla^2 (\rho \mathbf{v})$$

$$-\left(\tau-\frac{1}{2}\right)c_s^2\nabla\cdot\mathbf{v}\nabla\rho \tag{2.95}$$

$$+\left[\left(\tau-\frac{1}{2}\right)\left(\frac{C}{4}-c_s^2\right)+\frac{p(1-p)}{4C}(C-3)\right]\nabla\left[\nabla\cdot(\rho\mathbf{v})\right]$$

$$+\frac{\sqrt{3}}{8}\frac{p(1-p)(2p-1)}{C}\left\{2\nabla\left[\nabla\cdot(\rho\mathbf{B})\right]-\nabla^2(\rho\mathbf{B})\right\} \tag{2.96}$$

$$\frac{\partial\rho\mathbf{B}}{\partial t}+\nabla\cdot(\rho\mathbf{B}\mathbf{v}-\rho\mathbf{v}\mathbf{B})=$$

$$\left[\left(\tau-\frac{1}{2}\right)\frac{3C}{8}+\frac{3}{8}\frac{p(1-p)}{C}(C-1)\right]\nabla^2(\rho\mathbf{B})$$

$$-\left[\left(\tau-\frac{1}{2}\right)\frac{C}{4}+\frac{p(1-p)}{4C}(C-3)\right]\nabla\left[\nabla\cdot(\rho\mathbf{B})\right]$$

$$+\frac{\sqrt{3}}{8}\frac{p(1-p)(2p-1)}{C}\left\{2\nabla\left[\nabla\cdot(\rho\mathbf{v})\right]-\nabla^2(\rho\mathbf{v})\right\} \tag{2.97}$$

where P is the mechanical pressure. The unphysical terms in equations 2.95 and 2.97 can be eliminated by setting $p=\frac{1}{2}$, implying $C=\frac{3}{2}$. This gives us the following values for the transport coefficients:

$$\nu = \frac{3}{16}\tau \tag{2.98}$$

$$\nu_b = \frac{3\tau}{2}\left(\frac{1}{4}+\frac{3}{\alpha+12}\right)-\frac{1}{4}\left(1+\frac{9}{\alpha+12}\right) \tag{2.99}$$

$$\eta = \frac{9}{16}\left(\tau-\frac{4}{9}\right) \tag{2.100}$$

$$\eta_b = -\frac{1}{8}(3\tau-2) \tag{2.101}$$

It can be seen that in equations 2.95 and 2.97, that there are unphysical appearances of ρ in the terms which involve the magnetic field. This limits the validity of the model to flows where $\rho\approx$ constant. This constraint is not an intrinsic feature of the model, but arises from the definitions of $\mathbf{B}$ and $\mathbf{\Lambda}$ by equations 2.47 and 2.49 respectively. A simple solution to this problem is discussed in chapter 5.1. As it stands, however, the method does have the simplifying advantage that the local Alfvén speed is equal to the magnitude of the magnetic field. Furthermore, we have neglected some higher order terms in the above equations which are similar to the the higher order terms in equation 2.40. Unsurprisingly, these restrict the validity of the model to low Mach number, high β regimes.

2.4.4 An improved streaming process in the MHD model

The expressions 2.98,.. 2.101, which we have derived for the transport coefficients, reveal a potential shortcoming of the particular model which we have discussed here and was also noted in [1]. We have already mentioned that $\tau>\frac{1}{2}$ is a necessary condition for numerical stability which implies

that $\nu > \frac{3}{32}$ and $\eta > \frac{1}{32}$. This is unfortunate as it means that high Reynolds number flows must be modelled on a large lattice therefore increasing the computational expense of a simulation. As we noted in section 2.3.3, this problem does not arise in the ordinary hydrodynamic model, since the condition for numerical stability is the same as the condition for positive viscosity.

The origin of the problem in the MHD model is entirely due to the bi-directional streaming rules 2.51, which give rise to the positive definite contributions to the transport coefficients via the terms on the right hand sides of equations 2.84 and 2.86. This was in fact suggested by Martinez et al [1] as a possible cause, although no solution was proposed. The solution is in fact very straightforward: simply set $p = 0$ thereby restoring the model to a single streaming one.

Although the argument presented in this chapter and in [1] might appear to suggest that by setting $p = 0$, we are abandoning the essential feature of the model which distinguishes it from the hydrodanmic LB method, there are a couple of points which should be borne in mind, which show that this is not the case. Firstly, although we now have a single streaming model, the particle states are still characterised by pairs of lattice vectors $\mathbf{e}_a, \mathbf{e}_b$. This is necessary to ensure that we have sufficient degrees of freedom to allow arbitrary macroscopic fields. Secondly, our ability to include the Lorentz force in the momentum equation and also model the induction equation depends on our ability to specify a distribution function which gives rise to the second order moments 2.65, 2.66, which again results from the fact that we have retained sufficient degrees of freedom at the microscopic level.

The updating rule for our MHD model is now given by 2.9, except that f and Ω each have two subscripts corresponding to the lattice vectors $\mathbf{e}_a, \mathbf{e}_b$. The subsequent derivation of the MHD equations is identical to section 2.4, but now that $p = 0$, the Chapman-Enskog procedure is simplified considerably, the positive definite contributions to ν and η no longer appear and we also have the added bonus of eliminating the unphysical terms which appeared in equation 2.88. All that remains for us to do is simply state the new form of the equilibrium distribution, and the transport coefficients:

$$f_0^{(\mathrm{eq})} = \rho\left[\frac{\alpha}{\alpha+12} - v^2\right] \tag{2.102}$$

$$\begin{aligned} f_{ab}^{(\mathrm{eq})} = \frac{\rho}{12}\Bigg[&\frac{12}{\alpha+12} + 2\left(\mathbf{v}_{ab}\cdot\mathbf{v} + \mathbf{B}_{ab}\cdot\mathbf{B} - 2\left[(\mathbf{e}_b\cdot\mathbf{v})^2 - (\mathbf{e}_b\cdot\mathbf{B})^2\right]\right. \\ &+2\left[(\mathbf{e}_a\cdot\mathbf{v})(\mathbf{e}_b\cdot\mathbf{v}) - (\mathbf{e}_a\cdot\mathbf{B})(\mathbf{e}_b\cdot\mathbf{B})\right] \\ &\left.+\frac{2}{\sqrt{3}}\left[(\mathbf{e}_a\cdot\mathbf{v})(\mathbf{e}_b\cdot\mathbf{B}) - (\mathbf{e}_a\cdot\mathbf{B})(\mathbf{e}_b\cdot\mathbf{v})\right] + v^2 - \frac{1}{2}B^2\right)\Bigg] \end{aligned} \tag{2.103}$$

$$\nu = \frac{1}{4}\left(\tau - \frac{1}{2}\right) \tag{2.104}$$

$$\nu_b = \left(\frac{1}{2} + c_s^2\right)\left(\tau - \frac{1}{2}\right) \tag{2.105}$$

$$\eta = \frac{3}{4}\left(\tau - \frac{1}{2}\right) \tag{2.106}$$

$$\eta_b = -\frac{1}{2}\left(\tau - \frac{1}{2}\right) \tag{2.107}$$

2.4.5 Numerical Stability

In order that a numerical scheme be capable of producing accurate approximations to the solutions of the equations in question, it is necessary to show that the scheme does not allow the growth of any errors which may creep into the calculations. Establishing necessary and sufficient conditions for the numerical scheme can be a formidable task, especially for a set of non-linear equations like the lattice Boltzmann equation. A von Neumann stability analysis can, however, provide a useful set of necessary conditions for local, linear stability. Sterling and Chen [40] performed such an analysis for various hydrodynamic lattice Boltzmann methods, and here we apply it to the MHD model.

Let $f^{(0)}$ be a particular solution of the lattice Boltzmann equation, so that

$$\frac{\partial f_a^{(0)}}{\partial t} + \mathbf{e}_a \cdot \nabla f_a^{(0)} = -\frac{1}{\tau}\left(f_a^{(0)} - F_a(f^{(0)})\right) \tag{2.108}$$

where the function F maps $f^{(0)}$ to the equilibrium distribution with the same conserved quantities. Suppose also that $f^{(0)} + f'$ is another solution of the lattice Boltzmann equation, where f' is small so that F can be linearised about the solution $f^{(0)}$. Then

$$\frac{\partial f_a^{(0)}}{\partial t} + \frac{\partial f'_a}{\partial t} + \mathbf{e}_a \cdot \nabla f_a^{(0)} + \mathbf{e}_a \cdot \nabla f'_a = -\frac{1}{\tau}\left(f_a^{(0)} + f'_a - F_a(f^{(0)}) - \sum_b \frac{\partial F_a}{\partial f_b}(f^{(0)}) f'_b\right) + O(f'^2) \tag{2.109}$$

Taking the difference of these two equations, and neglecting the higher order terms leaves us with

$$\frac{\partial f'_a}{\partial t} + \mathbf{e}_a \cdot \nabla f'_a = -\frac{1}{\tau}\left(f'_a - \sum_b \frac{\partial F_a}{\partial f_b}(f^{(0)}) f'_b\right) \tag{2.110}$$

The derivatives of f'_a can now be replaced by discrete approximations. The original lattice Boltzmann method used

$$\frac{\partial f_a}{\partial t}(\mathbf{x}, t) = \frac{f_a(\mathbf{x}, t + \Delta t) - f_a(\mathbf{x}, t)}{\Delta t} \tag{2.111}$$

$$\mathbf{e}_a \cdot \nabla f_a(\mathbf{x}, t) = \frac{f_a(\mathbf{x}, t) - f(\mathbf{x} - \Delta x \mathbf{e}_a, t)}{\Delta x} \tag{2.112}$$

with $\Delta t = \Delta x = 1$ We will also use a Lax-Wendroff scheme for the advection operator, so that

$$\begin{aligned} e_{ax}\frac{\partial f_a}{\partial x}(x, y, t) = {} & \frac{f_a(x + \Delta x, y, t) - f_a(x - \Delta x, y, t)}{2\Delta x} \\ & - \frac{\Delta t e_{ax}^2}{\Delta x^2}\left(f_a(x + \Delta x, y, t) - 2f_a(x, y, t) + f_a(x - \Delta x, y, t)\right) \end{aligned} \tag{2.113}$$

and similarly for $e_{ay}\frac{\partial f_a}{\partial y}(x, y, t)$.

A complete analysis of the stability of equation 2.110 is not possible, as it requires prior knowledge of $f^{(0)}$ - a solution which we are attempting to find. However, conditions for local stability can be found if we assume that $f^{(0)}$ is sufficiently slowly varying that we can regard the quantities $\frac{\partial F_a}{\partial f_b}(f^{(0)})$ as constants.

Before proceeding further, it is useful to note the following result. If $F : R^n \to R^n$ is a differentiable function, such that $F(\mathbf{x}) = F(F(\mathbf{x}))$ for any $\mathbf{x}$ (ie F is idempotent under composition of functions), then the eigenvalues of the derivative of F at $\mathbf{x}$ (ie the matrix $DF(\mathbf{x})$, whose components are the partial derivatives $\frac{\partial F_i}{\partial x_j}(\mathbf{x})$) are either 0 or 1. The proof is as follows.

By the definition of a derivative,

$$F(\mathbf{x}+\epsilon\mathbf{y}) = F(\mathbf{x}) + \epsilon DF(\mathbf{x})\mathbf{y} + O(\epsilon^2) \tag{2.114}$$

and so,

$$\begin{aligned} F\left(F(\mathbf{x}+\epsilon\mathbf{y})\right) &= F\left(F(\mathbf{x}) + \epsilon DF(\mathbf{x})\mathbf{y} + O(\epsilon^2)\right) \\ &= F\left(F(x)\right) + \epsilon DF(\mathbf{x})^2\mathbf{y} + O(\epsilon^2) \end{aligned} \tag{2.115}$$

Also, since F is idempotent,

$$\begin{aligned} F\left(F(\mathbf{x}+\epsilon\mathbf{y})\right) &= F(\mathbf{x}+\epsilon\mathbf{y}) \\ &= F(\mathbf{x}) + \epsilon DF(\mathbf{x})\mathbf{y} + O(\epsilon^2) \end{aligned} \tag{2.116}$$

Equating the above expressions for $F\left(F(\mathbf{x}+\epsilon\mathbf{y})\right)$ and letting $\epsilon \to 0$, we have $DF(\mathbf{x})^2\mathbf{y} = DF(\mathbf{x})\mathbf{y}$. In particular, if $\mathbf{y}$ is an eigenvector of $DF(\mathbf{x})$, with eigenvalue λ, then this implies that $\lambda^2\mathbf{y} = \lambda\mathbf{y}$. Therefore, since $\mathbf{y} \neq 0$, $\lambda^2 = \lambda$ so that $\lambda = 0$ or 1.

It is obvious from its construction that the function which maps a distribution to the corresponding equilibrium distribution with the same conserved quantities, is itself idempotent, and so the matrix of partial derivatives has eigenvalues 0 or 1. Furthermore, we can readily find the multiplicity of these eigenvalues. Let f' be an eigenvector of $\frac{\partial F_a}{\partial f_b}(f^{(0)})$ with eigenvalue 0, so that f' is in the null space of $\frac{\partial F_a}{\partial f_b}(f^{(0)})$. Then

$$\begin{aligned} F(f^{(0)} + \epsilon f') &= F(f^{(0)}) + \epsilon \frac{\partial F_a}{\partial f_b}(f^{(0)})f' + O(\epsilon^2) \\ &= F(f^{(0)}) + O(\epsilon^2) \end{aligned} \tag{2.117}$$

Using the conservation of mass, we have

$$\begin{aligned} \sum_a f_a^{(0)} + \epsilon f_a' &= \sum_a F_a(f^{(0)} + \epsilon f') \\ &= \sum_a F_a(f^{(0)}) + O(\epsilon^2) \\ &= \sum_a f_a^{(0)} + O(\epsilon^2) \end{aligned} \tag{2.118}$$

so that

$$\sum_a \epsilon f'_a = O(\epsilon^2) \tag{2.119}$$

and

$$\sum_a f'_a = 0 \tag{2.120}$$

on letting $\epsilon \to 0$.

Similarly, conservation of momentum and magnetic field implies

$$\begin{aligned} \sum_a f'_a \mathbf{e}_a &= 0 \\ \sum_a f'_a \mathbf{B}_a &= 0 \end{aligned} \tag{2.121}$$

(This also shows that the $O(\epsilon^2)$ term in 2.118 vanishes)

In general, f' is an element of a 13 dimensional space. Furthermore, the conservation laws imply that if f' is null vector of $\frac{\partial F_a}{\partial f_b}(f^{(0)})$ then it satisfies 5 independent linear equations, and so is a member of $13 - 5 = 8$ dimensional subspace. Thus, since the null space of $\frac{\partial F_a}{\partial f_b}(f^{(0)})$ is 8 dimensional, then eigenvalue 0 has a multiplicity of 8. Provided that $\frac{\partial F_a}{\partial f_b}(f^{(0)})$ is not defective, (ie it has 13 linearly independent eigenvectors), then the eigenvalue 1 has a multiplicity of 5. In general, if there are n components of the distribution function, and c independent, conserved quantities, then the eigenvalue 1 has a multiplicity of c and the eigenvalue 0 has a multiplicity of $n - c$.

We are now in a position to explore the conditions for linear stability. Firstly, we shall analyse the stability of solutions of the continuous lattice Boltzmann equation. Expanding f' in terms of a Fourier series, we get the following equation for the amplitude of a particular Fourier mode:

$$\frac{\mathrm{d}f'_a}{\mathrm{d}t} = -\frac{1}{\tau}\left[f'_a - \sum_b \frac{\partial F_a}{\partial f_b}(f^{(0)}) f'_b\right] - i\mathbf{k}\cdot\mathbf{e}_a f'_a \tag{2.122}$$

which we rewrite as a matrix equation

$$\frac{\mathrm{d}f'}{\mathrm{d}t} = Mf' \tag{2.123}$$

where

$$M_{ab} = -\frac{1}{\tau}\left[\delta_{ab} - \frac{\partial F_a}{\partial f_b}(f^{(0)})\right] - i\mathbf{k}\cdot\mathbf{e}_a\delta_{ab} \tag{2.124}$$

The solution of the above matrix equation is thus

$$f' = \exp(tM) f'_0 \tag{2.125}$$

where f'_0 is the initial value of f'. A necessary and sufficient condition for the stability of these solutions is that the real parts of all the eigenvalues of M should be negative or zero. In particular, if $\mathbf{k} = 0$ (ie. the perturbations are uniform), then it is easy to see that the eigenvalues of M are 0, with a multiplicity of 5, and $-\frac{1}{\tau}$ with a multiplicity of 8. The eigenvectors of M are the eigenvectors

of $\frac{\partial F_a}{\partial f_b}(f^{(0)})$. Thus, our first stability constraint is $-\frac{1}{\tau} \leq 0$, so $\tau > 0$. ($\tau = \infty$ is, in principle, also allowed.) This condition is already satisfied by the physical constraint that the viscosity be positive.

For $\mathbf{k} \neq 0, \tau = \infty$, the eigenvalues of M are $i\mathbf{k} \cdot \mathbf{e}_a$ are purely imaginary, and therefore automatically satisfy the stability requirements. If $\mathbf{k} \neq 0$ and τ is finite, it is not possible to find general expressions for the eigenvalues of M as it requires finding the roots of a 13^{th} order polynomial. Instead, we find the eigenvalues of M numerically. There are 8 independent parameters which determine the eigenvalues of M, namely $\alpha, v_x, v_y, B_x, B_y, k_x, k_y$ and τ, but since $\mathbf{k}$ can be rescaled with the substituition $\mathbf{k} = \frac{1}{\tau}\mathbf{k}'$, the stability constraint is independent of τ, so without loss of generality, we can set $\tau = 1$.

Experimentation suggests that the stability constraints on $\mathbf{v}$ and $\mathbf{B}$ are severest for the Fourier modes with small, but non-zero $\mathbf{k}$. This should be expected as high $\mathbf{k}$ modes are more stongly affected by viscosity and resistivity. (If $\mathbf{k} = 0$, then stability is guaranteed.) Figs 2.1- 2.16 show the boundary of stability on various 2D slices through the 7D parameter space. Fig 2.1 suggests that $\alpha \approx 0.62$ maximises the region in which $\mathbf{v}$ satisfies the stability requirements. On the other hand, the stability region for $\mathbf{B}$ is greatest for small α. However, when $\alpha = 0.62, \mathbf{v} = 0$, B is constrained to be less than about 0.5, which is by no means too severe, as we would expect the lattice Boltzmann model to be inaccurate for large $\mathbf{B}$ anyway.

In figs 2.5, 2.6 we can see that the stability of a particular Fourier mode is more or less independent of the component of $\mathbf{v}$ orthogonal to $\mathbf{k}$. Furthermore, since the stabililty constraint must be satisfied for all $\mathbf{k}$ regardless of direction, this implies that the overall stability does not depend on the direction of $\mathbf{v}$. Further experimentation suggests that the optimal value of α is about 0.6 and that v and B should be smaller than about 0.3.

These are conditions for stability of solutions of the continuous lattice Boltzmann equation. The improved stability of the large k Fourier modes may be ascribed to the greater effects of viscosity at small length scales. It is tempting to regard the instabilities at large v as being indicative of the growth of shocks in a supersonic fluid. However, note that the above analysis strictly holds for linear perturbations about a uniform flow, and uniform flows in real fluids do not form shocks, regardless of the Mach number. Therefore, these instabilities at large v and B are simply indicative of the inaccuracy of the lattice Boltzmann method in those regimes.

Further instabilities may arise due to the discretisation of the lattice Boltzmann equation. Since only explicit finite difference schemes are used in this thesis, we shall write the discretised lattice Boltzmann equation for the pertubations as

$$\frac{f_a^{n+1} - f_a^n}{\Delta t} + D_a f_a^n = -\frac{1}{\tau}\left(f_a^n - \sum_b \frac{\partial F_a}{\partial f_b}(f^{(0)}) f_b^n\right) \tag{2.126}$$

where D_a is the finite difference form of the differential operator $\mathbf{e}_a \cdot \nabla$. The equation for a particular

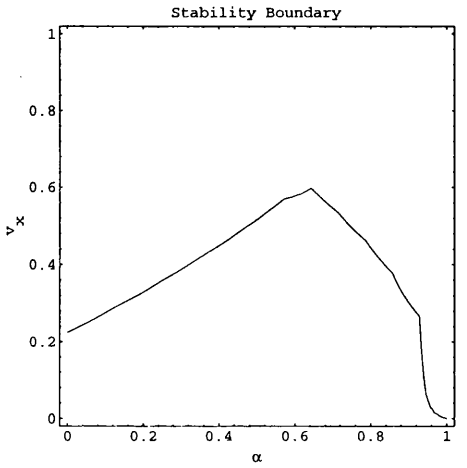

Figure 2.1: The stability boundary with $k_x = .01, k_y = v_y = B_x = B_y = 0$. The region of stability is below the line.

Fourier mode of f_a is then

$$\frac{f_a^{n+1} - f_a^n}{\Delta t} + D_a(\mathbf{k}) f_a^n = -\frac{1}{\tau}\left(f_a^n - \sum_b \frac{\partial F_a}{\partial f_b}(f^{(0)}) f_b^n\right) \tag{2.127}$$

Writing this in matrix form as

$$f^{n+1} = M f^n \tag{2.128}$$

where

$$M_{ab} = \left(1 - \frac{\Delta t}{\tau} - \Delta t D_a(\mathbf{k})\right)\delta_{ab} + \frac{\Delta t}{\tau}\frac{\partial F_a}{\partial f_b}(f^{(0)}) \tag{2.129}$$

then the solutions are

$$f^n = M^n f^0 \tag{2.130}$$

and the stability condition is that the magnitudes of the eigenvalues of M should all be less than or equal to 1. For the mode $\mathbf{k} = 0$, the eigenvalues of M are 1, with a multiplicity of 5 and $1 - \frac{\Delta t}{\tau}$ with a multiplicity of 8. This gives the stability condition that $0 \leq \Delta t \leq 2\tau$. In fact, it is better to have $0 \leq \Delta t \leq \tau$ so as to avoid oscillations in the finite difference solutions which are not exhibited in the continuous solutions.

The parameter space is now larger, since the finite differencing introduces the new parameters $\Delta t, \Delta x, \Delta y$. By rescaling $\Delta t = \tau \Delta t'$, we can arbitrarily set $\tau = 1$. Also, since the discretisation means that high wave number modes are not resolved, we can impose the restrictions $0 \leq k_x \Delta x \leq \pi$, $0 \leq k_y \Delta y \leq \pi$.

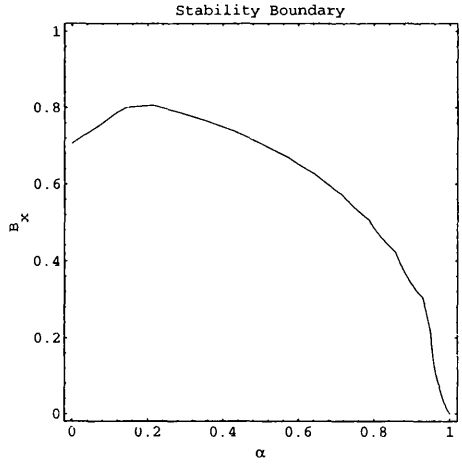

Figure 2.2: The stability boundary with $k_x = .01, k_y = v_x = v_y = B_y = 0$.

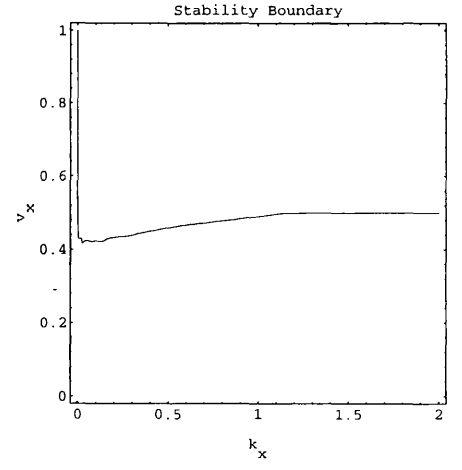

Figure 2.3: The stability boundary with $\alpha = 0.6, k_y = v_y = B_x = B_y = 0$.

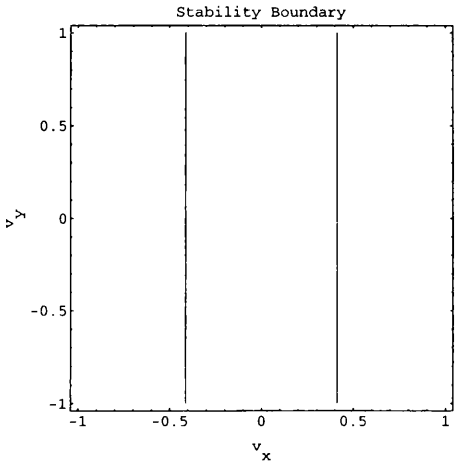

Figure 2.4: The stability boundary with $\alpha = 0.6, k_x = .01, k_y = B_x = B_y = 0$.

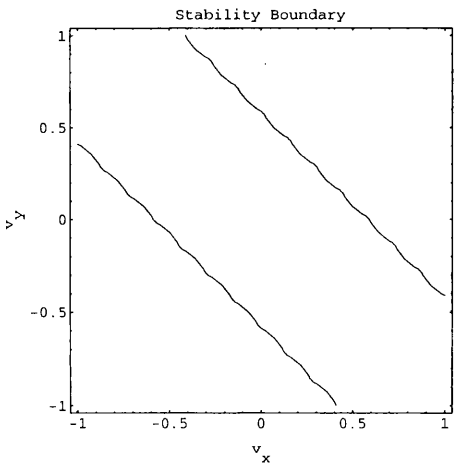

Figure 2.5: The stability boundary with $\alpha = 0.6, k_x = .01, k_y = .01, B_x = B_y = 0$.

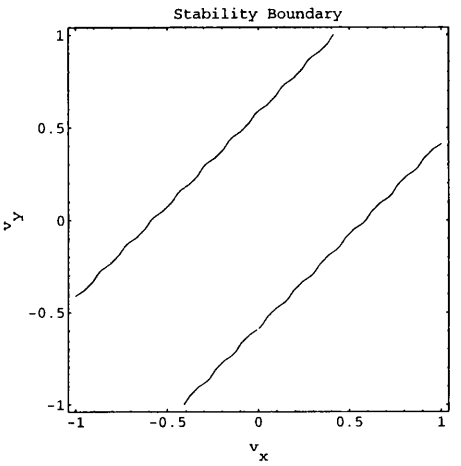

Figure 2.6: The stability boundary with $\alpha = 0.6, k_x = .01, k_y = -.01, B_x = B_y = 0$.

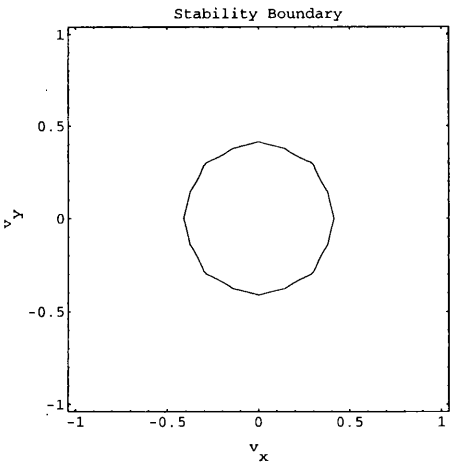

Figure 2.7: The stability boundary with $\alpha = 0.6, k_x^2 + k_y^2 = .001, B_x = B_y = 0$.

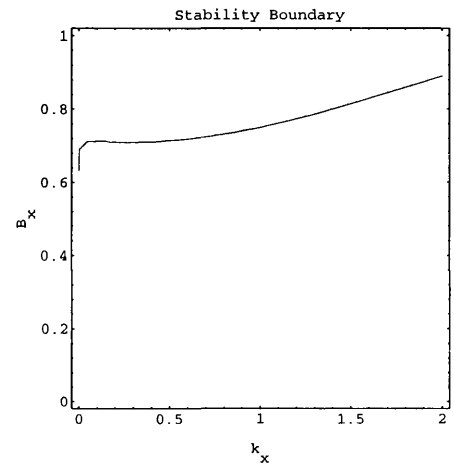

Figure 2.8: The stability boundary with $\alpha = 0.6, k_y = v_x = v_y = B_y = 0$.

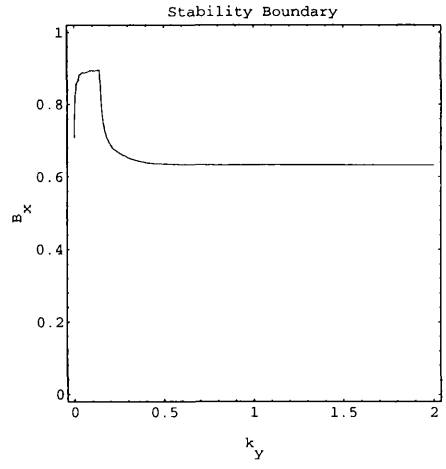

Figure 2.9: The stability boundary with $\alpha = 0.6, k_x = v_x = v_y = B_y = 0$.

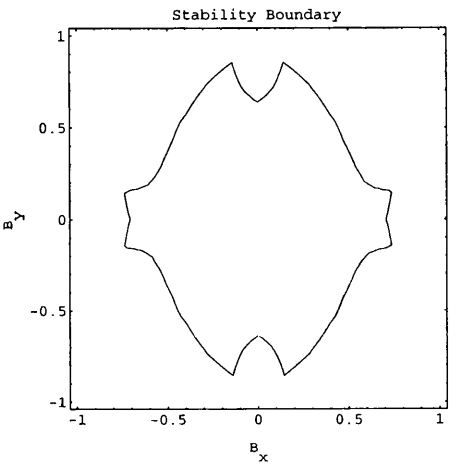

Figure 2.10: The stability boundary with $\alpha = 0.6, k_x = .01, k_y = v_x = v_y = 0$.

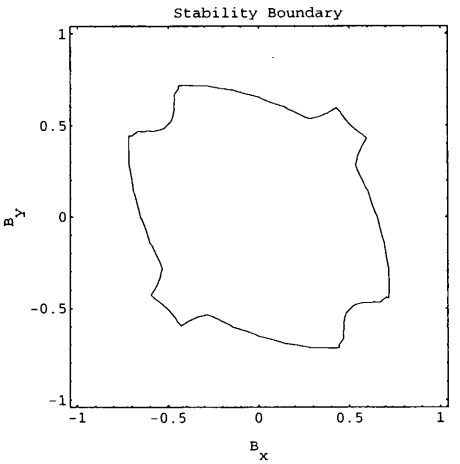

Figure 2.11: The stability boundary with $\alpha = 0.6, k_x = .01, k_y = .01, v_x = v_y = 0$.

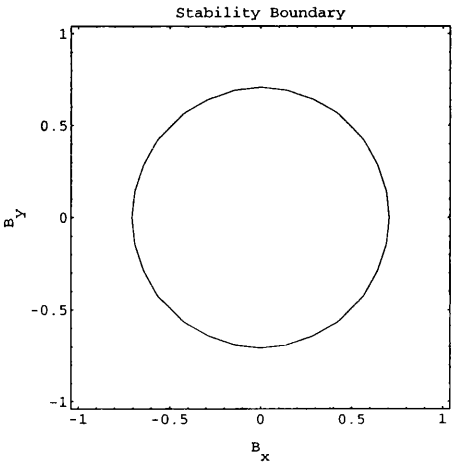

Figure 2.12: The stability boundary with $\alpha = 0.6, k_x^2 + k_y^2 = .001, v_x = v_y = 0$.

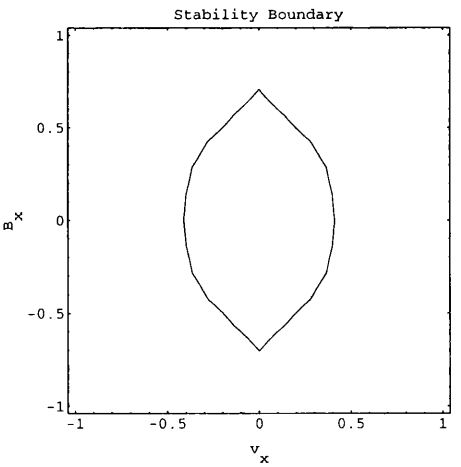

Figure 2.13: The stability boundary with $\alpha = 0.6, k_x = .01, k_y = v_y = B_y = 0$.

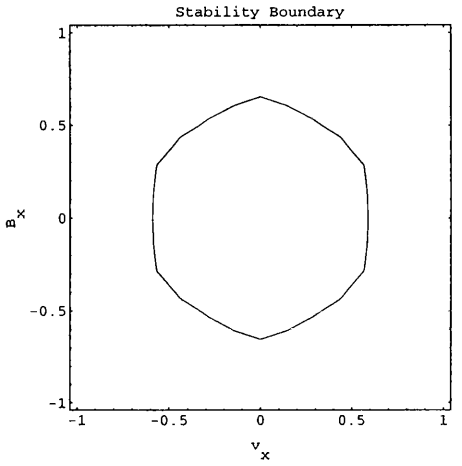

Figure 2.14: The stability boundary with $\alpha = 0.6, k_x^2 + k_y^2 = .001, v_y = B_y = 0$.

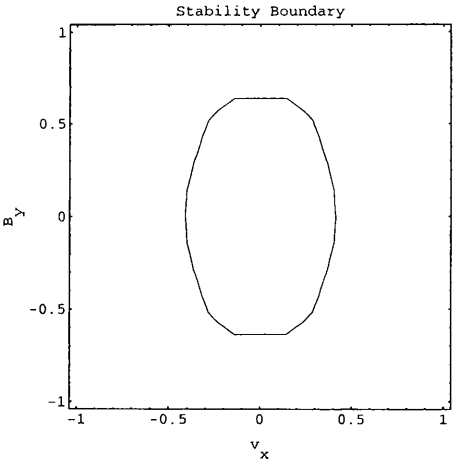

Figure 2.15: The stability boundary with $\alpha = 0.6, k_x = .01, k_y = v_y = B_x = 0$.

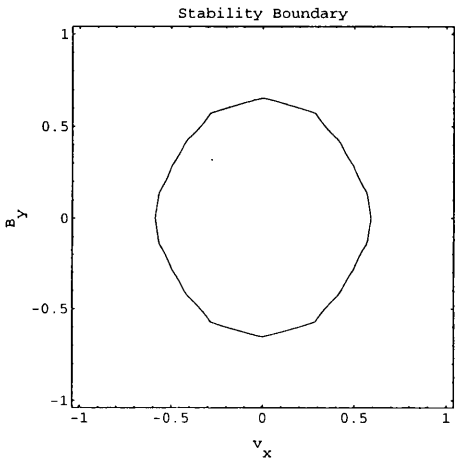

Figure 2.16: The stability boundary with $\alpha = 0.6, k_x^2 + k_y^2 = .001, v_y = B_x = 0$.

2.5 Other Discretisions of the Lattice Boltzmann Equation

We have already seen that a necessary condition for numerical stability of the lattice Boltzmann method is the $\tau > \frac{1}{2}$, and more detailed analysis indicates that the method should become unstable in certain flow regimes, especially when τ is close to $\frac{1}{2}$, and indeed various simulations have confirmed this [32, 41]. The stability could, in principle be improved by modifying the collision operator, (eg. stability is guaranteed if $\Omega = 0$). However, the simplicity of the collision operator is one of the appealing features of the lattice Boltzmann method, and a more fruitful approach has been discovered by Cao et al [41], which they applied to the hydrodynamic LB model, and here we shall apply their arguments to the MHD scheme.

We have already shown how the LB updating rule:

$$f_a(\mathbf{x}, t) = f_a(\mathbf{x} - \mathbf{e}_a, t-1) + \Omega_a(\mathbf{x} - \mathbf{e}_a, t-1) \tag{2.131}$$

approximates, to lowest order, to

$$\frac{\partial f_a}{\partial t} + \mathbf{e}_a \cdot \nabla f_a = \Omega_a \tag{2.132}$$

It has been noted [42, 41] that equation 2.131 is in fact an explicit, upwind, finite difference approximation to 2.132, with $||\mathbf{e}_a|| = \Delta t = \Delta x = 1$. Cao et al have developed this idea further, approaching the problem from a subtely different angle, by regarding equation 2.132 as describing the fundamental processes, and equation 2.131 as a particular means of solving equation 2.132.

From this point of view, the lattice Boltzmann technique becomes a far more general approach to solving fluid like equations, since we are no longer restricted to using equation 2.131 as our updating rule and any suitable approximation can be applied. Indeed, as described by Cao et al [41], and as we shall see, the points at which we calculate the values of f_a need not even correspond to the lattice points at which the particle collisions take place, but can be chosen to suit the geometry of the flow region.

With this change of emphasis, it may be more appropriate to regard the lattice Boltzmann method as an economical kinetic theory rather than the ensemble average of CA lattice gases. It should be borne in mind however, that we are still not solving the real kinetic equations, partly because of the small velocity space, and especially so in the MHD model due to the unusual representation of the magnetic field.

Returning to equation 2.132, we note that it is a set of linear, hyperbolic equations, coupled via the collision operator Ω. The stability of such equations is a standard problem in computational fluid dynamics and as was discussed in section 1.2 a common constraint on a wide class of explicit methods is the Courant-Friedrichs-Lewy (CFL) condition: $\frac{u\Delta t}{\Delta x} \leq 1$, where u is a characteristic speed of the system (eg a convection speed, a wave speed etc.) [5]. In equation 2.131, we have $u = ||\mathbf{e}_a|| = \Delta t = \Delta x = 1$, so that the CFL condition is only marginally satisfied, hence instabilities as $\tau \to \frac{1}{2}$ should be expected and have been observed by several authors [32]. Multi-speed lattice

Boltzmann methods, which model thermal flows [34], are even more severely constrained by stability considerations [43, 41] and are restricted to flows with a rather narrow range of temperature.

By adopting the approach of Cao et al, we can relax the restriction $\Delta t = \Delta x = 1$ and apply any standard technique to discretise the linear convection equation. In their paper, Cao et al use a central difference formula for $\mathbf{e}_a \cdot \nabla f$, on a rectangular grid:

$$\mathbf{e}_a \cdot \nabla f \approx e_x \frac{f_{j+1,k} - f_{j-1,k}}{2\,\Delta x} + e_y \frac{f_{j,k+1} - fj, k-1}{2\,\Delta y}$$

which lead to an unconditionally unstable method if employed along with a simple forward difference approximation for $\frac{\partial f}{\partial t}$ (ie. $\frac{f^{n+1}-f^n}{\Delta t}$), but can be stabilised by using a Runge-Kutta method to advance f forward in time.

2.5.1 A Lax-Wendroff discretisation of the lattice Botzmann equation

We shall firstly discuss this approach in relation to a simple 1D, lincar convection equation and then apply it to the lattice Boltzmann equation.

If we consider one of the simplest discretisations of

$$\frac{\partial f}{\partial t} + u\frac{\partial f}{\partial x} = 0 \tag{2.133}$$

namely the forward-time, centred-space approximation:

$$\frac{f_j^{n+1} - f_j^n}{\Delta t} + u\frac{f_{j+1}^n - f_{j-1}^n}{2\,\Delta x} = 0 \tag{2.134}$$

we note that it has two major drawbacks.

Most importantly, and fatally, it is unconditionally unstable. To see this, we apply a Fourier analysis to the equation obeyed by the errors in f, (which is equation 2.134, since it is linear), so that $\delta f_j^{n+1} \propto G e^{ij\theta}\delta f_j^n$. Then

$$\frac{G-1}{\Delta t} + u\frac{e^{i\theta} - e^{-i\theta}}{2\,\Delta x} = 0 \tag{2.135}$$

so

$$G = 1 - i\frac{u\Delta t}{\Delta x}\sin\theta \tag{2.136}$$

For stability, we require that δf remain bounded so that $|G| \leq 1$ for all θ, which clearly cannot be satisfied by 2.136.

An additional drawback is that while the centred-space approximation of $\frac{\partial f}{\partial x}$ is of order $O(\Delta x^2)$, the forward time approximation of $\frac{\partial f}{\partial t}$ is only of order $O(\Delta t)$, so that expanding 2.134 and keeping the lowest order truncation errors, we have:

$$\frac{\partial f}{\partial t} + \frac{1}{2}\Delta t\frac{\partial^2 f}{\partial t^2} + u\frac{\partial f}{\partial x} + \frac{1}{6}u\,\Delta x^2\frac{\partial^3 f}{\partial x^3} = 0 \tag{2.137}$$

The Lax-Wendroff FD approximation introduces additional terms to 2.134 in order to cancel the term of order $O(\Delta t)$ appearing in 2.137. Noting that if f satistifes 2.133, then it also satisfies

$$\frac{\partial^2 f}{\partial t^2} = u^2 \frac{\partial^2 f}{\partial x^2} \tag{2.138}$$

so that a second order scheme can be obtained by discretising the equation

$$\frac{\partial f}{\partial t} + u\frac{\partial f}{\partial x} - \frac{1}{2}\Delta t\, u^2 \frac{\partial^2 f}{\partial x^2} = 0 \tag{2.139}$$

Using the usual approximations for $\frac{\partial f}{\partial t}$, $\frac{\partial f}{\partial x}$ and $\frac{\partial^2 f}{\partial x^2}$ gives us the FD formula

$$\frac{f_j^{n+1} - f_j^n}{\Delta t} + u\frac{f_{j+1}^n - f_{j-1}^n}{2\,\Delta x} - \frac{1}{2}\Delta t\, u^2 \frac{f_{j+1}^n - 2f_j^n + f_{j-1}^n}{\Delta x^2} + O(\Delta t^2, \Delta x^2) = 0 \tag{2.140}$$

A Fourier stability analysis gives us the expression for the amplification factor G:

$$G = 1 + C^2(\cos\theta - 1) - iC\sin\theta \tag{2.141}$$

where $C = \frac{u\Delta t}{\Delta x}$ and $|G| \leq 1$, for all θ, if $|C| \leq 1$. The above approach is easily extended to more dimensions and in 2D, the stability constraint is $C_x^2 + C_y^2 \leq 1$, where $C_x = \frac{u_x \Delta t}{\Delta x}, C_y = \frac{u_y \Delta t}{\Delta y}$. If we discretise the lattice Boltzmann equation using this method, we get the following:

$$\begin{aligned}
&\frac{f_{ajk}^{n+1} - f_{ajk}^n}{\Delta t} + e_{ax}\frac{f_{aj+1k}^n - f_{aj-1k}^n}{2\,\Delta x} \\
&+e_{ay}\frac{f_{ajk+1}^n - f_{ajk-1}^n}{2\,\Delta y} - \frac{1}{2}\Delta t\, e_{ax}^2 \frac{f_{aj+1k}^n - 2f_{ajk}^n + f_{aj-1k}^n}{\Delta x^2} \\
&-\frac{1}{2}\Delta t\, e_{ay}^2 \frac{f_{ajk+1}^n - 2f_j^n ajk + f_{ajk-1}^n}{\Delta x^2} = -\frac{1}{\tau}\left(f_{ajk}^n - f_{ajk}^{(\mathrm{eq})^n}\right)
\end{aligned} \tag{2.142}$$

The trunctation error of this discretisation is

$$\frac{1}{2}\Delta t\left(e_{ax}e_{ay}\frac{\partial^2 f_a}{\partial x\,\partial y} - 2\,\mathbf{e}_a\cdot\nabla\Omega_a + \sum_b \frac{\partial \Omega_a}{\partial f_b}\Omega_b\right)$$

The final term in the truncation error can be simplified by applying the conservation laws. If we use the generic symbol C_k to represent the conserved quantities ρ,$\rho\mathbf{v}$ etc and c_{ak} the corresponding microscopic quantity, then by using the fact that the equilibrium distribution is a function of the conserved quantites we have

$$\begin{aligned}
\sum_b \frac{\partial \Omega_a}{\partial f_b}\Omega_b &= \sum_b \Omega_b \frac{\partial}{\partial f_b}\frac{f_a^{(\mathrm{eq})} - f_a}{\tau} \\
&= -\frac{1}{\tau}\Omega_a + \sum_b \Omega_b \sum_k \frac{\partial f_a^{(\mathrm{eq})}}{\partial C_k}\frac{\partial C_k}{\partial f_b}
\end{aligned} \tag{2.143}$$

Now

$$C_k = \sum_a f_a c_{ak} \tag{2.144}$$

so that

$$\frac{\partial C_k}{\partial f_b} = c_{bk} \tag{2.145}$$

On substitution into 2.143 we have

$$\begin{aligned} \sum_b \frac{\partial \Omega_a}{\partial f_b}\Omega_b &= -\frac{1}{\tau}\Omega_a + \sum_b \Omega_b \sum_k \frac{\partial f_a^{(\mathrm{eq})}}{\partial C_k} c_{bk} \\ &= -\frac{1}{\tau}\Omega_a \end{aligned} \tag{2.146}$$

after changing the order of summation and applying the conservation laws. This discretisation is of lower order than 2.140, but it does have better stability properties than the traditional lattice Boltzmann scheme and, as we shall see, proves to be quite an effective means for solving the lattice Boltzmann equation. The order $O(\Delta t)$ trunctation errors can be cancelled by introducing additional finite difference terms into the equation, but since they involve the $\frac{\partial^2}{\partial x\,\partial y}$ operator, this necessitates a larger neighbourhood for each grid point, and is therefore computationally more expensive.

Chapter 3

Simulations of Standard MHD Problems

Now that we have discussed in detail the lattice Boltzmann method for MHD we now turn our attention to the some standard problems which can be modelled by the method so that the results can be compared with the analytic solutions or with the results of established work.

3.1 Flow down a channel

3.1.1 Analytic solutions

Incompressible flow down a channel is one of the simplest problems in MHD and one of the few problems which can be solved exactly without the need of linear approximations, because the non-linear terms vanish. The particular examples which we shall examine here are Hartmann flow [44] and time dependent Poiseuille flow [45].

Hartmann flow

This is a standard problem in magnetohydrodynamics [44] and was originally used by Matrinez et al [1] to test the lattice Boltzmann MHD model. The fluid is forced by a uniform, constant total pressure gradient, down a channel with walls at $y = \pm L$, and a uniform magnetic field is applied perpendicular to the walls. Our boundary conditions are $\mathbf{v} = 0$ and $\mathbf{B} = (0, B_0)$ at $y = \pm L$. We shall look for steady state solutions of the form $\mathbf{v} = (v(y), 0)$ and $\mathbf{B} = (b(y), B_0)$.

With these considerations, the MHD equations reduce to

$$\nu \frac{\mathrm{d}^2 v}{\mathrm{d}y^2} + B_0 \frac{\mathrm{d}b}{\mathrm{d}y} + f = 0 \tag{3.1}$$

$$\eta \frac{\mathrm{d}^2 b}{\mathrm{d}y^2} + B_0 \frac{\mathrm{d}v}{\mathrm{d}y} = 0 \tag{3.2}$$

where the constant f is the pressure gradient and the units are chosen so that $\rho = 1$.

It is easy to show that the solution of this pair of equations, which satisfies our boundary conditions is:

$$v(y) = \frac{fL}{B_0}\sqrt{\frac{\eta}{\nu}}\coth(H)\left[1 - \frac{\cosh(Hy/L)}{\cosh(H)}\right] \tag{3.3}$$

$$b(y) = \frac{fL}{B_0}\left[\frac{\sinh(Hy/L)}{\sinh(H)} - \frac{y}{L}\right] \tag{3.4}$$

where the Hartmann number $H = B_0 L/\sqrt{\nu\eta}$.

Time dependent Poiseuille flow

The situation here is that of the previous section, except that we impose $\mathbf{B} = 0$ and we now look for time dependent solutions of the form $\mathbf{v} = (v(y,t), 0)$, with the initial condition $v(y,0) = 0$. The reason for switching off the magnetic field will be made clear later.

There is now only one equation to solve:

$$\frac{\partial v}{\partial t} - \nu \frac{\partial^2 v}{\partial y^2} = f \tag{3.5}$$

In order to find the general solution of equation 3.5 we firstly need a particular solution. It is easily shown that one such solution is

$$v(y,t) = \frac{fL^2}{2\nu}\left[1 - \left(\frac{y}{L}\right)^2\right] \tag{3.6}$$

which is expression 3.3 in the limit $B_0 \to 0$.

The next step is to find the general solution of the homogeneous equation

$$\frac{\partial v}{\partial t} - \nu \frac{\partial^2 v}{\partial y^2} = 0 \tag{3.7}$$

We can take a Fourier expansion of 3.7 to get the following ODE in the Fourier coefficients:

$$\frac{\mathrm{d}\overline{v}_n}{\mathrm{d}t} = -k_n^2 \nu \overline{v}_n \tag{3.8}$$

where $k_n = n\pi/2L$. The solution of the above equation is then

$$\overline{v}_n = V_n e^{-k_n^2 \nu t} \tag{3.9}$$

and so the general solution of 3.7 is

$$v(y,t) = \sum_{n=0}^{\infty} V_n e^{-k_n^2 \nu t} \begin{cases} \cos(k_n y) & \text{if } n \text{ is odd} \\ \sin(k_n y) & \text{if } n \text{ is even} \end{cases} \tag{3.10}$$

If a non-zero magnetic field were included, and a similar analysis performed to solve the equations, then it turns out that the eigenfunctions which satisfy the boundary conditions $v(\pm L, t) = b(\pm L, t) = 0$ are not orthogonal, thus greatly complicating the task of finding the relevant coefficients.

The general solution of 3.5 is the sum of the particular solution 3.6 and the general solution 3.10 of the homogeneous equation 3.7. To find the constants V_n, which satisfy the initial condition $v(y, 0) = 0$, we require the Fourier expansion of 3.6

$$\frac{f}{2\nu L^2}\left[1 - \left(\frac{y}{L}\right)^2\right] = \frac{f}{\nu L^2}\sum_{\text{odd}\, n} \frac{8(-1)^{\frac{n-1}{2}}\cos(k_n y)}{(n\pi)^3} \tag{3.11}$$

and it is easily checked that the solution of 3.5 with the required initial and boundary conditions is

$$v(y,t) = \frac{f}{2\nu L^2}\left[1 - \left(\frac{y}{L}\right)^2 - \sum_{\text{odd}\, n} \frac{8(-1)^{\frac{n-1}{2}} e^{-k_n^2 \nu t}\cos(k_n y)}{(n\pi)^3}\right] \tag{3.12}$$

3.1.2 Lattice-Boltzmann simulations

Simulations were carried out on a lattice, 60 cells wide, in the y-direction, and, since the problem is independent of x, 1 cell long, with periodic boundary conditions in the x-direction. The boundary conditions at $y = \pm L$ were achieved simply by setting the values of the distribution function to the appropriate equilibrium distribution.

To implement the pressure gradient, an additional procedure was included in the code, which redistributes the distribution function after the streaming step and before the collision step. This is equivalent to the inclusion of an additional term in equation 2.51:

$$f_{ab}(\mathbf{x}, t) = (1 - p)\left[f_{ab}(\mathbf{x} - \mathbf{e}_a, t - 1) + \ldots\right] + p[\ldots] + F \tag{3.13}$$

An appropriate form for F can be derived from the considerations that in one timestep $\Delta\rho = 0$, $\Delta(\rho\mathbf{v}) = (f, 0)$, $\Delta(\rho\mathbf{B}) = 0$ [1]:

$$F_{ab} = fC_{ab} \tag{3.14}$$

where

$$C_{11} = C_{12} = -C_{41} = -C_{42} = 1 \tag{3.15}$$

$$C_{51} = -C_{62} = \frac{3 - p}{2 - p} \tag{3.16}$$

$$C_{52} = -C_{61} = \frac{3 - 2p}{2 - p} \tag{3.17}$$

The values of f must be kept small, so that deviations from the equilibrium distribution do not become too large, thereby affecting the accuracy of the lattice-Boltzmann method. A value of 2×10^{-5} was used in our simulations. The Hartmann number H was varied by varying the strength of the magnetic field. The results of the simulations are shown in figures 3.1- 3.3. As with the tests of Martinez et al [1], the graphs show good agreement between the lattice Boltzmann results and the analytic solutions for both the steady state Hartmann flow problem and the time dependent Poiseuille flow.

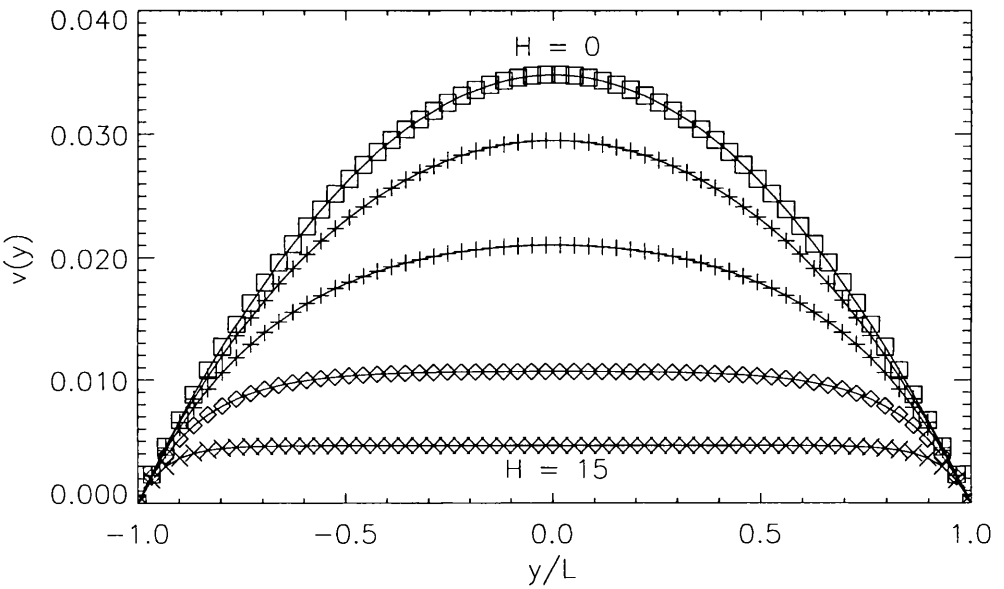

Figure 3.1: Velocity profile of Hartmann flow, for $H = 0, 1.5, 3, 6.5, 15$. The solid lines show the analytical results; the symbols show the results of the lattice Boltzmann simulations. The other parameters for these runs are: $L = \frac{59\sqrt{3}}{4}$, $f = 2 \times 10^{-5}$, $\tau = 1$ and the streaming parameter $p = \frac{1}{2}$.

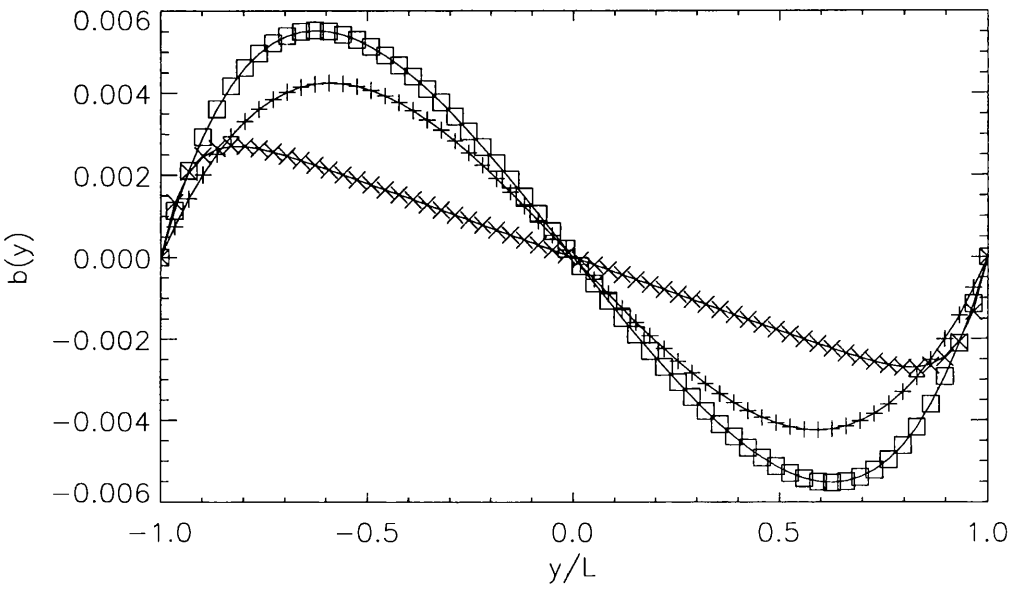

Figure 3.2: Magnetic field profile of Hartmann flow, for $H = 1.5$ (+ symbol), $H = 3$ (□ symbol) and $H = 15$ (× symbol). The solid lines show the analytical results; the symbols show the results of the lattice Boltzmann simulations. The other parameters for these runs are: $L = \frac{59\sqrt{3}}{4}, f = 2 \times 10^{-5}, \tau = 1$ and the streaming parameter $p = \frac{1}{2}$.

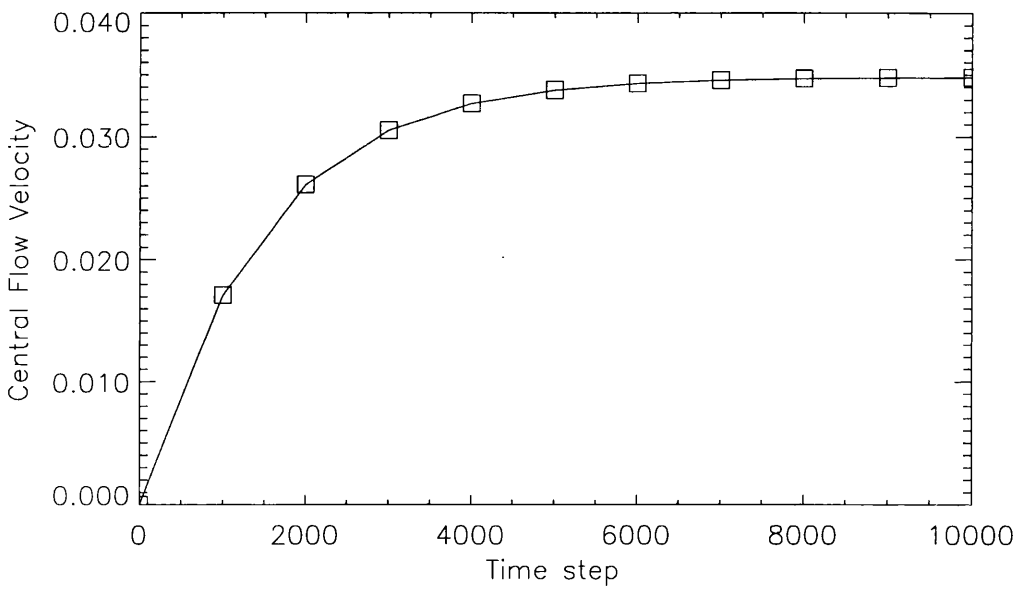

Figure 3.3: Evolution of Central flow velocity of time dependent Poiseuille Flow. The solid lines show the analytical results; the symbols show the results of the lattic Boltzmann simulations. This simulation corresponds to the situation in figure 3.1 with $H = 0$. The final velocity profile (as $t \to \infty$) is shown in figure 3.1.

3.2 Damped Alfvén waves

3.2.1 The linearized equations and the dispersion relation

As a result of the interaction with the electromagnetic field, plasmas can support a much richer variety of wave motion than neutral fluids. The simplest example is the shear Alfvén wave, which results from the magnetic tension and is analogous to a wave travelling along a taut wire.

We consider small perturbations of a homogeneous, incompressible plasma, which is at rest and permeated by a uniform magnetic field, $B_0\hat{\mathbf{x}}$. Writing the perturbed velocity and magnetic fields as $\mathbf{v}$, $\mathbf{b}$, and assuming any non-linear terms to be negligible, the MHD equations become

$$\frac{\partial \mathbf{v}}{\partial t} = -\nabla(p + B_0 b_x) + B_0 \frac{\partial \mathbf{b}}{\partial x} + \nu \nabla^2 \mathbf{v} \tag{3.18}$$

$$\frac{\partial \mathbf{b}}{\partial t} = B_0 \frac{\partial \mathbf{v}}{\partial x} + \eta \nabla^2 \mathbf{b} \tag{3.19}$$

Since the plasma is incompressible, $\nabla \cdot \mathbf{v} = 0$, on taking the divergence of equation 3.18, we obtain

$$\nabla^2(p' + B_0 b_x) = 0 \tag{3.20}$$

where p' is the pressure perturbation. Since p' and $\mathbf{b}$ must remain bounded over all space, it follows from harmonic function theory that $p' + B_0 b_x$ must be constant. So equation 3.18 becomes

$$\frac{\partial \mathbf{v}}{\partial t} = B_0 \frac{\partial \mathbf{b}}{\partial x} + \nu \nabla^2 \mathbf{v} \tag{3.21}$$

If we look for solutions of the form $e^{i(\mathbf{k}\cdot\mathbf{x} - \omega t)}$ then we get

$$-i\omega \mathbf{v} = iB_0 k_x \mathbf{b} - \nu k^2 \mathbf{v} \tag{3.22}$$

$$-i\omega \mathbf{b} = -\eta k^2 \mathbf{b} + iB_0 k_x \mathbf{v} \tag{3.23}$$

which can be rewritten as the following matrix equation

$$\begin{bmatrix} i\omega - \nu k^2 & iB_0 k_x \\ iB_0 k_x & i\omega - \eta k^2 \end{bmatrix} \begin{bmatrix} \mathbf{v} \\ \mathbf{b} \end{bmatrix} = 0 \tag{3.24}$$

In order that the solutions the solutions be non-trivial, the determinant of the 2×2 matrix must be zero, which gives us the following dispersion relation

$$\omega = \left\{ \pm \left[B_0 k_x - \frac{1}{4} k^4 (\nu - \eta)^2 \right]^{\frac{1}{2}} + i \frac{1}{2} k^2 (\nu + \eta) \right\} \tag{3.25}$$

and the relationship between the amplitudes of the velocity and magnetic perturbations:

$$\mathbf{b} = \frac{\omega + i\nu k^2}{k_x B_0} \mathbf{v} \tag{3.26}$$

3.2.2 Simulations

As for the simulations of flow down a channel, a lattice one cell long in the x-direction was used. Periodic boundary conditions were applied across the x and y boundaries and the initial conditions were chosen to specify a sinusoidal variation in the perturbed magnetic and velocity fields, so that

$$\mathbf{b}(x, y, 0) = (b_0 \cos(ky), 0) \tag{3.27}$$

$$\mathbf{u}(x, y, 0) = (u_0 \cos(ky - \phi), 0) \tag{3.28}$$

In order to satisfy the periodic boundary conditions, we must have $k = \frac{2n\pi}{L_y}$ for some integer n, where L_y is the size of the lattice in the y-direction. The unperturbed magnetic field is set to be $\mathbf{B}_0 = (B_0 \sin\theta, B_0 \cos\theta)$ where θ is the angle between the ambient field and the wave vector.

The results of two such simulations are shown in figures 3.4- 3.6. As with the simulations of 1D channel flow, the lattice Boltzmann results compare well with the analytic solutions. Figure 3.6 shows the fractional error, (defined as $\left(\int_0^{L_y}(\Delta v^2 + \Delta b^2)dy / \int_0^{L_y}(v^2 + b^2)dy\right)^{\frac{1}{2}}$, where Δv, Δb are the differences between the analytic and LB solutions and v and b are the analytic solutions) in the simulations. The larger fractional errors of figure 3.6 may be attributed to the fact that the waves in this simulation are more strongly damped, so that the wave amplitude becomes small very quickly. The errors are also observed to oscillate at twice the frequency of the Alfvén wave itself. The reason for this is that the LB model is valid only in the incompressible limit and does not strictly obey an incompressible equation of state. There is thus a non-linear coupling between the incompressible, transverse Alfvén wave and the compressible, longitudinal wave. The longitudinal mode is forced by the oscillations in the magnetic pressure, which, due to its quadratic dependence on the magnetic field, results in the observed frequency at twice the frequency of the linear wave.

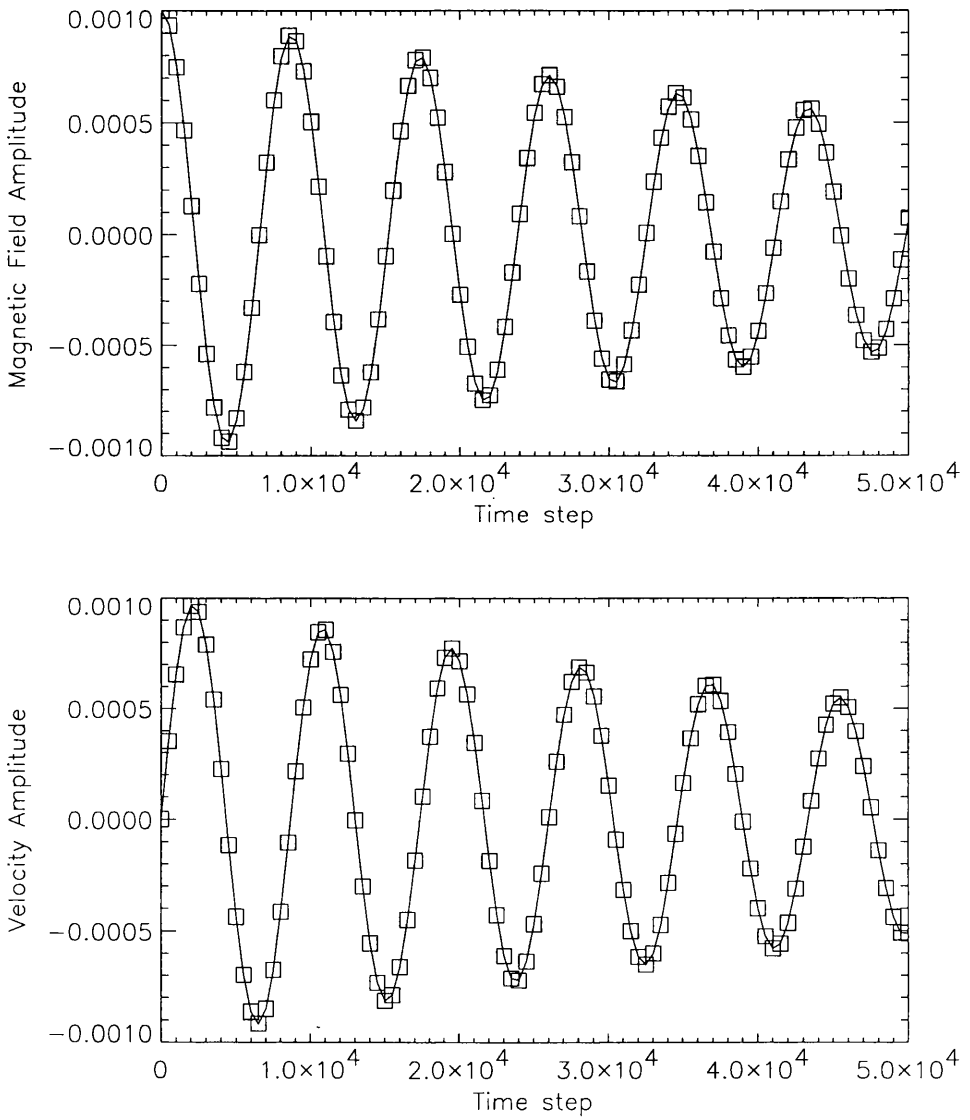

Figure 3.4: These graphs show the evolution of the perturbed fields of a standing Alfvén wave at a fixed point in space. $B_0 = 0.1$, $b_0 = 0.001$, $u_0 = 0$, $k = \pi/500\sqrt{3}$, $\tau = 1$. The analytic solution is indicated by the solid line, the lattice Boltzmann results by the symbols.

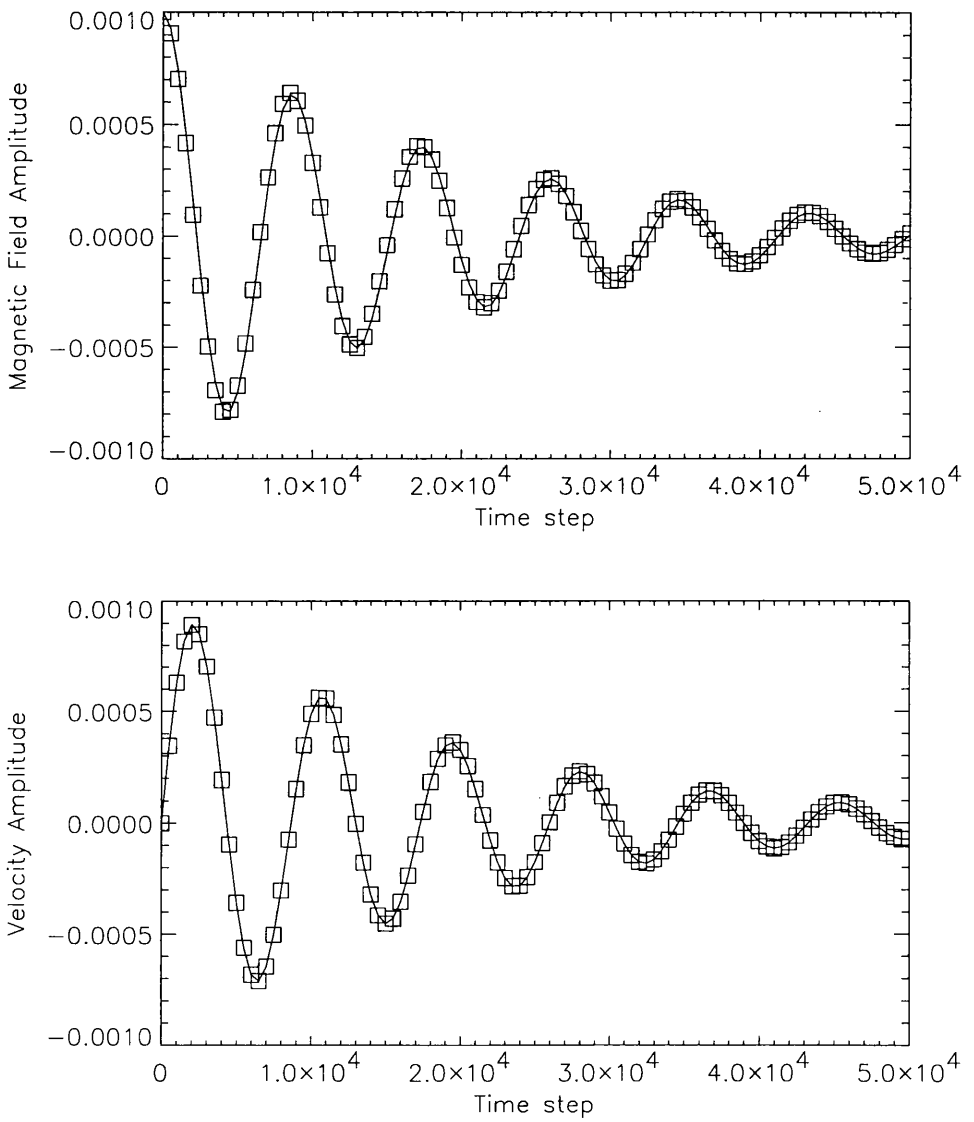

Figure 3.5: These graphs show the evolution of the perturbed fields of a standing Alfvén wave at a fixed point in space. $B_0 = 0.1$, $b_0 = 0.001$, $u_0 = 0$, $k = \pi/250\sqrt{3}$, $\tau = 1$. The analytic solution is indicated by the solid line, the lattice Boltzmann results by the symbols.

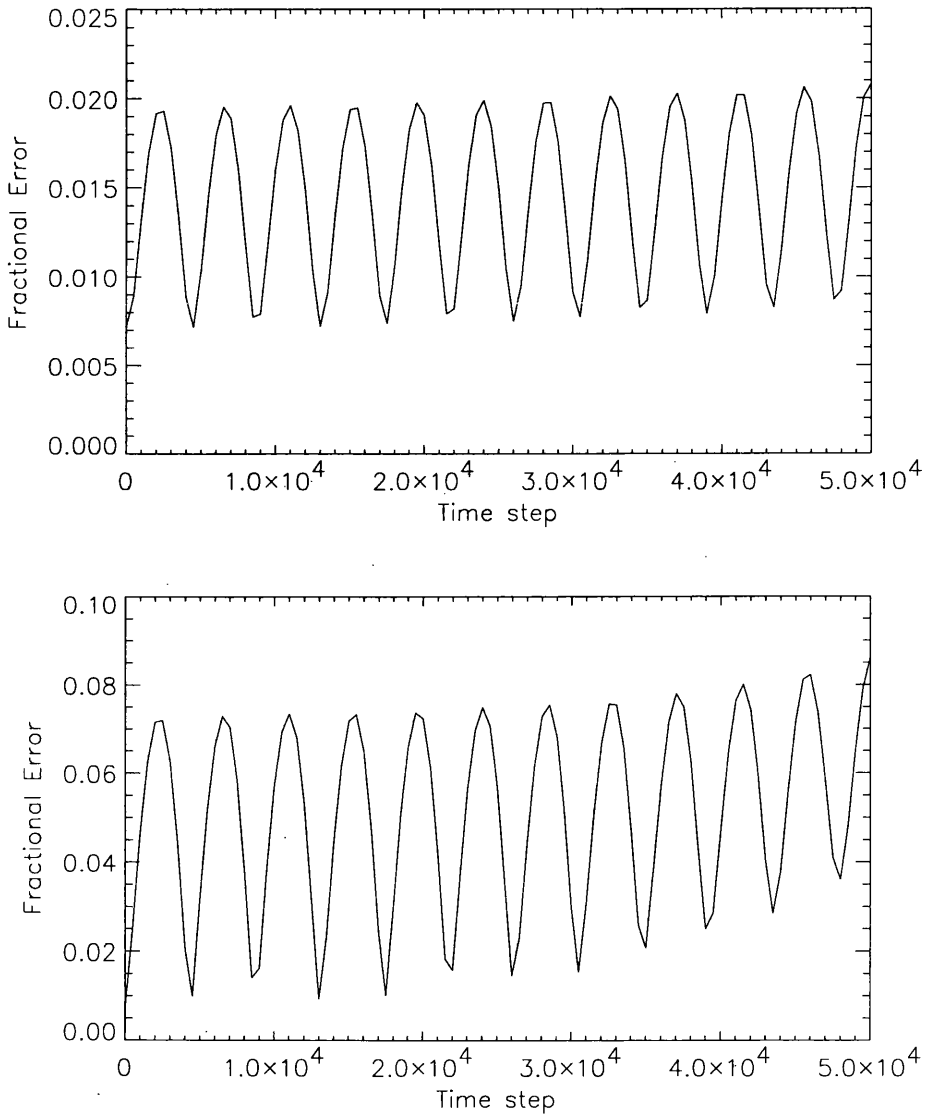

Figure 3.6: This graph shows the evolution of the fractional error between the lattice Boltzmann results and the analytic solution for each of the two Alfvén wave simulations. The error oscillates at twice the frequency of the Alfvén wave due to a non-linear coupling between the Alfvén wave and the longitudinal compression wave.

3.3 Coalescence of magnetic islands

An area of considerable interest in plasma physics is the process of magnetic reconnection. Plasmas in both laboratory and astrophysical situations are sometimes observed to persist in apparently stable states for relatively long periods of time until a considerable amount of energy is released in a sudden burst. In the solar atmosphere, for instance, this process is manifested as solar flares and coronal mass ejections. In a tokamak plasma, such disruptions can lead to a loss of confinement and thus are a major obstacle to the achievement of controlled fusion.

The basic mechanism behind such sudden discharges of energy is magnetic reconnection. Throughout most of the plasma, Ohmic dissipation is generally negligible, so that the magnetic field lines are frozen into the fluid. This has important implications, which are most easily understood in two dimensions, for then the frozen flux condition implies that the topology of the field lines cannot change. Thus, it is possible for the plasma to be found in a configuration in which it is unable to relax to a state of minimum energy because to do so would require a change in the field line topology. This can constrain the plasma to persist in a state of high magnetic energy. However, the frozen flux condition is, of course, an approximation, and in general there will be regions where Ohmic dissipation is significant. These regions appear as thin current sheets, which form when field lines of opposite sense are compressed together. Within these current sheets, the frozen flux condition no longer applies, and the field lines are able to break and reconnect with a different topology, thus enabling the sudden discharge of energy. In three dimensions, the process is not so readily understood in terms of field line topology, but the same basic process occurs, with the formation of thin current sheets enabling the energy discharge.

Here we apply the lattice Boltzmann method to an example of a reconnecting system, namely the coalescence of magnetic islands. The basic configuration consists of a magnetic field, uniform as $y \to \infty$, which reverses direction in a thin current sheet. There are two types of reconnection process which can occur in this system, tearing and coalescence [46]. Tearing produces topologically disconnected magnetic islands, which correspond to local enhancements in the current density. These magnetic islands experience a mutual attraction, much like the magnetic forces between current carrying wires, which pulls the islands together, forcing reconnection to take place and allowing the islands to coalesce. The tearing mode is a comparatively slow process, its linear time scale generally being at least two orders of magnitude greater than the Alfvén time scale. Coalescence is much faster. Its time scale is only one order of magnitude longer than the Alfvén time scale and is quite insensitive to the value of the resistivity, since the instability is driven by ideal processes [47]. Magnetic island coalescence is therefore a convenient problem with which to test the lattice Boltzman method in more complex situations.

The linear stability of island coalescence was studied analytically by Finn and Kaw [48], and numerical models of the reconnecting system have been conducted in the linear and non-linear regimes by Pritchett and Wu [47] and Biskamp and Welter [49]. It will be useful to use their results

for comparison with the lattice Boltzmann simulations. The system is described by the magnetic potential

$$\psi = B_\infty a \log\left(\cosh(y/a) + \varepsilon\cos(x/a)\right), \tag{3.29}$$

where the magnetic field is $\mathbf{B} = \left(\frac{\partial\psi}{\partial y}, -\frac{\partial\psi}{\partial x}\right)$. The Lorentz force is balanced by the pressure field

$$p = p_\infty - B_\infty^2 + \frac{B_\infty^2\cosh(y/a)}{\cosh(y/a) + \varepsilon\cos(x/a)}. \tag{3.30}$$

The configuration describes a current sheet of width a, in which there is a chain of magnetic islands, whose width w is give by $\cosh(w/2a) = 1 + 2\varepsilon$. Finn and Kaw [48] showed, via the energy principle that this equilibrium is linearly unstable for $\varepsilon > 0.12$. The later numerical work of Pritchett and Wu [47], showed that there is no threshold value of ε, below which the system is stable. The discrepancy with the results of Finn and Kaw was attributed to the trial function they used, which was insufficiently general and did not include the most unstable modes. Pritchett and Wu also modelled the non-linear evolution of the instability and observed the eventual coalescence of the islands when the resistivity was non-zero. The reconnecting process was studied in more detail by Biskamp and Welter [49]. They focussed their attention on the current sheet which forms between the islands during coalescence, and deduced various scaling laws for the upstream and downstream fields and the dimensions of the current sheet.

The perturbation was calculated in a similar manner to that employed by Pritchett and Wu: a traditional finite difference code was used to evolve the linearised set of MHD equations until the solution was swamped by the fastest growing mode. The solution was then multiplied by a small factor (typically $.01/\max v$) to give the initial perturbation. Pritchett and Wu found that with the distant boundary at $y = 5a$ and a magnetic Reynolds number ($S = B_\infty a/\eta$) of 200, the growth rate was $0.132\ B_\infty/a$. For the same conditions, our growth rate was $0.129\ B_\infty/a$, the small discrepancy presumably being due to differences in the details of the finite difference codes. The inclusion of a viscosity $\nu = \eta/3$, (which is necessary for the lattice Boltzmann simulations) marginally reduced the growth rate to $0.125\ B_\infty/a$.

The full simulations were carried out on a grid of 320×161 points, using the Lax-Wendroff FD discretisation of the lattice Boltzmann equation described in section 2.5.1. The evolution of the system with $S = 200$ is shown in figures 3.7, 3.8. As was observed by Pritchett and Wu, the islands accelerate towards each other and enter a reconnection phase which leads to eventual coalescence. The velocity field is seen to reverse direction after this stage, which is due to the island vibrating under the action of the magnetic tension, in an analogous manner to the vibrations of a soap bubble or drop of liquid.

Examination of the reconnection phase in detail reveals that the reconnection occurs within a thin, intense current sheet (figure 3.9). At sufficiently high S, this current sheet is itself prone to tearing instabilities [49, 50]. Figure 3.10 shows such an example at $S = 800$. A profile of the current density at $x = 2\pi$ shows that the current sheet is poorly resolved. Biskamp [46] remarks that such

poor numerical resolution is likely to result in the tearing instability being observed in a current sheet which should really be stable, so this particular simulation should not be taken too seriously.

A total of 5 simulations were performed at values of S between 200 and 400. Figures 3.11- 3.12 show the scaling laws obeyed in the current sheet, which are

$$\begin{aligned} B &\sim S^{0.27\pm0.03} \\ u &\sim S^{-0.5\pm0.1} \\ v &\sim S^{0.39\pm0.07} \\ \delta &\sim S^{-0.9\pm0.2} \end{aligned} \tag{3.31}$$

Where B is the upstream magnetic field, u the upstream velocity, v the downstream velocity and δ the current sheet thickness. For comparison, the scaling laws observed by Biskamp and Welter [49] were

$$\begin{aligned} B &\sim S^{\frac{1}{3}} \\ u &\sim S^{-\frac{1}{3}} \\ v &\sim S^{\frac{1}{3}} \\ \delta &\sim S^{-\frac{2}{3}} \end{aligned} \tag{3.32}$$

The width of the current sheet Δ was independent of S in both our simulations and those of Biskamp and Welter. Despite the large scatter in the data, the scaling laws calculated using the LB method are in fair agreement with Biskamp and Welter's results. In particular we have $u\Delta \sim v\delta$ as required by mass continuity and the downstream velocity is close to the upstream Alfvén speed as is predicted by considering current sheet dynamics [46, 51, 52]. The biggest discrepancy is in the scaling law for the current sheet thickness δ. This is likely to be due to the rather poor resolution of the current sheet, causing inaccuracies in the simulations. A non-uniform mesh, with a high concentration of grid points in the current sheet region could resolve this problem without making the computation particularly more expensive. It should also be noted that in Biskamp and Welter's simulations their was no viscosity, whereas here the viscosity is one third the resistivity, which is likely to cause further discrepancy.

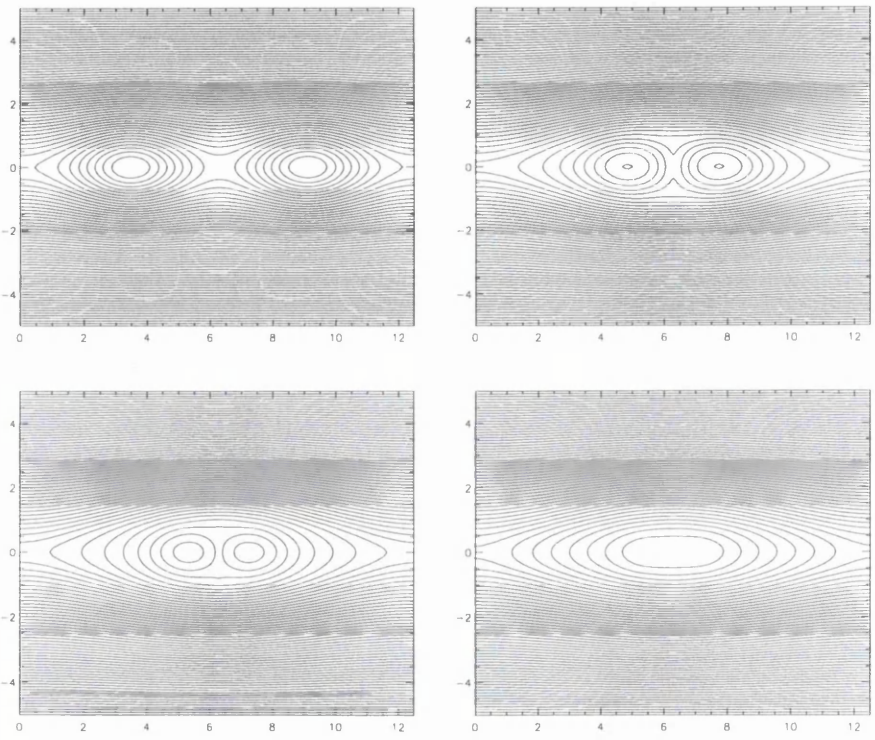

Figure 3.7: The evolution of the magnetic field lines during coalescence. The initial conditions (top left) are unstable to small perturbations, and the islands can be seen to move towards each other under their mutual attraction and eventually coalesce. $S = 200$, $\epsilon = 0.3$ in these simulations and the plots show the magnetic field lines at $t = 0, 84, 115, 146$ in units of $(kB_0)^{(-1)}$.

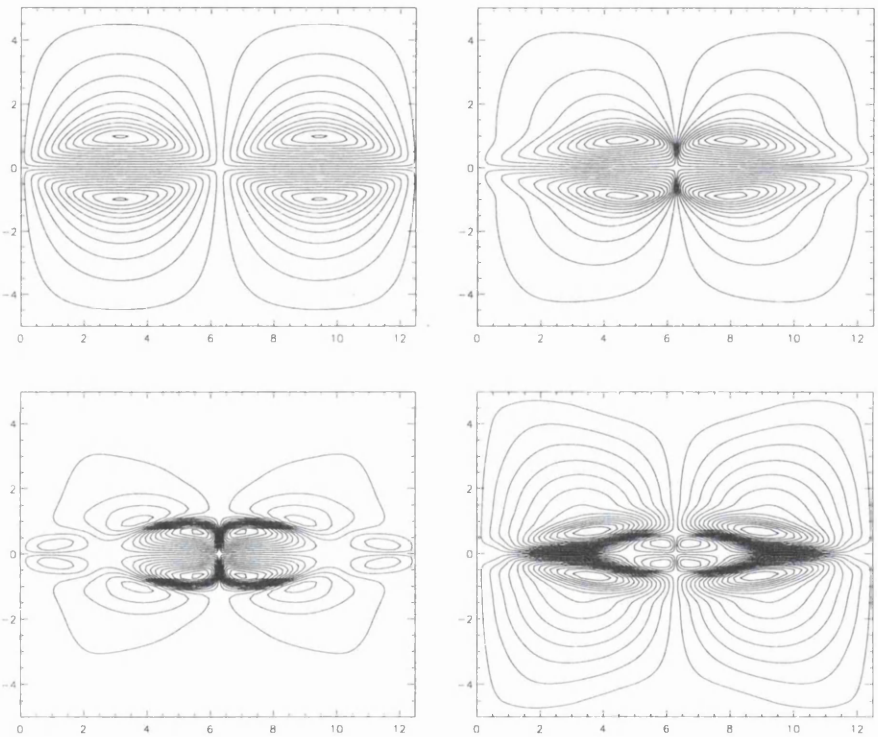

Figure 3.8: The stream lines corresponding to the magnetic field plots shown in figure 3.7. The flow can be observed to reverse after coalescence which is due to oscillations of the new island under the influence of magnetic tension.

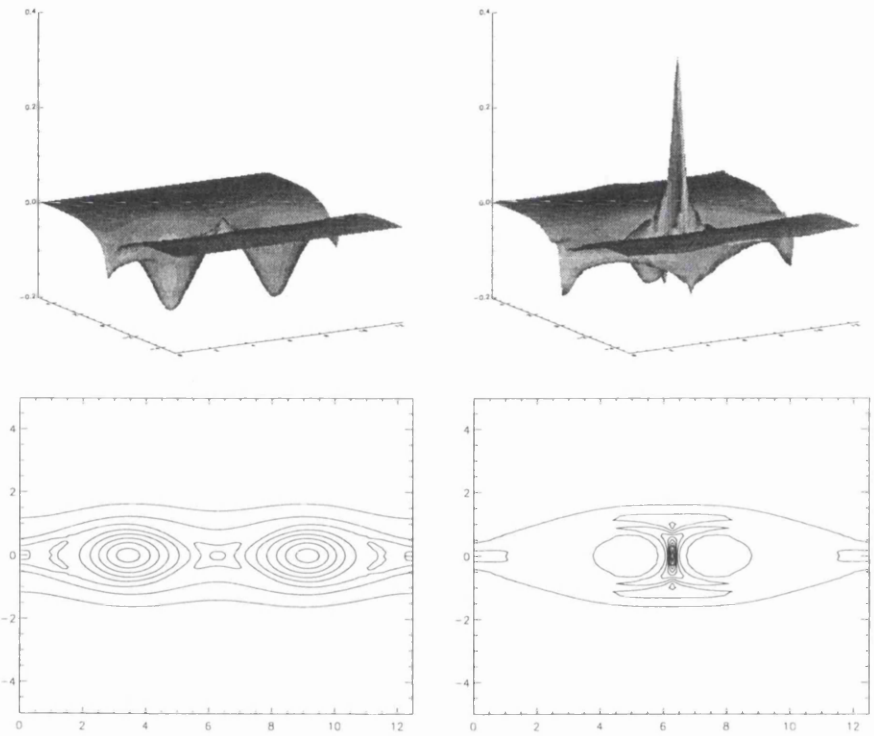

Figure 3.9: A thin, intense current sheet forms in the reconnecting region between the two islands. The plots on the left show the inital current density, on the right, the current density at the time of maximum field compression, (roughly $t = 84(kB_0)^{(-1)}$).

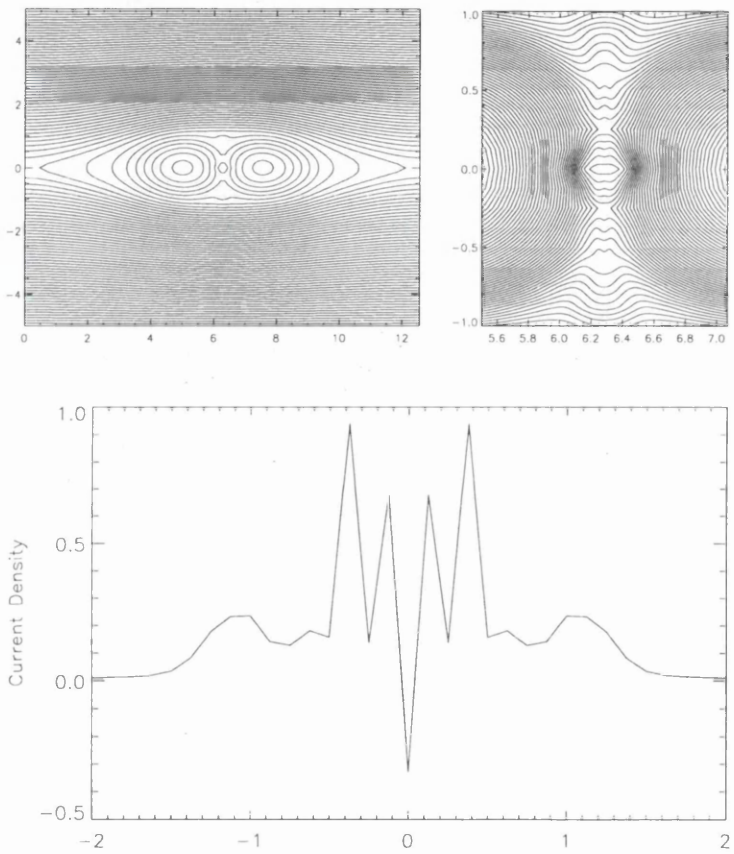

Figure 3.10: The current sheet can be observed to undergo tearing. $S = 800$ in this simulation. The profile of the current density along the current sheet indicates that this is really a non-linear numerical instability due to poor resolution rather than a physical effect. However, the instability does genuinely occur at sufficiently high $S > 10^4$ [46].

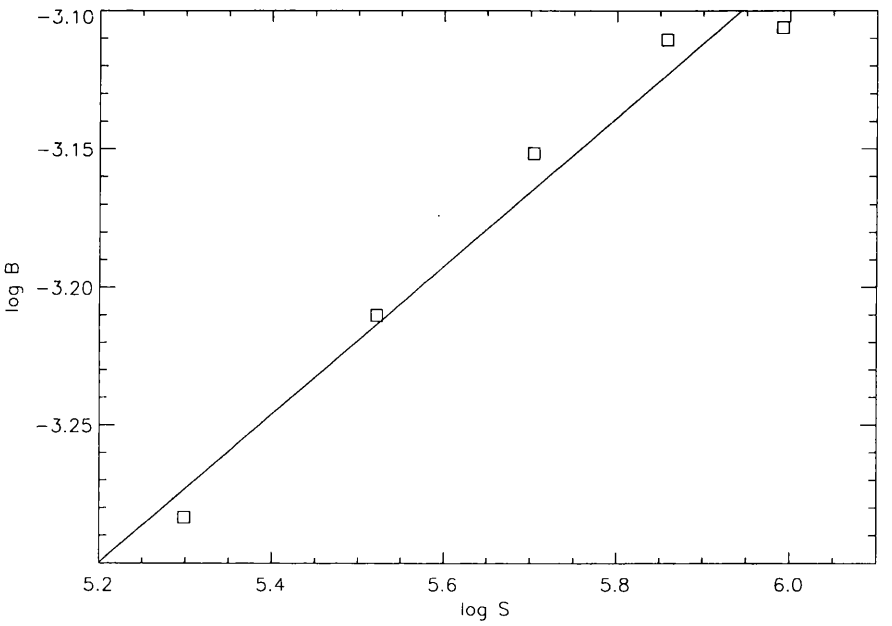

Figure 3.11: The scaling law obeyed by the upstream magnetic field near the current sheet. $B \sim S^{0.27\pm0.03}$.

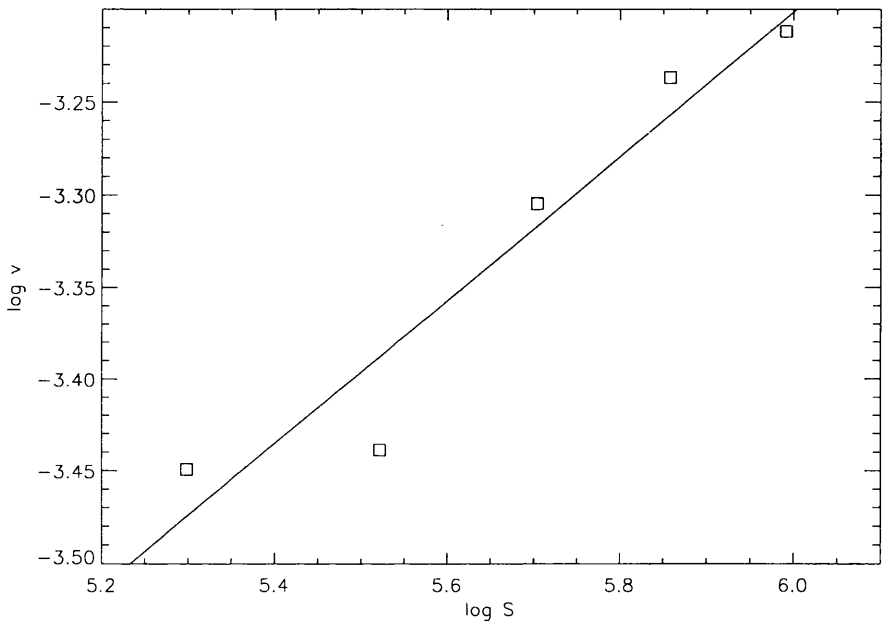

Figure 3.12: The scaling law obeyed by the downstream velocity near the current sheet. $v \sim S^{0.39 \pm 0.07}$.

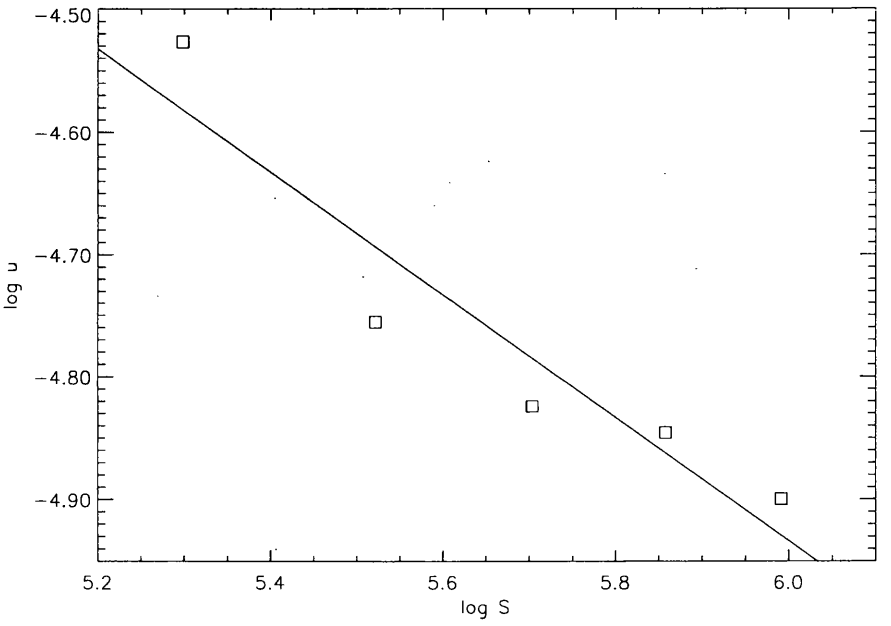

Figure 3.13: The scaling law obeyed by the upstream velocity near the current sheet. $u \sim S^{-.5\pm0.1}$.

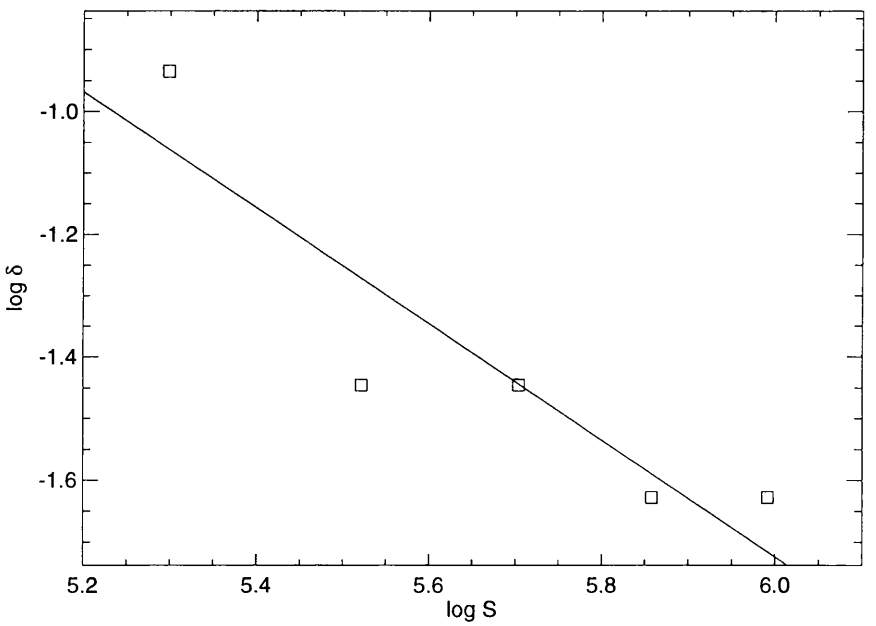

Figure 3.14: The scaling law obeyed by the current sheet thickness. $\delta \sim S^{-0.9\pm0.2}$.

Chapter 4

Vortex Shedding in Solar Active Regions

4.1 Flux Tube Geometry and Sunspot Motions

Now that we have shown that the lattice Boltzmann method is a valid technique for modelling MHD, we turn our attention to a problem of practical interest in solar physics, namely the effect of an erupting coronal loop on the photosphere.

A coronal loop (or flux tube) is an arc of plasma, which protrudes from the solar photosphere and is supported against its own weight by a magnetic field. The footpoints of the loop, where it intersects with the surface of the photosphere, appear in optical wavelengths as dark sunspots. As the loop erupts from the photosphere the sunspots move apart. The paths which they follow can be used to infer the loop geometry. This has been investigated by Leka et al [53]. If the loop is a simple arc, then the sunspots will diverge along a straight line; on the other hand, if there is a twist in the loop, the sunspots will follow a meandering path, as shown in figure 4.1.

This analysis, however, depends on the assumption that the sunspot motions are really due to the geometry of the tube and not a result of the loop being dragged along by bulk motions of the photosphere. A possible means of distinguishing these scenarios is to examine the vorticity in the ambient plasma. If we imagine that the sunspots are following a meandering path, then it should be clear from figure 4.2 that the vorticity in the ambient photospheric plasma should be different depending on what causes the sunspot motions.

If the sunspot motion is due to the geometry of the flux tube, then the plasma is being stirred by the tube and (if the Reynolds number is sufficiently high) a trail of vortices should be left in the wake of the motion. Alternatively, if the flux tube is being dragged along by the plasma, then the vortex shedding should occur ahead of the sunspot. An analysis of the vorticity in the region of a

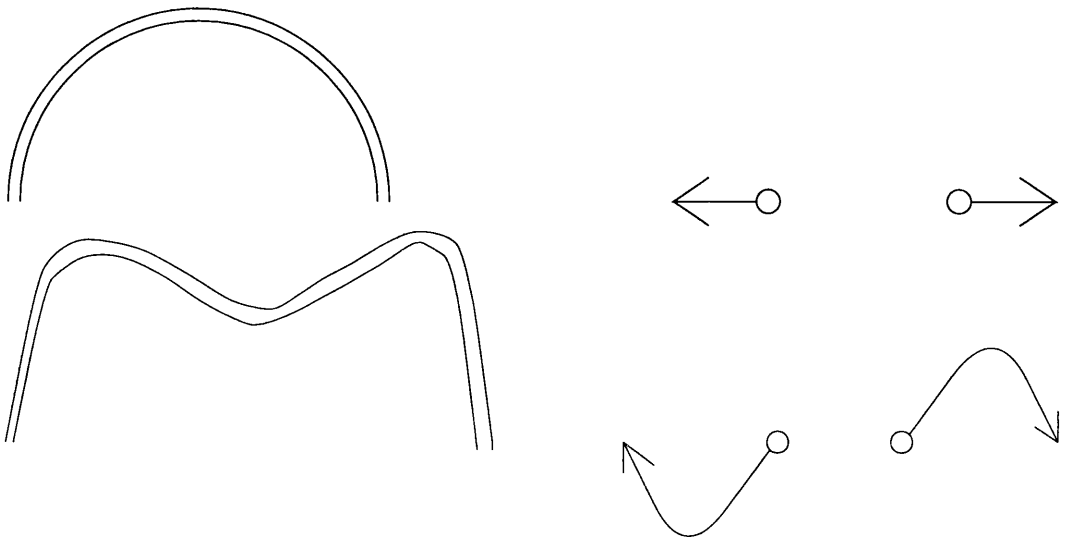

Figure 4.1: Sketch of flux tubes and their sunspots. The top figure shows a simple arc shaped flux tube. As the tube erupts from the photosphere, the footpoints move apart in a linear fashion. If the flux tube is twisted (bottom figure), the footpoints follow a meandering path.

pair of sunspots has been carried out by Strous [54].

4.2 Vortex Shedding by an Obstacle

The reasoning behind figure 4.2, however, assumes that the ambient plasma is behaving purely hydrodynamically, and it is natural to ask what effect a magnetic field would have. The crucial effect is the mechanism by which vorticity, which is generated by relative motion between the plasma and flux tube, is transported through the photosphere.

To simplify our simulations, we will crudely model the flux tube as if it were an impermeable cylinder, with a no-slip boundary condition and restrict ourselves to two dimensional flows. the hydrodynamical version of this problem has been extensively studied [55], and even modelled by a lattice Boltzmann method [56, 57, 58, 59, 60]. It can be shown that the problem can be parameterised by a single dimensionless quantity, the Reynolds number, which is a measure of the relative importance of the non-linear convective term in the momentum equation to the viscous term. Using a dimensional argument to derive this quantity, we can write $\nabla \approx (2a)^{-1}$, where a is the radius of the cylinder, so that

$$R_e = \frac{||\rho \mathbf{v}.\nabla \mathbf{v}||}{||\rho \nu \nabla^2 \mathbf{v}||} = \frac{(2a)^{-1}U^2}{\nu(2a)^{-2}U} = \frac{2aU}{\nu} \tag{4.1}$$

where U is the relative flow speed between the fluid and the cylinder.

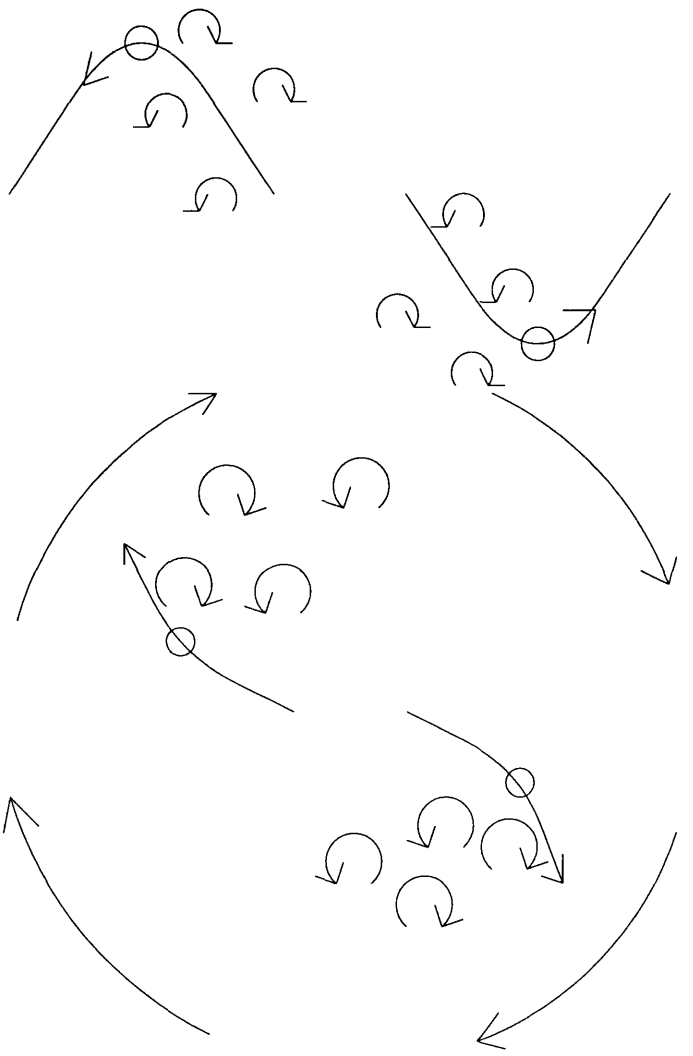

Figure 4.2: This figure is a sketch of the vortex shedding patterns in the wake of sunspots, in two different scenarios. In the top figure, the ambient motion of the photosphere is negligible and the vortex shedding occurs behind the sunspots. In the lower figure, there is a bulk clockwise rotation of the photosphere, causing the vortices to be shed in a different direction.

If we take the curl of the momentum equation in 2D so that

$$\frac{\partial \omega}{\partial t} = -\mathbf{v} \cdot \nabla \omega + \nu \nabla^2 \omega \tag{4.2}$$

then we can see that we have two mechanisms for transporting vorticity. The first term on the right hand side of equation 4.2 transports vorticity by convection - ie a vortex will move because the fluid as a whole is moving - and the second term allows vorticity to diffuse through fluid. It can easily be seen that dimenionsally, the ratio of these two terms is also equal to the Reynolds number.

For large R_e viscosity is negligible far away from the boundary, where spatial gradients are small and a particular solution of the inviscid equations is that of an irrotational steady state [55]. In such a case, where the fluid is also incompressible, the flow can be described by a complex potential [45], $w(z)$, where $z = x + iy$ and $v_x = \Re w'(z), v_y = -\Im w'(z)$. Noting that $w(z) = Uz$ is the potential for uniform flow, we can apply the Milne-Thomson Theorem [45] to generate a potential describing flow past a circular cylinder. This states that if a flow described by a potential $f(z)$, whose singularities all lie in the region $|z| > a$, then the potential $f(z) + \bar{f}(\frac{a^2}{z})$ describes a flow past a circular cylinder which has the same singularities as $f(z)$. Thus the potential we require is $U(z + \frac{a^2}{z})$ and the velocity field is

$$v_x = U\left(1 - \frac{a^2 \cos 2\theta}{r^2}\right) \tag{4.3}$$

$$v_y = -U\frac{a^2 \sin 2\theta}{r^2} \tag{4.4}$$

where

$$r\cos\theta = x \tag{4.5}$$

$$r\sin\theta = y \tag{4.6}$$

This velocity field is a good description of the flow far away from the cylinder, and is in fact a singular perturbation of the viscous Navier- Stokes equations. Notice that the no-slip boundary condition is not satisfied, so that the irrotational assumption is not valid at smaller distances. Very close to the boundary, the flow field will vary over much shorter length scales than a, so the viscous terms will become significant in this region.

For small $R_e \ll 1$, the viscous terms dominate, and the vorticity diffuses isotropically away from the boundary. In such a situation, the flow possesses fore and aft symmetry. As R_e increases towards unity, convection becomes more important and the fore and aft symmetry of the flow is broken. It is possible to find approximate solutions in this case [55].

For larger R_e, the non-linearity of the convection term, which now begins to dominate, prevents us from finding even approximate analytic solutions and either numerical simulations or direct experimentation are required [55]. For $10 \leq R_e \leq 60$, regions of circulating flow form in the immediate wake of the cylinder and for $R_e > 60$ these regions of circulation become unstable and

begin to shed vortices. When the Reynolds number exceeds approximately 1000, more instabilities set in and the wake becomes turbulent and three dimensional. Although the singular perturbation discussed above represents a solution at $R_e = \infty$, this flow does not occur as $R_e \to \infty$. The reason for this being that turbulence generated by the instabilities has very small length scales, so that as $\nu \to 0$, $\nabla^2 \mathbf{v} \to \infty$ in such a way that the viscous stresses in the wake cannot be neglected.

If we include a magnetic field, then Alfvén waves provide an additional means of transporting vorticity away from the boundary. To see this, recall the equations, derived in section 3.2.1, for small, linear perturbations about a homogenous, static equilibrium ($\rho = 1$)

$$\frac{\partial \mathbf{v}}{\partial t} = \mathbf{B}_0 \cdot \nabla \mathbf{b} \tag{4.7}$$

$$\frac{\partial \mathbf{b}}{\partial t} = \mathbf{B}_0 \cdot \nabla \mathbf{v} \tag{4.8}$$

Eliminating $\mathbf{b}$, we have

$$\frac{\partial^2 \mathbf{v}}{\partial t^2} = (\mathbf{B}_0 \cdot \nabla)^2 \mathbf{v} \tag{4.9}$$

taking the curl of which gives us

$$\frac{\partial^2 \omega}{\partial t^2} = (\mathbf{B}_0 \cdot \nabla)^2 \omega \tag{4.10}$$

Thus if the vorticity is localised in space, it will be propagated as a wave packet parallel (or anti-parallel) to the magnetic field at the Alfvén speed.

Additionally, if we have an Alfvén wave packet which consists purely of modes propagating in one direction, then it can be shown that the non-linear terms in the MHD equations cancel exactly, so the above statement will hold even for large velocity fields.

4.3 Model parameters

The observations on which we shall base our simulations are those of Strous et al. [61]. They obtained flow fields of an active region by tracking identifiable features in the photosphere and then smoothing their data to reduce noise, before calculating the (2 dimensional) divergence and vorticity fields.

In order to calculate an appropriate Reynolds number, we require the diameter of a sunspot, the flow speed and the viscosity. The diameter and flow speed are straight forward; typical values are $D \approx 5\text{Mm}$ and $U_0 \approx 0.35 - 1.0\text{km s}^{-1}$. However, great care must be taken over what value to use for the viscosity. The basic problem is that the observational data has a resolution of $\approx 0.2\text{Mm}$ and, after smoothing, only the features with a scale of $\approx 7.6\text{Mm}$ are left behind. The observations are thus incapable of resolving the small scale features of the flow (which can be of the order of a few cm). However, the unresolved features cannot simply be ignored because, due to the nonlinearity of the equations, they play a significant role in the transport of large scale momentum and vorticity.

If our simulations are to make any sense, then we require some means of parameterising the unresolved turbulence [62, 63]. Turbulence has long been one of the most intractable problems in

basic physics and any ad hoc model can, at best, only give order-of-magnitude estimates. Bearing this in mind, we shall adopt an eddy viscosity parameterisation. This approach draws an analogy between the small scale eddies and the molecules of a gas and postulates that the smallest eddies transport the momentum of the large scale flow in a similar manner to molecular viscosity.

To make this more concrete, suppose that a flow field can be expressed as $\mathbf{u} = \mathbf{U} + \tilde{\mathbf{u}}$ where $\mathbf{U} =< \mathbf{u} >$ is some sort of average flow, (either an ensemble or a temporal average) and $\tilde{\mathbf{u}}$ is the small scale turbulence, such that $< \tilde{\mathbf{u}} >= 0$. Then we can write the (incompressible) momentum equation as follows:

$$\rho\left[\frac{\partial}{\partial t}(\mathbf{U}+\tilde{\mathbf{u}}) + \nabla\cdot((\mathbf{U}+\tilde{\mathbf{u}})(\mathbf{U}+\tilde{\mathbf{u}}))\right] = -\nabla(P+\tilde{p}) + \nabla\cdot\mu\nabla(\mathbf{U}+\tilde{\mathbf{u}}) \tag{4.11}$$

which, upon expanding the non-linear terms and averaging becomes

$$\rho\left[\frac{\partial \mathbf{U}}{\partial t} + \mathbf{U}\cdot\nabla\mathbf{U}\right] = -\nabla P + \nabla\cdot\mu\nabla\mathbf{U} - \rho\nabla\cdot < \tilde{\mathbf{u}}\tilde{\mathbf{u}} > \tag{4.12}$$

The crucial term here is $\nabla\cdot < \tilde{\mathbf{u}}\tilde{\mathbf{u}} >$ which gives rise to the turbulent transport of momentum. The parameterisation of this term in terms of the mean flow field is an important aspect of modelling turbulence. In the eddy viscosity parameterisation, it is postulated that

$$< \tilde{\mathbf{u}}\tilde{\mathbf{u}} >= -\nu_T\left(\nabla\mathbf{U} + (\nabla\mathbf{U})^T\right) \tag{4.13}$$

where ν_T is the kinematic eddy viscosity. Generally ν_T is an anisotropic tensor quantity which is dependant on the flow field. Various schemes exist for calculating ν_T (eg the $k-\epsilon$ model [62]) but for simplicity, we shall take ν_T to be constant in our simulations. We can justify this assumption on the grounds that the photospheric plasma is already turbulent due to convective motions deep within the sun, and therefore variations in the eddy viscosity will be much less significant than in a situation in which the photospheric flow is laminar and all the turbulence is generated by the motion of the erupting flux tube.

Although the eddy viscosity parameterisation is inevitably a gross simplification, it does have the most important desirable feature that we would expect of a model of turbulence, namely that the large scale eddies dissipate their energy by exciting smaller scale eddies. These small scale eddies excite yet smaller scale eddies and this energy cascade continues until the eddies are so small that the effects of molecular viscosity cannot be neglected and the viscous dissipation of kinetic energy into heat imposes a lower bound on the size of the eddies. It is almost as if the fluid is searching for the fastest available mechanism for dissipating its kinetic energy; ultimately viscous heating is the only means by which the kinetic energy can be dissipated (in a neutral fluid), but if this is not fast because the length scales are too large, then the fluid generates smaller length scales by exciting smaller eddies.

We can treat the small scale structure of the magnetic field in a similar manner to derive the

following equations:

$$\rho\left(\frac{\partial \mathbf{U}}{\partial t}+\mathbf{U}\cdot\nabla\mathbf{U}\right)=-\nabla\left(p+\frac{1}{2}B^2+\frac{1}{2}<\tilde{\mathbf{b}}^2>\right)+\mathbf{B}\cdot\nabla\mathbf{B}$$
$$+\rho\nu\nabla^2\mathbf{U}-\rho\nabla\cdot<\tilde{\mathbf{u}}\tilde{\mathbf{u}}>+<\tilde{\mathbf{b}}\cdot\nabla\tilde{\mathbf{b}}> \quad (4.14)$$

$$\frac{\partial \mathbf{B}}{\partial t} = \nabla\times(\mathbf{U}\times\mathbf{B})+\nabla\times\left\langle\tilde{\mathbf{u}}\times\tilde{\mathbf{b}}\right\rangle+\eta\nabla^2\mathbf{B} \quad (4.15)$$

For the sake of simplicity, we shall simply parameterise the contributions of $<\tilde{\mathbf{b}}\tilde{\mathbf{b}}>$ to the momentum equation by an eddy viscosity and parameterise the turbulent contributions to the induction equation by an eddy resistivity in a manner analogous to the eddy viscosity parameterisation. Substituting these parameterisations into equations 4.14 and 4.15 recovers the original MHD equations with ν and η replaced by ν_T and η_T. This parameterisation is particularly convenient because the mean field variables obey the same equations as the total fields, but with larger transport coefficients. This allows us to forget about the small scale structure of the flow and so we can use the same numerical techniques which work at low Reynolds numbers.

4.4 Simulations on a uniform grid

In the following simulations, the size of the lattice is 350 by 350 cells. In order to see the vortices forming in the wake of the flow, this restricts the diameter of the cylinder to about 150 cells, which with a maximum velocity of about 0.15 and a minimum viscosity of 0.1875 (when the streaming parameter $p=\frac{1}{2}$ and relaxation time $\tau=\frac{1}{2}$), gives us a maximum Reynolds number of 240. This value of R_e is within the region where vortex shedding can take place, and is therefore of relevance to the situation discussed above.

It was remarked in section 2.4.4 that setting $p=0$ is a better choice as it would allow small transport coefficients as $\tau\rightarrow\frac{1}{2}$. However, in the traditional lattice Boltzmann method, this creates severe nonlinear instability problems which can be dealt with by using different discretisations of the lattice Boltzmann equation. This will be explored later.

The initial conditions away from the boundary are specified by the complex potential $w(z)=U(z+\frac{a^2}{z})$, so that the velocity field is specified by equation 4.3. With this velocity field, the vorticity is initially zero everywhere expect at the boundary where it is singular. However, on the lattice, spatial structures smaller than one lattice spacing cannot be resolved, effectively rendering the vorticity field finite and the boundary layer to be one cell thick.

Typical results are shown in figures 4.3- 4.8. For Reynolds numbers of the order of 100, and without any magnetic field, the flow evolves according to our expectations, so that as the vorticity is carried away from the boundary, regions of circulation form in the wake of the cylinder.

As we increase the strength of the magnetic field, we can see that it has the effect of decreasing the vorticity in the wake of the cylinder, and in fact, the regions of circulation have been suppressed

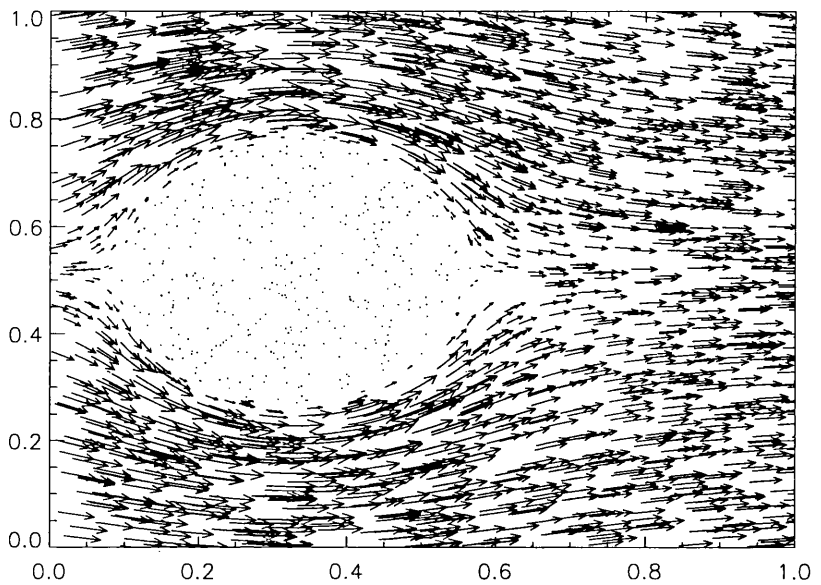

Figure 4.3: The initial velocity field in the simulations of flow past a flux tube

altogether when B_0 is comparable to U. It can also be seen that there is a substantial increase in the vorticity close to the upstream boundary, for a perpendicular field. This can be attributed to the bending of the field lines as they wrap around the cylinder.

When the ambient field is aligned parallel to the flow, similar results are obtained with regard to the suppression of vortices but no region of increased vorticity is observed immediately upstream of the cylinder, since the field lines are not wrapped around the cylinder as they are carried along by the flow.

4.5 Simulations on a non-uniform grid

The simulations of section 4.4 were performed using the original lattice Boltzmann method, ie. on a a uniform hexagonal grid. It was mentioned in section 2.5 and originally observed by Cao et al [41] and by He et al [64] and He and Doolen [60, 59] that this approach has a number of limitations; namely the CFL condition is only marginally satisfied, making the method prone to numerical instabilities as the Reynolds number increases; the uniform hexagonal grid does not take advantage

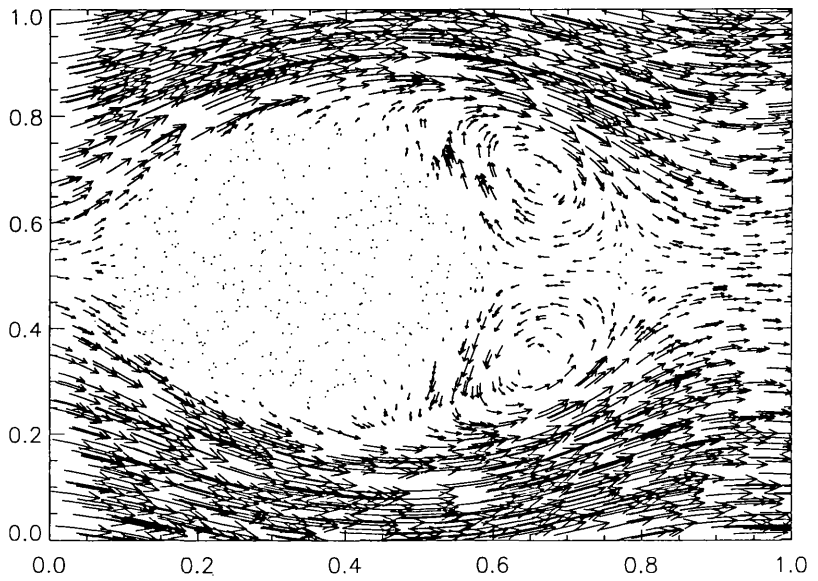

Figure 4.4: Vortex formation in the wake of a flux tube, $R_e = 120$. After 1000 time steps ($\approx \frac{2a}{U}$) regions of circulation have clearly formed in the immediate wake of the flux tube

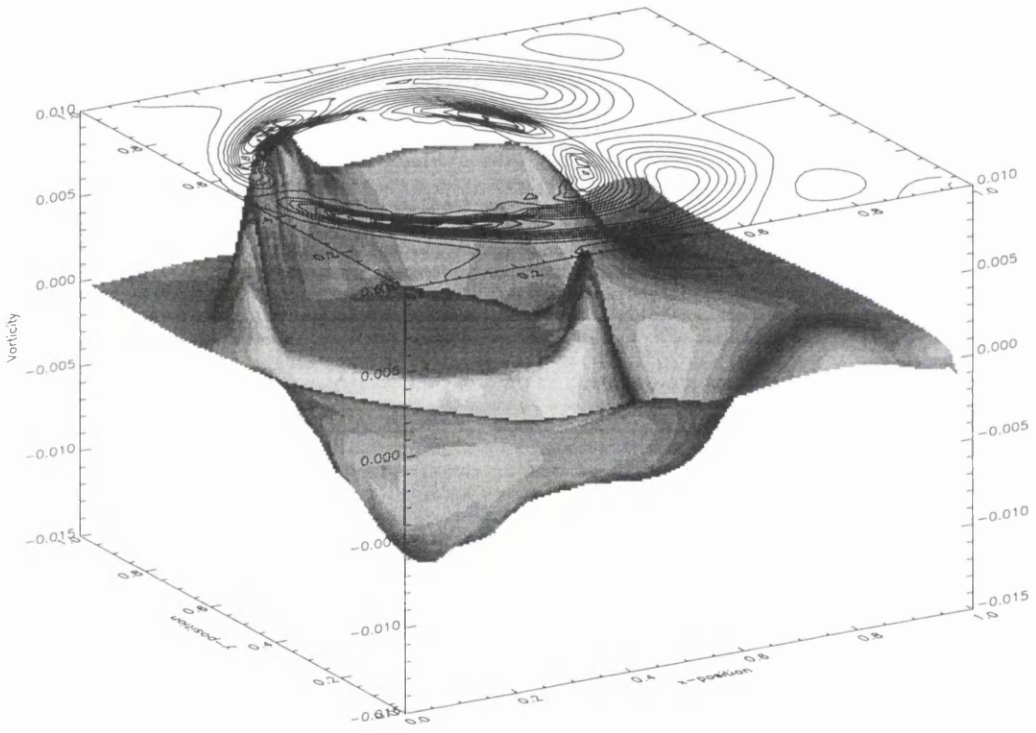

Figure 4.5: Vorticity of the flow shown in figure 4.4

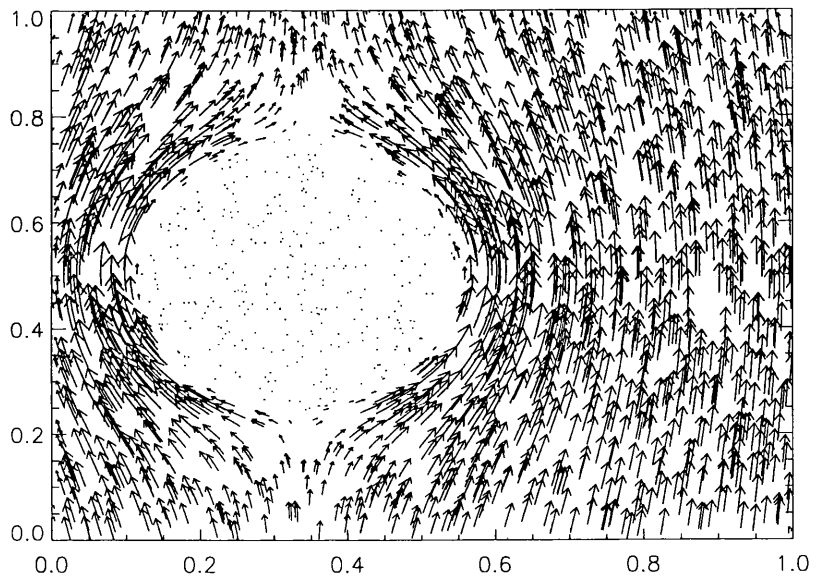

Figure 4.6: The initial magnetic field aligned perpendicular to the flow. $B_0 = U$

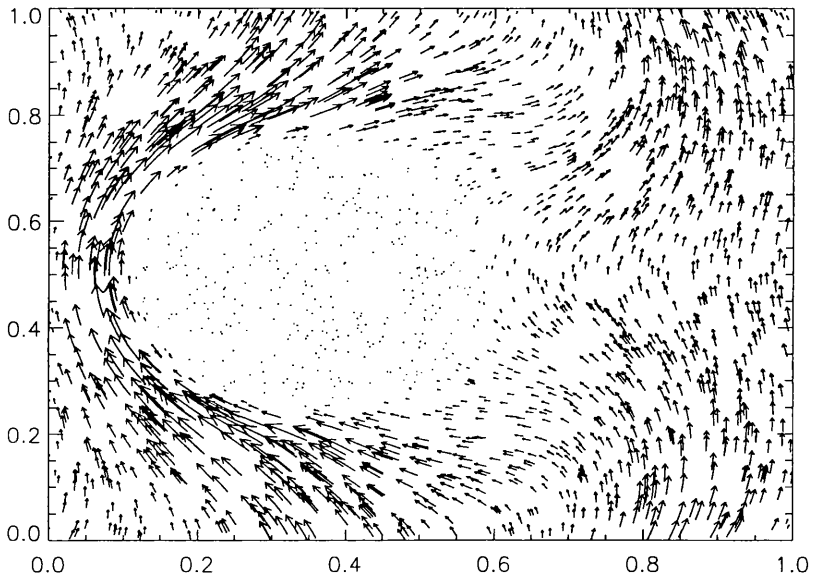

Figure 4.7: The magnetic field after the flow has evolved for 1000 time steps. Notice how the field lines have been bent round the flux tube and reconnect in the wake

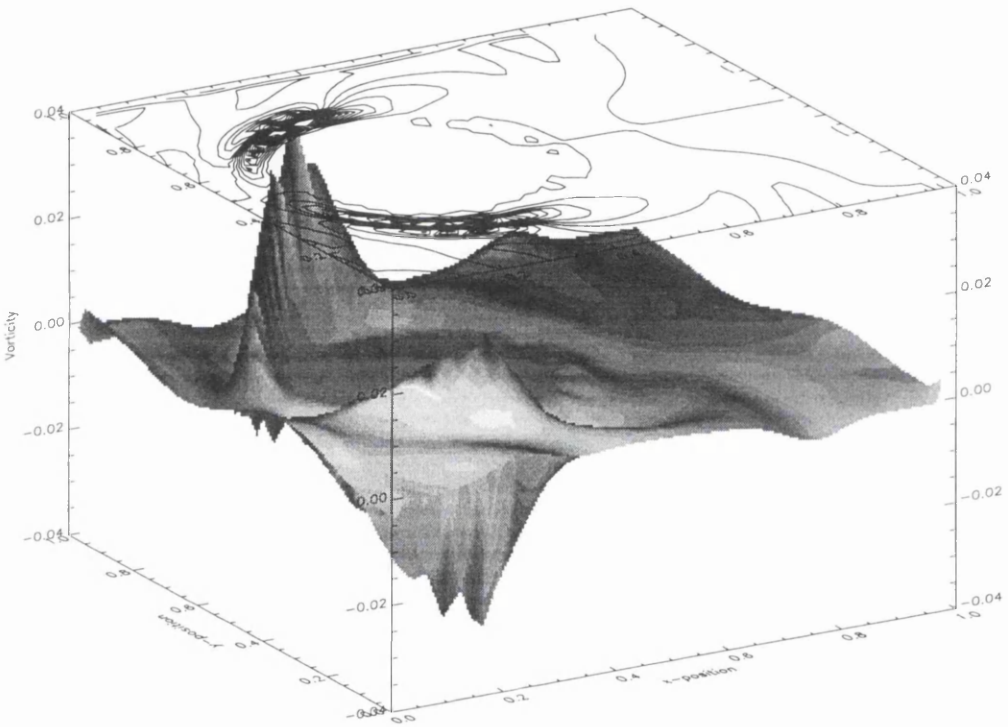

Figure 4.8: The vorticity of the flow with a perpendicular ambient magnetic field. Notice that as well as the suppression of vortices in the wake of the flux tube, there is an enhanced vorticity immediately before the flux tube, due to the effects of bending of the field lines as they are convected past the flux tube.

of the particular boundary conditions; and, most seriously, a uniform grid increases considerably the computational expense because it demands that as much time be devoted to regions of uniform flow as to regions with rapid variations.

He and Doolen have modelled flow past a cylinder on a non-uniform grid using a LB method [60, 59]. They note that it is not necessary that the computational grid coincide with the lattice on which the particles move. Their approach still appears to be strongly influenced by the historical development of the LB method from the CA lattice gas, as they introduce a new step into the lattice Boltzmann method which interpolates between the computational grid and the particle lattice in the course of the calculation [64, 60, 59], A simpler procedure, as noted by Cao et al [41] is to discretise the lattice Boltzmann equation directly, as was done in sections 2.5.1 and 3.3 and this is the procedure that we follow here.

The $M \times N$ computational grid is the same as that of He and Doolen [60, 59]. A grid point is specified by the coordinates (ξ_j, η_k), where $\xi_j = j\Delta\xi, \eta_k = k\Delta\eta$, $0 \leq j \leq M-1, 0 \leq k \leq N-1$ and $\Delta\xi = \xi_\infty/(M-1), \Delta\eta = 2/(N-1)$. The grid point (ξ_j, η_k) is mapped onto a Cartesian coordinate system by the conformal transformation

$$x + iy = a \exp \pi(\xi_j + i\eta_k) \tag{4.16}$$

The lattice Boltzmann equation becomes, in the (ξ, η) coordinates

$$\frac{\partial f_a}{\partial t} + e_{a\xi}\frac{\partial f_a}{\partial \xi} + e_{a\eta}\frac{\partial f_a}{\partial \eta} = -\frac{1}{\tau}(f_a - f_a^{(\mathrm{eq})}) \tag{4.17}$$

where

$$e_{a\xi} = e_{ax}\frac{\partial \xi}{\partial x} + e_{ay}\frac{\partial \xi}{\partial y} \tag{4.18}$$

$$e_{a\eta} = e_{ax}\frac{\partial \eta}{\partial x} + e_{ay}\frac{\partial \eta}{\partial y} \tag{4.19}$$

Equation 4.17 is then easily discretised by any of the standard means. In the simulations presented here, a Lax-Wendroff scheme is used, so the discrete form is

$$\begin{aligned}\frac{f^{n+1}_{ajk} - f^n_{ajk}}{\Delta t} + e_{a\xi}\frac{f^n_{aj+1k} - f^n_{aj-1k}}{2\Delta\xi} - \Delta t e^2_{a\xi}\frac{f^n_{aj+1k} - 2f^n_{ajk} + f^n_{aj-1k}}{\Delta\xi^2} \\ + e_{a\eta}\frac{f^n_{ajk+1} - f^n_{ajk-1}}{2\Delta\eta} - \Delta t e^2_{a\eta}\frac{f^n_{ajk+1} - 2f^n_{ajk} + f^n_{ajk-1}}{\Delta\eta^2} = -\frac{1}{\tau}(f^n_{ajk} - f^{(\mathrm{eq})n}_{ajk})\end{aligned} \tag{4.20}$$

The simulations on the uniform grid were restricted by their size to modelling the growth of the two recirculating eddies in the immediate wake of the cylinder. The non-uniform grid permits simulations over a much larger region, and it is possible to model periodic vortex shedding [59, 60] In order to observe this process, it is necessary to excite the instability of the symmetric flow observed in section 4.4. Like He and Doolen [60] we achieve this by adding an asymmetric perturbation to

the initial symmetric flow:

$$u_x = U' \frac{ay}{r^2} \tag{4.21}$$

$$u_y = -U' \frac{ax}{r^2} \tag{4.22}$$

The boundary conditions for the vortex shedding simulations are exactly the same as before, ie $\mathbf{v} = 0, \mathbf{B} = 0$ on $r = a$, $\mathbf{v}, \mathbf{B}$ are uniform as $r \to \infty$. These are achieved by using the simple bounce back rule at the edge of the cylinder [65, 66] (although better schemes are possible [65, 67, 68, 69, 70, 71, 72, 73, 42, 74, 66, 75]) and by setting the distribution function, f to be the appropriate equilibrium distribution on ξ_∞.

In these simulations, some care had to be taken in choosing the grid spacing. Various conditions for the linear stability of the lattice Boltzmann method were explored in section 2.4.5 and it was shown that the velocity and magnetic fields should remain within certain bounds, the transport coefficients should be positive (which is also a physical requirement) and, depending on the discretisation scheme being used, the CFL condition should be satisfied. If, however, the physical system is itself unstable due to non-linearities, like the flows being studied here, then new instablities in the numerical method arise.

As has been remarked before, the non-linear term in the Navier-Stokes equation couples the large scale and small scale motions and, if the flow is unstable, gives rise to the energy cascade, whereby kinetic energy is transfered from large eddies to small ones. The length scale of the smallest structures (the Kolmogorov scale) is determined by the balance of input of kinetic energy with viscous dissipation. In two dimensions, the situation is somewhat different. Small scale vortices tend to merge together to form larger, coherent structures which account for most of the kinetic energy. This is known as the inverse energy cascade [46], and since it tends to transfer energy from large wave numbers to small wavenumbers, it inhibits the dissipative effects. The vorticity, however, still exhibits a direct cascade, which corresponds to the generation of thin sheets between counter-rotating eddies, where the vorticity gradient is large and where the dissipation is strongest. The problems arise when the computational grid is too coarse to resolve the smallest structures of a flow. In this situation the coupling between different wave numbers still occurs, but the poor resolution means that the small structures, which should dissipate the kinetic energy, are aliased and appear as weakly dissipating, large structures on the numerical grid [4]. This failure to dissipate energy is known as a non-linear instability and is a result of the coarseness of the grid, not the particular discretisation of the fundamental equations. The consequences of the instability may well depend on the scheme used: it may result in a local violation of the CFL condition, for example, thus allowing linear numerical instabilities to grow.

There are two basic solutions to this problem. The simplest is to increase the resolution of the grid to ensure that no aliasing occurs. This of course increases the computational expense, and is not really feasible at very high Reynolds numbers. Instead, as in the approach we have taken,

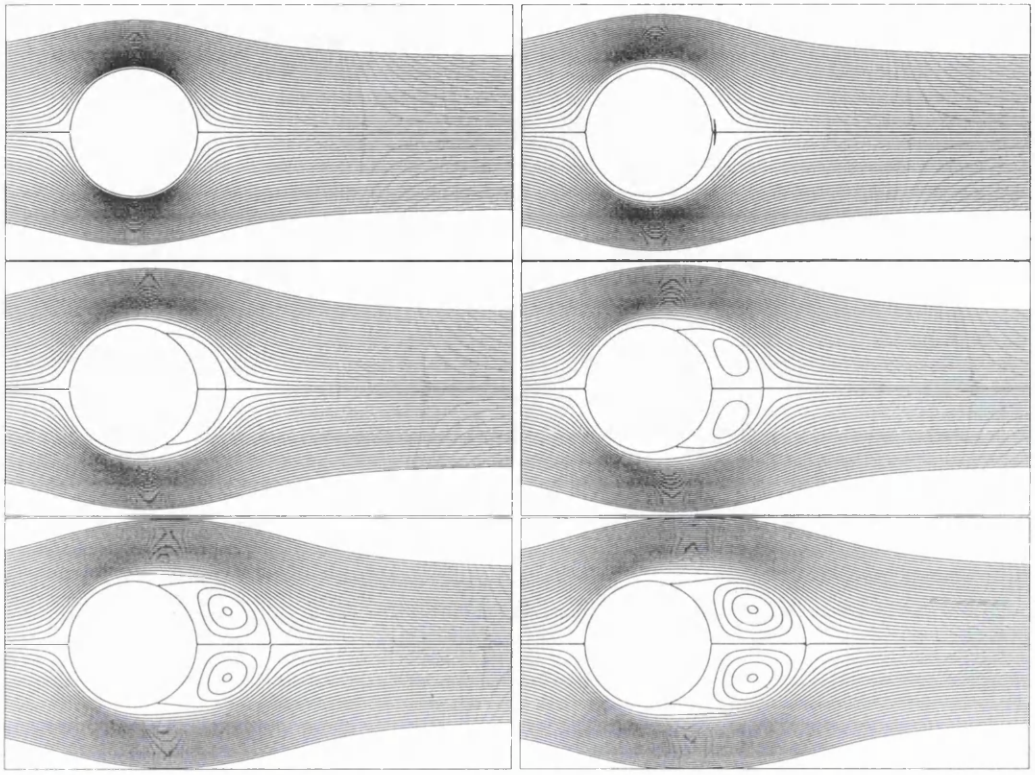

Figure 4.9: Streamlines of showing the growth of the recirculating regions of the unperturbed symmetric flow, at a Reynolds number of 200. $B_0 = 0$

a relatively coarse grid can be used to model a slowly varying mean flow, and the effects of the unresolved eddies can be modelled using some parameterisation, such as an effective eddy viscosity.

In setting up the simulations, there is an important constraint on the model parameters which arises when the component of the magnetic field perependicular to the ambient flow becomes significant. It should be noted first of all that this situation is similar to a conducting wire moving through a magnetic field, and thus experiencing an induced emf which forces a current along the wire. We can easily estimate the size of this current by applying Ohm's law: $\mathbf{E} + \mathbf{v} \times \mathbf{B} = \eta \mathbf{j}$. The externally applied electric field, $\mathbf{E}$, is zero and, since the magnetic field is perpendicular to the flow, $\|\mathbf{v} \times \mathbf{B}\| = U_0 B_0$. Thus the current density $j = U_0 B_0 / \eta$. Now, if we assume that the current is distributed uniformly across the cross section of the cylinder, the total current $I = j\pi a^2 = U_0 B_0 \pi a^2 / \eta$. A current flowing along a straight wire produces a magnetic field outside the wire, whose magnitude varies as $B = I/2\pi r = U_0 B_0 a^2 / 2\eta r$. In our computational domain, this field has a maximum value when $r = a$, so $\max B = U_0 B_0 a / 2\eta = R_e B_0 \nu / 4\eta$. Since we shall examine cases where $R_e > 100$, this implies that the magnetic field will attain values which are considerably larger than the ambient

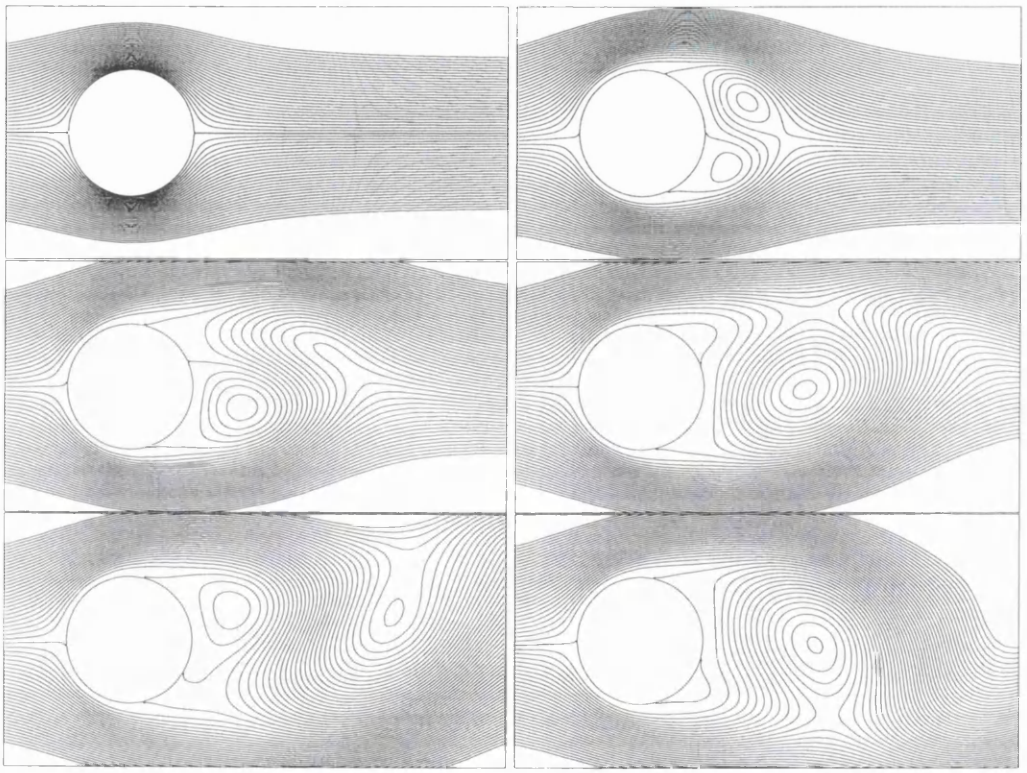

Figure 4.10: Streamlines of the initial growth and shedding of the vortices at a Reynolds number of 200, at time intervals of $3.15a/U$. $B_0 = 0$

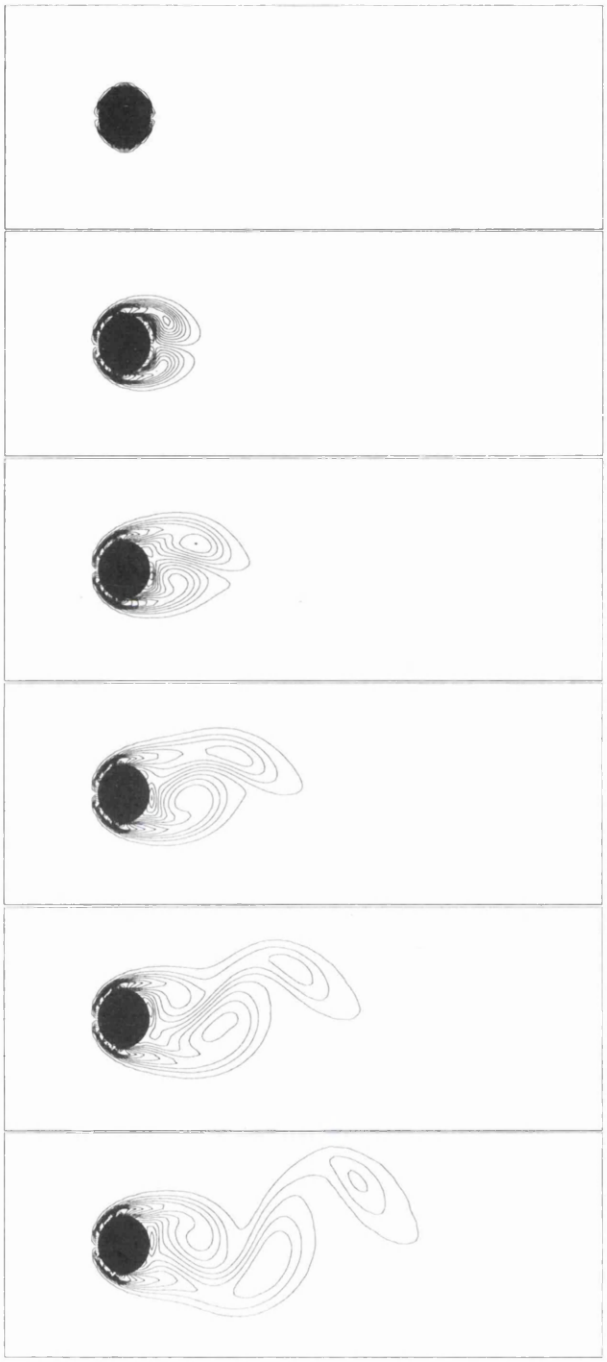

Figure 4.11: Vorticity contours of the initial growth and shedding of the vortices at a Reynolds number of 200. $B_0 = 0$

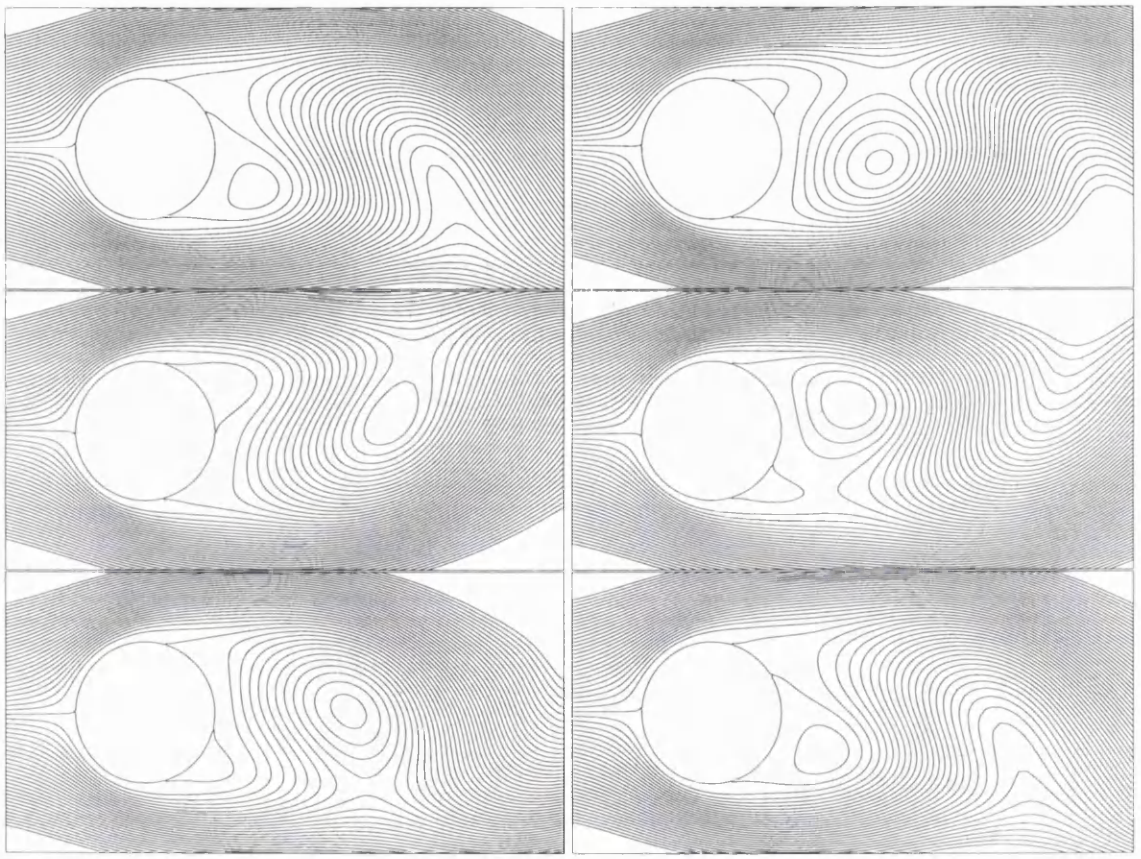

Figure 4.12: Streamlines of a complete shedding cycle at a Reynolds number of 200, at time intervals of $0.585a/U$. $B_0 = 0$

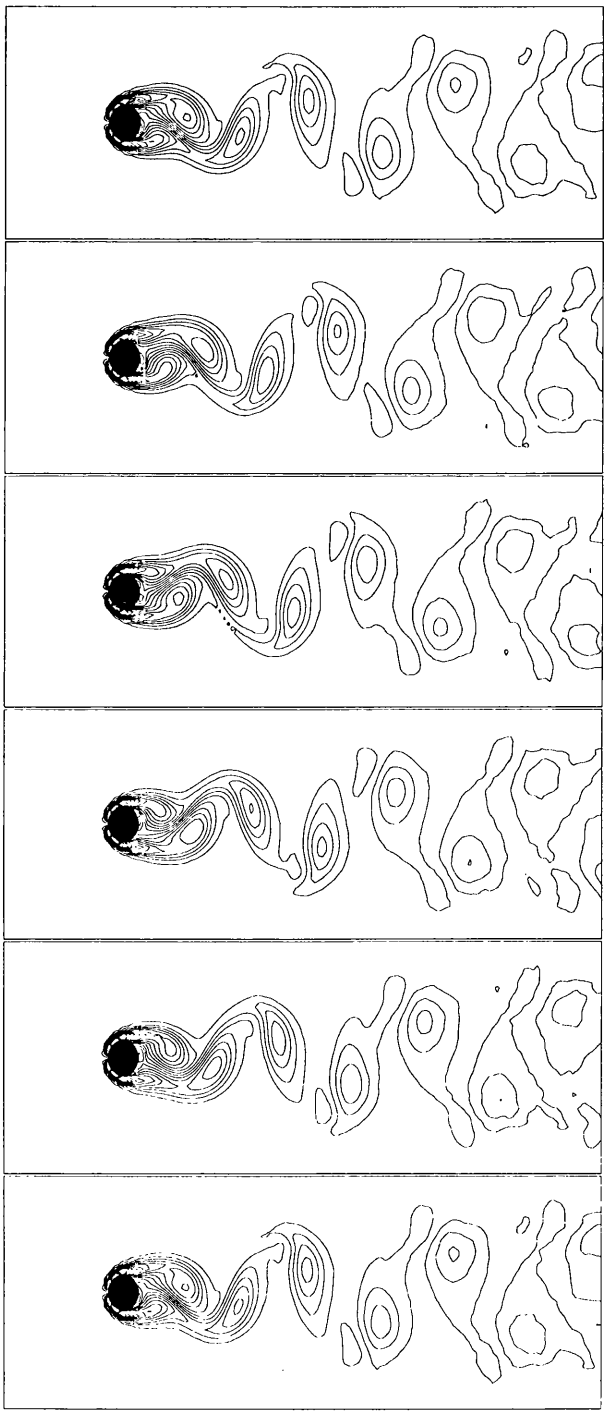

Figure 4.13: Vorticity contours of a complete shedding cycle at a Reynolds number of 200. $B_0 = 0$

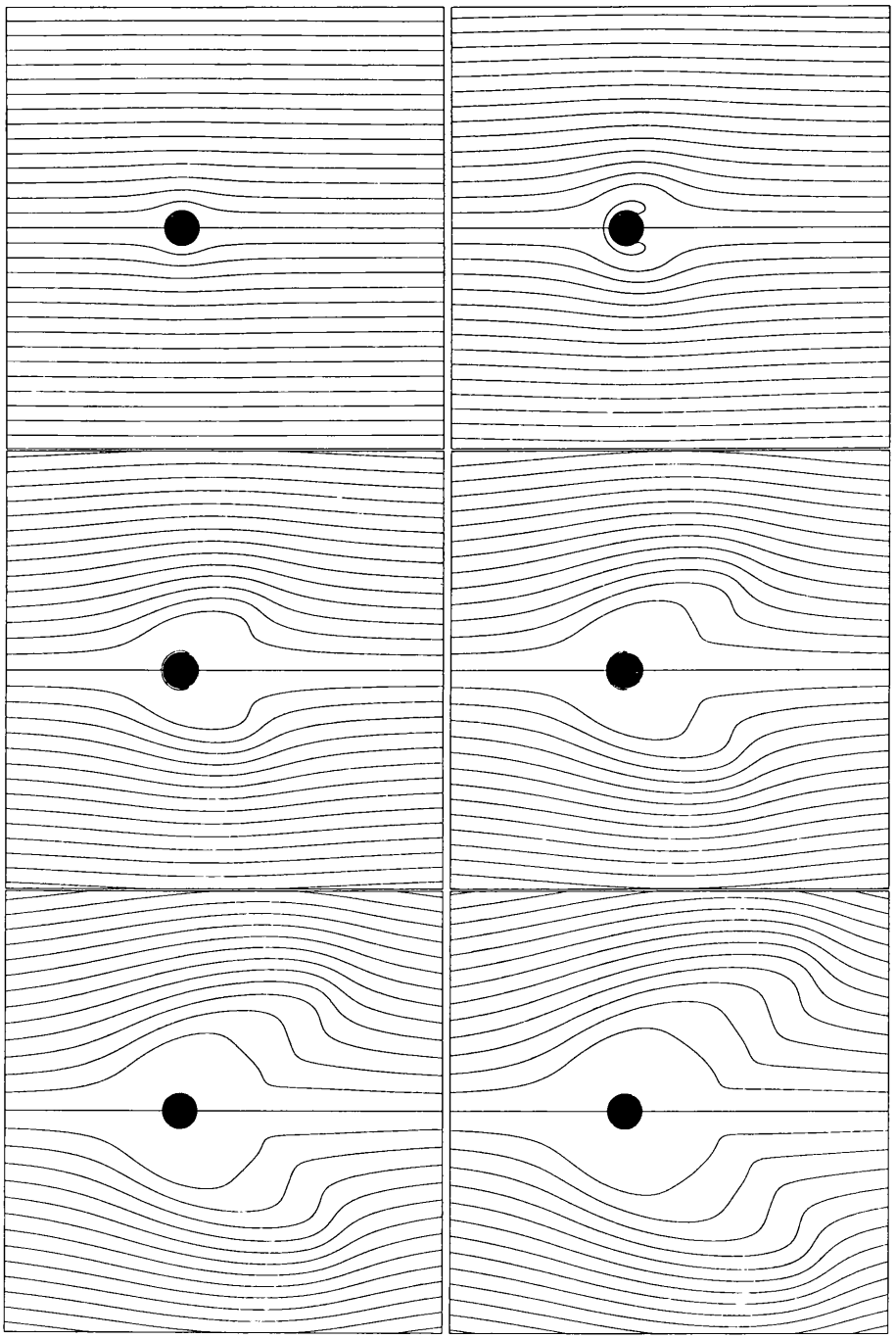

Figure 4.14: The initial evolution of the streamlines with a perpendicular magnetic field. The vortex shedding process has clearly been suppressed due to the stabilising effect of the magnetic field and a slow shock front can be seen developing in the wake.

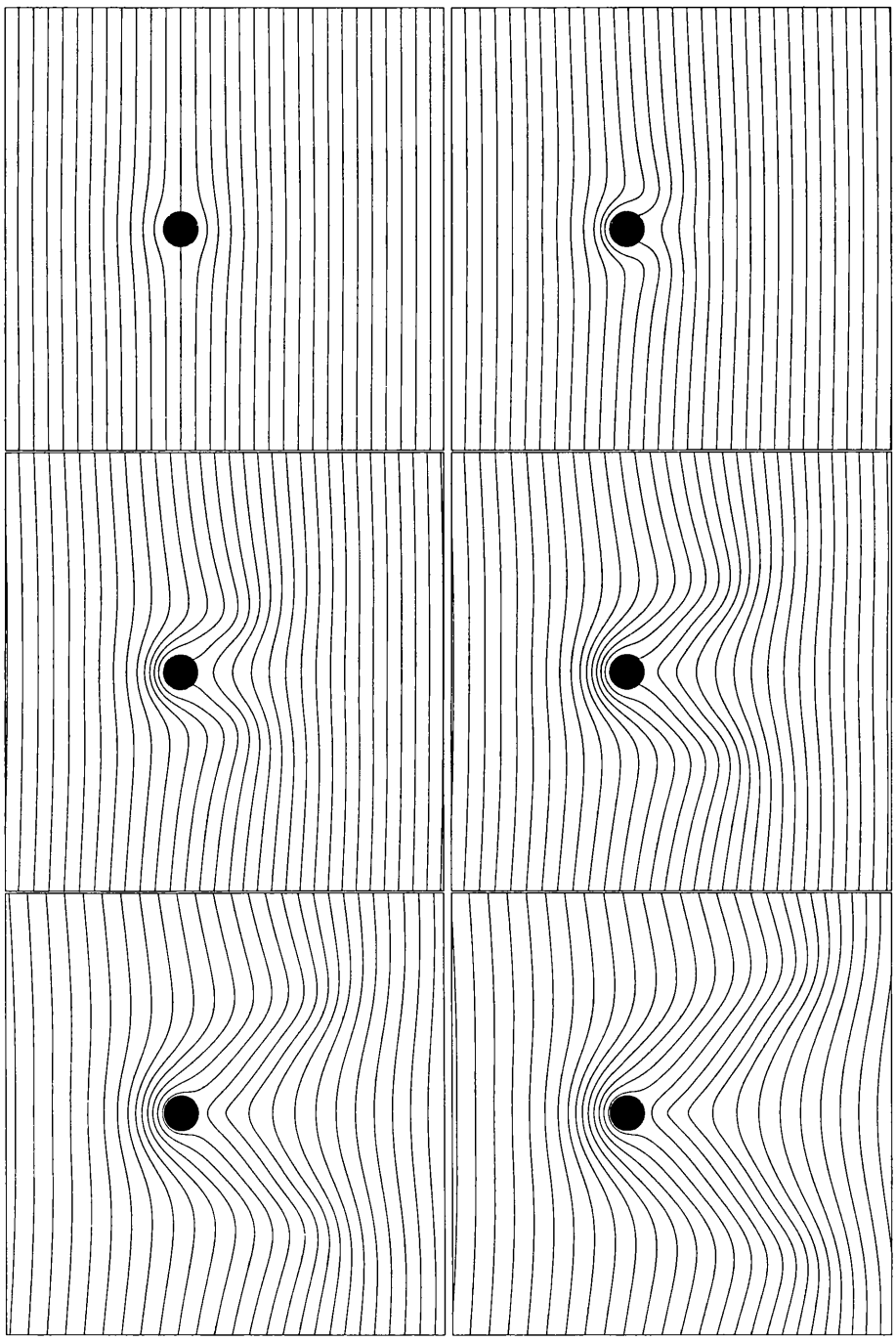

Figure 4.15: The initial evolution of the magnetic field. The field lines are advected past the obstacle and are wrapped around it. The bending of the field lines propagates vorticity away from the boundary.

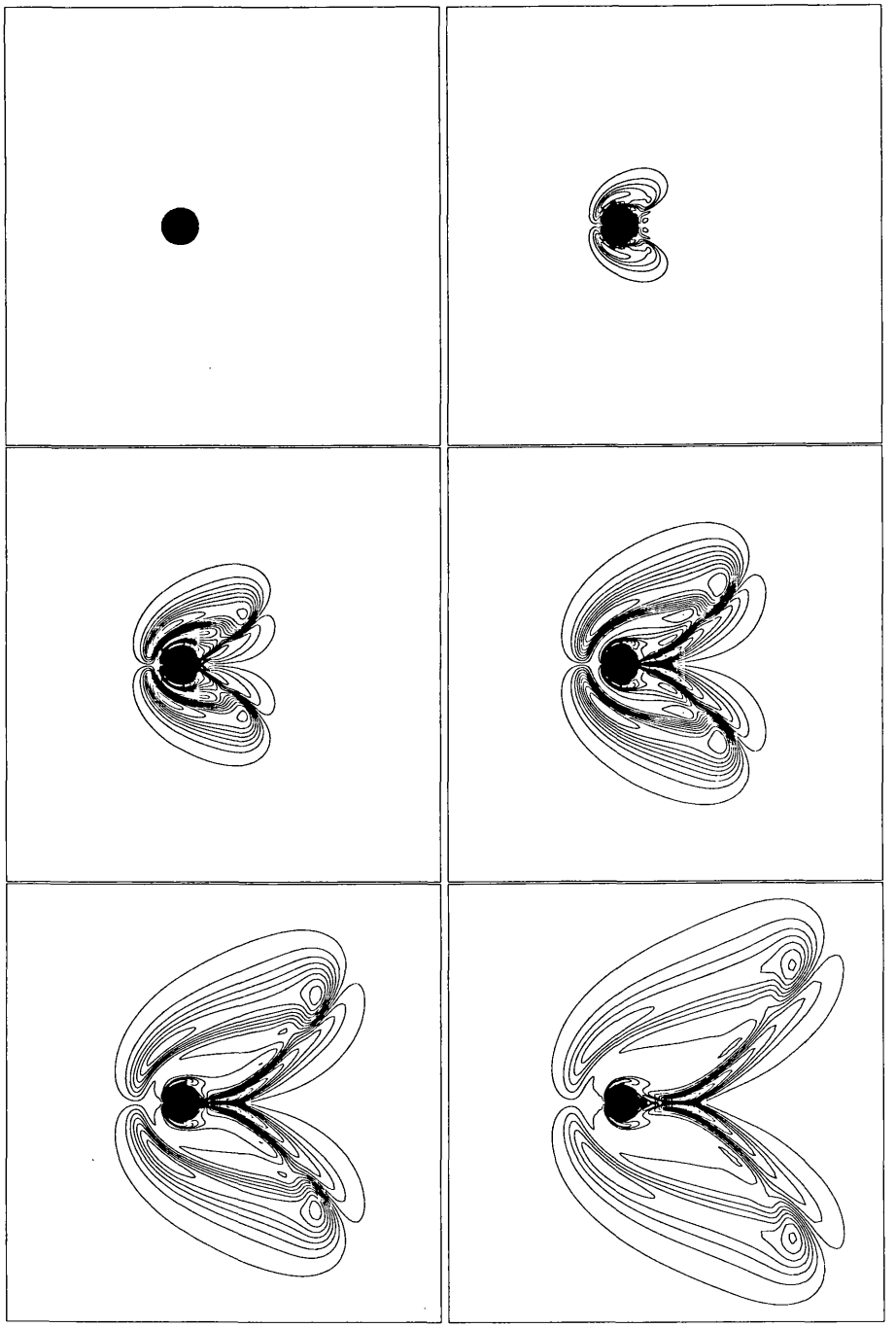

Figure 4.16: The initial evolution of the vorticity field. Comparison with the magnetic field plots shows that the vorticity is propagated by Alfvén waves in the magnetic field.

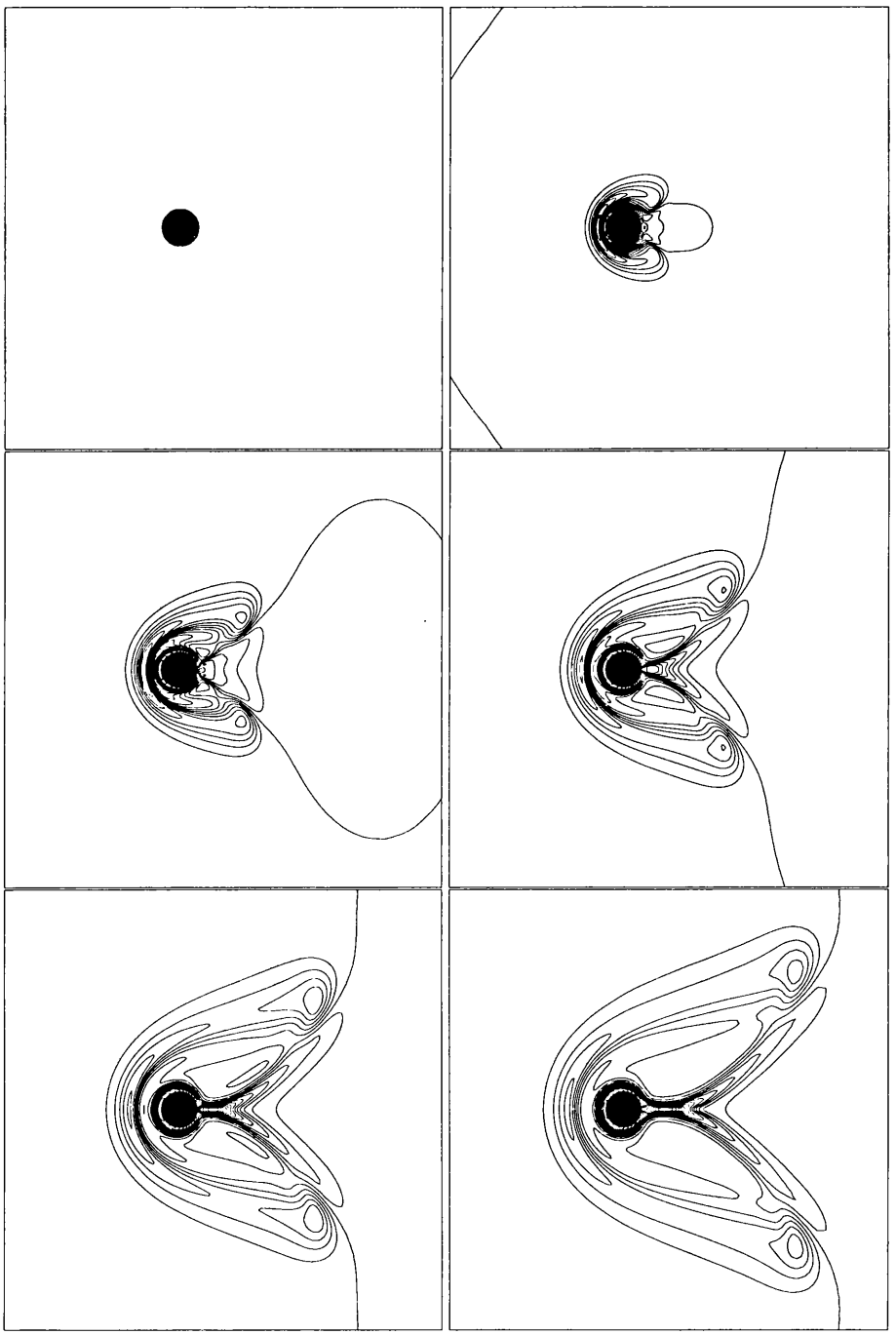

Figure 4.17: The initial evolution of the current density field. Inspection of the equation of Alfvén waves shows that the current density should propagate in a similar manner to the vorticity and is confirmed in these plots.

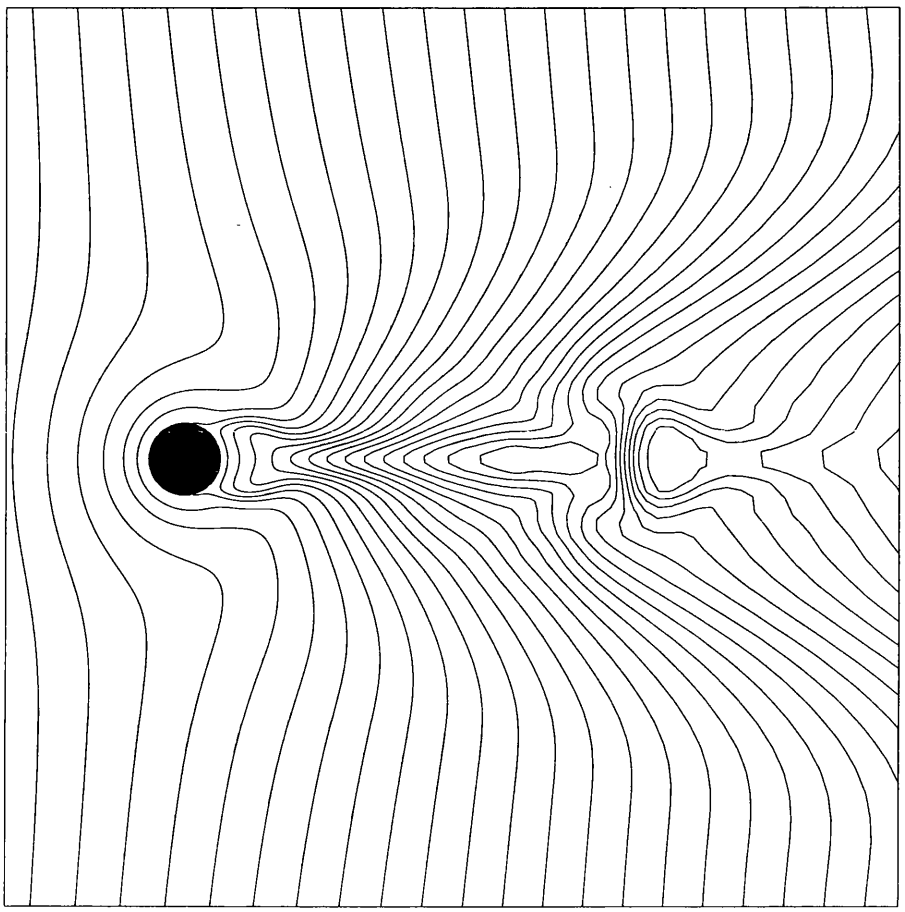

Figure 4.18: Magnetic field lines at $t = 118a/U_0$. Tearing and plasmoid formation can be observed in the curent sheet which forms in the wake

field prescribed by the initial and boundary conditions and this has important implications for how we set up the simulations. In particular, we must ensure that $\max B = R_e B_0 \nu / 4\eta < \frac{1}{2}$, so that the lattice Boltzmann method remains stable. Since we are interested in situations in which B_0 can be as large as U_0, this implies that $U_0 < \eta / 2\nu R_e$, and in order to maintain our desired values of R_e, we must have $a = \nu R_e / 2U_0 > \nu^2 R_e / \eta$.

Obviously the above analysis is a gross simplification. Nevertheless, experimentation does indicate that the analysis provides useful estimates on the bounds of the parameters and these constraints prove to be quite severe, so that the simulations become considerably more expensive as the component of the magnetic field perpendicular to the flow becomes larger.

Results of the simulations are shown in figures 4.9- 4.18 The cases in which there is no magnetic field are similar to the simulations performed by He and Doolen [59, 60]. In the unperturbed

situation, the flow eventually settles down to a steady state, with circulating regions in the immediate wake (figure 4.9). With the perturbation switched on, the advantages of the non-uniform grid become clear. It is now possible to observe the vortex shedding process when the instabilities of the symmetric flow are excited (figures 4.10- 4.11). Eventually the flow settles down to a periodic state, with vortices of opposite sense being shed alternately. Contour plots of the vorticity field over a complete cycle highlight the process particularly clearly (figures 4.12 - 4.13).

When the magnetic field is switched on, we see that it has a stabilising effect on the flow as B_0 increases (figures 4.14- 4.17). A comparison of the contour plots of vorticity with the magnetic field (figures 4.15, 4.16, 4.17) indicates quite clearly that the stabilising mechanism is the Alfvénic propagation of vorticity along the magnetic field lines, rather than the additional dissipation due to the resistivity of the fluid. This can be seen in both cases where the magnetic field is aligned either parallel or perpendicular to the flow.

The simulations with a perpendicular magnetic field are particularly interesting (figure 4.15). The structure of the field arises as a result of the field lines being advected by the flow and wrapped around the obstacle. As the field lines are compressed together, strong spatial gradients are generated and a current sheet develops in the wake. Reconnection takes place within the current sheet, which allows the field lines to be advected beyond the obstacle and subsequently accelerate the fluid in the wake. In some instances (figure 4.18), magnetic islands (plasmoids) break off the current sheet and are advected away. This process is, in some respects similar to the plasmoid formation in the earth's magnetotail, as a result of the interaction of the magnetosphere with the solar wind.

Another interesting effect can be seen in the initial stages of the evolution of the flow. Examining the streamlines at a time just after the start of the simulation (fig 4.14) reveals two circulating regions before the obstacle, rather than in its wake. To understand how this arises, consider again linearised Alfvén waves in a uniform magnetic field. The perturbed fields obey the equations:

$$\frac{\partial \mathbf{v}}{\partial t} = \mathbf{B}_0 \cdot \nabla \mathbf{b} \tag{4.23}$$

$$\frac{\partial \mathbf{b}}{\partial t} = \mathbf{B}_0 \cdot \nabla \mathbf{v} \tag{4.24}$$

so that the Fourier modes obey

$$-i\omega \mathbf{v} = iB_0 k \cos\theta \mathbf{b} \tag{4.25}$$

$$-i\omega \mathbf{b} = iB_0 k \cos\theta \mathbf{v} \tag{4.26}$$

The Alfvén wave dispersion relation is

$$\omega^2 = B_0^2 k^2 \cos^2\theta \tag{4.27}$$

or

$$\omega = \pm B_0 k \cos\theta, \tag{4.28}$$

the two solutions for ω corresponding to waves travelling in opposite directions. Thus we have $\mathbf{v} = -\mathbf{b}$ if the wave is travelling parallel to the magnetic field or $\mathbf{v} = \mathbf{b}$ if the wave is travelling anti-parallel to the magnetic field.

Now, if we have a configuration in which the magnetic field is initially unperturbed, then the initial conditions can be decomposed into the Fourier modes travelling parallel to the magnetic field, with velocity field $\frac{1}{2}\mathbf{v}$ and magnetic perturbation $-\frac{1}{2}\mathbf{v}$, and modes travelling anti-parallel to the magnetic field, with velocity field $\frac{1}{2}\mathbf{v}$ and magnetic perturbation $\frac{1}{2}\mathbf{v}$. Thus an initially localised perturbation in the velocity field will spilt into two, and disturbances will be transmitted in opposite directions along the magnetic field.

The initial condition of our simulations is like this configuration, albeit distorted by the geometry. The magnetic field is initially unperturbed, and we have a localised region of strong vorticity at the boundary of the obstacle. Thus, we should expect, say, the negative vorticity on the top part of the boundary to propagate in opposite directions along the magnetic field. The vorticity propagating away from the obstacle in the positive y direction can clearly be seen in figure 4.16, whilst the vorticity propagating in the opposite direction appears as a circulating region in front of the obstacle. The vorticity which propagates round from the opposite side of the obstacle has the opposite sign and eventually interferes destructively with the vorticity from the top half of the obstacle, so that the circulating regions at the front are very weak and eventually disappear altogether.

Chapter 5

Generalising Lattice Boltzmann MHD

In this chapter, we derive generalisations of the lattice Boltzmann MHD model which we have been using. Firstly we present a 2D generalisation which includes the thermal energy of the fluid and then we present a 3D, isothermal model.

5.1 Thermal Energy in Lattice Boltzmann MHD

5.1.1 The Energy Equations of Magnetohydrodynamics

Until now, our discussion of lattice Boltzmann MHD and our MHD simulations have ignored energy conservation. The MHD equations have been closed by assuming that the temperature is constant so that the fluid obeys Boyle's law:

$$p = c^2 \rho \tag{5.1}$$

This condition can be arrived at by assuming that either the thermal conductivity is infinite, or that the system is in contact with a heat bath so that energy need not be conserved. In fact, by considering the microscopic dynamics of our present lattice Boltzmann model, it is obvious that energy is not conserved in general.

In order to include energy in our model, we first of all need the correct energy equation for magnetohydrodynamics, an issue that was brushed over in section 1.1.2. There are a number of contributions to this [76]. Firstly, we have the heat equation:

$$\rho\left(\frac{\partial \phi}{\partial t} + \mathbf{v}\cdot\nabla\phi\right) = -p\nabla\cdot\mathbf{v} - \nabla\cdot\mathbf{q} + \eta j^2 + \nu(\nabla\mathbf{v}) : (\nabla\mathbf{v}) + \nu_b(\nabla\cdot\mathbf{v})^2 - L_r + H \tag{5.2}$$

where ϕ is the internal energy per unit mass; $-p\nabla\cdot\mathbf{v}$ is the rate at which work is done on the gas by compressing it; $\mathbf{q}$ is the heat flux which equals $\kappa\nabla\phi$, κ being the thermal diffusivity; ηj^2 is the

ohmic dissipation; the terms involving $\nabla \mathbf{v}$ are heating due to viscous dissipation; L_r is the radiation flux and H is the heat from all other sources, like nuclear fusion in a tokamak or solar plasma. From now on we shall neglect L_r and H.

We can also obtain the equation of mechanical energy by taking the dot product of the momentum equation 1.40 with $\mathbf{v}$:

$$\rho\left[\frac{\partial \frac{1}{2}v^2}{\partial t} + \mathbf{v}\cdot\nabla(\frac{1}{2}v^2)\right] = -\mathbf{v}\cdot\nabla p + \mathbf{v}\cdot(\mathbf{j}\times\mathbf{B}) + \nu\mathbf{v}\cdot(\nabla^2\mathbf{v}) + \nu_b\mathbf{v}\cdot\nabla(\nabla\cdot\mathbf{v}) \tag{5.3}$$

Finally, we have an equation for the electromagnetic energy which follows from Poyntings theorem [3]:

$$\frac{\partial}{\partial t}\left(\frac{\epsilon_0 E^2}{2} + \frac{B^2}{2\mu_0}\right) + \mathbf{E}\cdot\mathbf{j} + \nabla\cdot(\mathbf{E}\times\mathbf{B}) = 0 \tag{5.4}$$

where, for the moment, we re-introduce the constants ϵ_0 and μ_0. This tells us that the rate of change of electromagnetic energy is due to the rate at which work is done on the charges plus the energy flux of electromagnetic radiation. Since $\epsilon_0 = \frac{1}{\mu_0 c^2}$ and $c \approx \infty$ in the MHD approximation, we shall neglect the electric component of the energy density from now on. Thus, on setting $\mu_0 = 1$ again, we are left with

$$\mathbf{E}\cdot\mathbf{j} = -\frac{\partial \frac{1}{2}B^2}{\partial t} - \nabla\cdot(\mathbf{E}\times\mathbf{B}) \tag{5.5}$$

Combining equations 5.2, 5.3 and 5.5, we get an equation for the total energy:

$$\begin{aligned}\rho\left[\frac{\partial}{\partial t}(\phi + \frac{1}{2}v^2) + \mathbf{v}\cdot\nabla(\phi + \frac{1}{2}v^2)\right] + \frac{\partial \frac{1}{2}B^2}{\partial t} + \nabla\cdot(\mathbf{E}\times\mathbf{B}) = \\ -p\nabla\cdot\mathbf{v} - \nabla\cdot\mathbf{q} + \eta j^2 + \nu(\nabla\mathbf{v}) : (\nabla\mathbf{v}) + \nu_b(\nabla\cdot\mathbf{v})^2 - \mathbf{v}\cdot\nabla p \\ +\mathbf{v}\cdot(\mathbf{j}\times\mathbf{B}) + \nu\mathbf{v}\cdot(\nabla^2\mathbf{v}) + \nu_b\mathbf{v}\cdot\nabla(\nabla\cdot\mathbf{v}) - \mathbf{E}\cdot\mathbf{j}\end{aligned} \tag{5.6}$$

This equation can be considerably simplified if we note that $\mathbf{v}\cdot(\mathbf{j}\times\mathbf{B}) = -\mathbf{j}\cdot(\mathbf{v}\times\mathbf{B})$ and $\mathbf{E}$ is eliminated using equation 1.37, so that all the electromagnetic contributions to the right hand side vanish. Further simplification occurs if we introduce the viscous stress tensor $\sigma = -\nu(\nabla\mathbf{v}) + (\nabla\mathbf{v})^T + (\nu_b - \nu)(\nabla\cdot\mathbf{v})\mathbf{I}$ [45], so that equation 5.6 can be written

$$\begin{aligned}\frac{\partial}{\partial t}(\rho\phi + \frac{1}{2}\rho v^2 + \frac{1}{2}B^2) + \nabla\cdot\Big[\rho\phi\mathbf{v} + \frac{1}{2}\rho v^2\mathbf{v} - (\mathbf{v}\times\mathbf{B})\times\mathbf{B} \\ +p\mathbf{v} + \mathbf{q} + \mathbf{v}\cdot\sigma + \eta\mathbf{j}\times\mathbf{B}\Big] = 0\end{aligned} \tag{5.7}$$

All that is now needed is the equation of state:

$$p = \frac{\rho k T}{m} = \frac{2\rho\phi}{N} = a\rho\phi \tag{5.8}$$

where k is Boltzmann's constant, m is the molecular mass of the gas and N is the number of degrees of freedom of a molecule.

5.2 Microscopic Dynamics

5.2.1 Compressibility in Lattice Boltzmann Magnetohydrodynamics

On examining the fluid equations of lattice Boltzmann MHD (equations 2.95 and 2.97), we are immediately struck with a problem: there are unphysical appearances of the density in the terms involving the magnetic field. This restricts the validity of the model to flows where $\rho \approx$ constant. Clearly this is undesirable if we wish to include thermodynamics, since it effectively closes the system, and therefore an additional energy equation should have no effect on the flow.

The origin of the unphysical appearances of ρ arises simply from the definitions of the magnetic field and the equilibrium distribution:

$$\sum_{a,b} f_{ab}\mathbf{B}_{ab} = \rho\mathbf{B} \tag{5.9}$$

$$\sum_{a,b} f_{ab}^{(\mathrm{eq})}\mathbf{v}_{ab}\mathbf{v}_{ab} = p\mathbf{I} + \rho(\mathbf{vv} - \mathbf{BB}) \tag{5.10}$$

$$\sum_{a,b} f_{ab}^{(\mathrm{eq})}\mathbf{B}_{ab}\mathbf{v}_{ab} = \rho(\mathbf{Bv} - \mathbf{vB}) \tag{5.11}$$

If we change our definitions of $\mathbf{B}$ and $f^{(\mathrm{eq})}$ by removing the appearances of ρ from the magnetic contributions to the right hand sides of equations 5.9, 5.10 and 5.11, so that

$$\sum_{a,b} f_{ab}\mathbf{B}_{ab} = \mathbf{B} \tag{5.12}$$

$$\sum_{a,b} f_{ab}^{(\mathrm{eq})}\mathbf{v}_{ab}\mathbf{v}_{ab} = p\mathbf{I} + \rho\mathbf{vv} - \mathbf{BB} \tag{5.13}$$

$$\sum_{a,b} f_{ab}^{(\mathrm{eq})}\mathbf{B}_{ab}\mathbf{v}_{ab} = \mathbf{Bv} - \mathbf{vB} \tag{5.14}$$

then it is easily shown that unphysical appearances of ρ disappear from the fluid equations so that the correct form of the MHD equations is recovered. Thus, by a simple modification, the lattice Boltzmann technique is no longer restricted to incompressible MHD.

5.2.2 Particle States

The basic reason for the lack of thermodynamics in the lattice Boltzmann model is that the moving particles are monoenergetic. In the absence of rest particles, energy conservation is equivalent to conservation of particle number and therefore results in a trivial energy equation for the system. Rest particles are introduced in order to achieve a properly structured momentum equation, not for energy considerations and it is easily seen that their presence violates energy conservation.

The obvious means of introducing multi-energetic particles is to expand the neighbourhood of a cell to include cells beyond the nearest neighbours. As mentioned in section 2.3.4, this has already been done for hydrodynamics [38, 34]. Here we shall follow the same procedure and derive a thermal MHD model.

The particles move on the usual hexagonal lattice, with the six lattice vectors $\mathbf{e}_a$, $a = 1, \ldots 6$. We define two types of particle: magnetic and non-magnetic. There are thirteen non-magnetic particles, one of which is at rest and has number density f_0. The other twelve carry momentum $\lambda \mathbf{e}_a$, and have number density $f_{a\lambda}$, $a = 1, \ldots, 6$, $\lambda = 1, 2$. There are thirty magnetic particles, six of which are at rest, with number density g_a and carry a magnetic field $\mathbf{e}_a$,$a = 1, \ldots, 6$. Twelve of the magnetic particles correspond to the moving particles of the non-thermal MHD model described in section 2.4, and carry momentum $\mathbf{e}_a$, and magnetic field $\mathbf{B}_{ab}$ and have a number density g_{ab1}, $a = 1, \ldots, 6$, $b = 0, 1$. The other twelve magnetic particles carry momentum $2\mathbf{e}_a$ and magnetic field $(-1)^b \mathbf{e}_a$ and have a number density g_{ab2} The non-magnetic particles carry $\lambda^2/2$ units of energy and the magnetic particles carry $1/2 + \lambda^2/2$ units of energy where $\lambda = 0, 1, 2$ is the particle speed.

The macroscopic fields are defined in the usual way:

$$\rho = f_0 + \sum_{a,\lambda} f_{a\lambda} + \sum_a g_a + \sum_{a,b,\lambda} g_{ab\lambda} \tag{5.15}$$

$$\rho \mathbf{v} = \sum_{a,\lambda} f_{a\lambda} \lambda \mathbf{e}_a + \sum_{a,b,\lambda} g_{ab\lambda} \lambda \mathbf{e}_a \tag{5.16}$$

$$\mathbf{B} = \sum_a g_a \mathbf{e}_a + \sum_{a,b} \left(g_{ab1} \mathbf{B}_{ab} + (-1)^b g_{ab2} \mathbf{e}_a \right) \tag{5.17}$$

$$\epsilon = \sum_{a,\lambda} f_{a\lambda} \frac{1}{2} \lambda^2 + \sum_a \frac{1}{2} g_a + \sum_{a,b,\lambda} \frac{1}{2} (1 + \lambda^2) g_{ab\lambda} \tag{5.18}$$

$$\mathbf{\Pi} = \sum_{a,\lambda} f_{a\lambda} \lambda^2 \mathbf{e}_a \mathbf{e}_a + \sum_{a,b,\lambda} g_{ab\lambda} \lambda^2 \mathbf{e}_a \mathbf{e}_a \tag{5.19}$$

$$\mathbf{\Lambda} = \sum_{a,b} \left(g_{ab1} \mathbf{B}_{ab} \mathbf{e}_a + (-1)^b g_{ab2} \lambda \mathbf{e}_a \mathbf{e}_a \right) \tag{5.20}$$

$$\mathbf{Q} = \sum_{a,\lambda} f_{a\lambda} \frac{1}{2} \lambda^3 \mathbf{e}_a + \sum_{a,b,\lambda} g_{ab} \frac{1}{2} (1 + \lambda^2) \lambda \mathbf{e}_a \tag{5.21}$$

where, in addition to the previously defined quantities, ϵ is the total energy density and $\mathbf{Q}$ is the energy flux vector.

5.2.3 The equilibrium distribution

Now we need to make the appropriate choice of equilibrium distribution in order to recover the correct thermal MHD equations. Since the energy flux vector contains terms which are cubic in

the vector fields, it is necessary to expand the equilibrium distribution to third order. There is considerable freedom in how this can be done and we shall adopt the following choice:

$$f_{a\lambda}^{(\mathrm{eq})} = A_\lambda + C_\lambda v^2 + D_\lambda B^2 + F_\lambda \mathbf{v}\cdot\mathbf{e}_a + G_\lambda(\mathbf{v}\cdot\mathbf{e}_a)^2 + H_\lambda(\mathbf{v}\cdot\mathbf{e}_a)^3 + J_\lambda B^2(\mathbf{v}\cdot\mathbf{e}_a) + K_\lambda(\mathbf{B}\cdot\mathbf{v})(\mathbf{B}\cdot\mathbf{e}_a) \quad (5.22)$$

where $a = 1, \ldots, 6$, $\lambda = 0, 1, 2$ and $f_{a0} = f_0$,

$$g_a^{(\mathrm{eq})} = L + NB^2 + P\mathbf{B}\cdot\mathbf{e}_a \quad (5.23)$$

$$g_{ab1}^{(\mathrm{eq})} = R + SB^2 + T\mathbf{v}\cdot\mathbf{e}_a + U\mathbf{B}\cdot\mathbf{B}_{ab} + V_1(\mathbf{B}\cdot\mathbf{B}_{ab})^2 + \frac{1}{3}[(\mathbf{v}\cdot\mathbf{e}_a)(\mathbf{B}\cdot\mathbf{B}_{ab}) - (\mathbf{B}\cdot\mathbf{e}_a)(\mathbf{v}\cdot\mathbf{B}_{ab})] \quad (5.24)$$

$$g_{ab2}^{(\mathrm{eq})} = V_2(\mathbf{B}\cdot\mathbf{e}_a)^2 \quad (5.25)$$

In the analysis of chapter 2, the equilibrium distribution was chosen in order that the ideal MHD equations be satisfied to lowest order, and the the Chapman-Enskog procedure established the form of the dissipative terms. In a more general model, such as this, the Chapman-Enskog procedure reveals, as we shall see, additional constraints on the equilibrium distribution which are necessary in order to eliminate some unphysical first order terms. Therefore, we shall derive some expressions from the Chapman-Enskog procedure which will be useful in our derivation of the equilibrium distribution. Recall that the first order perturbation of the distribution function is given by the expression

$$f_i^{(1)} = -\tau\left(\frac{\partial}{\partial t_1} + \mathbf{v}_i\cdot\nabla\right) f_i^{(\mathrm{eq})} \quad (5.26)$$

where f_i is an arbitrary component of $(f_0, f_{a\lambda}, g_a, g_{ab})$ and $\mathbf{v}_i$ the corresponding velocity. So the dissipative terms in the flux tensors are thus:

$$\begin{aligned}\mathbf{\Pi}^{(1)} &= -\tau\sum_i \frac{\partial}{\partial t_1}(f_i^{(\mathrm{eq})}\mathbf{v}_i\mathbf{v}_i) + \nabla\cdot(f_i^{(\mathrm{eq})}\mathbf{v}_i\mathbf{v}_i\mathbf{v}_i) \\ &= -\tau\frac{\partial\mathbf{\Pi}^{(0)}}{\partial t_1} - \tau\nabla\cdot\sum_i f_i^{(\mathrm{eq})}\mathbf{v}_i\mathbf{v}_i\mathbf{v}_i \end{aligned} \quad (5.27)$$

$$\mathbf{\Lambda}^{(1)} = -\tau\frac{\partial\mathbf{\Lambda}^{(0)}}{\partial t_1} - \tau\nabla\cdot\sum_i f_i^{(\mathrm{eq})}\mathbf{B}_i\mathbf{v}_i\mathbf{v}_i \quad (5.28)$$

$$\mathbf{Q}^{(1)} = -\tau\frac{\partial\mathbf{Q}^{(0)}}{\partial t_1} - \tau\nabla\cdot\sum_i f_i^{(\mathrm{eq})}E_i\mathbf{v}_i\mathbf{v}_i \quad (5.29)$$

and since $\mathbf{\Pi}^{(0)}, \mathbf{\Lambda}^{(0)}, \mathbf{Q}^{(0)}$ can be expressed in terms of the macroscopic fields, we can derive expressions for $\frac{\partial\mathbf{\Pi}^{(0)}}{\partial t_1}$ etc using the inviscid fluid equations thus:

$$\begin{aligned}\frac{\partial\Pi_{ij}^{(0)}}{\partial t_1} &= -\left[a^2\rho\phi\partial_k v_k + a\partial_k(\rho\phi v_k)\right]\delta_{ij} \\ &\quad -\partial_k(\rho v_i v_j v_k) - (v_i\partial_j + v_j\partial_i)(a\rho\phi + \frac{1}{2}B^2) \\ &\quad +B_k(v_i\partial_k B_j + v_j\partial_k B_i) - B_k(B_i\partial_k v_j + B_j\partial_k v_i) + \partial_k(B_i B_j v_k)\end{aligned} \quad (5.30)$$

$$\begin{aligned}\frac{\partial \Lambda_{ij}^{(0)}}{\partial t_1} &= -\frac{1}{\rho}(B_i\partial_j - B_j\partial_i)(a\rho\phi + \frac{1}{2}B^2) \\ &+\frac{B_k}{\rho}(B_j\partial_k B_i - B_i\partial_k B_j) - \partial_k\left[(v_iB_j - B_iv_j)v_k\right] \\ &+B_k(v_i\partial_k v_j - v_j\partial v_i)\end{aligned} \tag{5.31}$$

$$\begin{aligned}\frac{\partial Q_i^{(0)}}{\partial t_1} &= -(a+1)\left[a\rho\phi u_i\partial_k u_k + \phi\partial_i(a\rho\phi + \frac{1}{2}B^2) - \phi\partial_k(B_iB_k) + \partial_k(\rho u_i u_k\phi)\right] \\ &+\frac{1}{2}v^2\left[\partial_k(B_iB_k) - \partial_i(a\rho\phi + \frac{1}{2}B^2)\right] - \partial_k(\frac{1}{2}\rho v^2 v_i v_k) \\ &+v_iv_j\left[\partial_k(B_jB_k) - \partial_j(a\rho\phi + \frac{1}{2}B^2)\right] + 2B_jv_i\partial_k(v_jB_k - B_jv_k) \\ &+\frac{B^2}{\rho}\left[\partial_k(B_iB_k) - \partial_i(a\rho\phi + \frac{1}{2}B^2) - \rho v_k\partial_k v_i\right] - B_iv_j\partial_k(v_jB_k - B_jv_k) \\ &-\frac{B_iB_j}{\rho}\left[\partial_k(B_jB_k) - \partial_j(a\rho\phi + \frac{1}{2}B^2) - \rho v_k\partial_k v_j\right] - B_jv_j\partial_k(v_iB_k - B_iv_k)\end{aligned} \tag{5.32}$$

We can now derive the correct form for the distribution function. The terms of order $O(v^0, B^0)$ give us

$$A_0 + 6A_1 + 6A_2 + 6L + 12R = \rho \tag{5.33}$$

$$3A_1 + 12A_2 + 3L + 12R = \rho\phi \tag{5.34}$$

$$3A_1 + 12A_2 + 6R = a\rho\phi \tag{5.35}$$

on subsitution into equations 5.15,5.18 and 5.19 respectively. Substitution into equation 5.29 gives us

$$\tau\left[\frac{3}{2}\nabla A_1 + 24\nabla A_2 + 6\nabla R\right] = \kappa\nabla\phi + \tau a(a+1)\left[\phi^2\nabla\rho + \rho\phi\nabla\phi\right] \tag{5.36}$$

so that

$$\frac{\partial}{\partial\rho}\left(\frac{3}{2}A_1 + 24A_2 + 6R\right) = a(a+1)\phi^2 \tag{5.37}$$

$$\frac{\partial}{\partial\phi}\left(\frac{3}{2}A_1 + 24A_2 + 6R\right) = \frac{\kappa}{\tau} + a(a+1)\rho\phi \tag{5.38}$$

In the above expressions it is clear that $\frac{3}{2}A_1 + 24A_2 + 6R$ is sufficiently smooth that the operators $\frac{\partial}{\partial\rho}$ and $\frac{\partial}{\partial\phi}$ commute (since the second order partial derivatives are continuous functions of ρ and ϕ). Therefore, for consistency, we must have

$$\begin{aligned}\frac{\partial}{\partial\phi}\left[a(a+1)\phi^2\right] &= \frac{\partial}{\partial\rho}\left[\frac{\kappa}{\tau} + a(a+1)\rho\phi\right] \\ \Longrightarrow \frac{\partial}{\partial\rho}\left(\frac{\kappa}{\tau}\right) &= a(a+1)\phi \\ \Longrightarrow \kappa &= a(a+1)\tau\rho\phi + q(\phi)\end{aligned} \tag{5.39}$$

where q is an arbitrary function. This similar to the constraint on the thermal diffusivity that was derived by Boghosian and Coveney [77], namely

$$\kappa = 2\left(\tau - \frac{1}{2}\right)\rho\phi + q(\phi) \tag{5.40}$$

. The appearance of the factor $\tau - \frac{1}{2}$ rather than τ is due to the particular discretisation of the LB equation which they considered, and the factor 2 appears because in their 2D model, additional constraints, derived in a similar manner, set $a = 1$. The general form of the above constraint is, in fact, determined completely by the structure of the macroscopic equations and the form of the collision operator and cannot be modified by the choice of particle states [77]. Similar constraints will be derived for the viscosities and resistivity.

Integrating either equation 5.37 or equation 5.38 then gives us

$$\frac{3}{2}A_1 + 24A_2 + 6R = a(a+1)\rho\phi^2 + r(\phi) \tag{5.41}$$

where where $r'(\phi) = q(\phi)$.

We can now obtain the following:

$$A_0 = \rho + a(a+1)\rho\phi^2 + r(\phi) + R - (2 + \frac{1}{2}a)\rho\phi \tag{5.42}$$

$$A_1 = \frac{4}{9}a\rho\phi - \frac{2}{9}a(a+1)\rho\phi^2 - \frac{2}{9}r(\phi) - \frac{4}{3}R \tag{5.43}$$

$$A_2 = \frac{1}{18}a(a+1)\rho\phi^2 - \frac{1}{36}a\rho\phi + \frac{1}{18}r(\phi) - \frac{1}{6}R \tag{5.44}$$

$$L = \frac{1}{3}(1-a)\rho\phi - 2R \tag{5.45}$$

The order $O(v^1, B^0)$ contributions to the equilibrium distribution obey the following:

$$3F_1 + 6F_2 + 6T7 = \rho \tag{5.46}$$

$$\frac{3}{2}F_1 + 12F_2 + 6T = (a+1)\rho\phi \tag{5.47}$$

$$\tau\left(\frac{3}{4}F_1 + 6F_2 + \frac{3}{2}T\right) = \mu = \lambda + a(a+1)\rho\phi \tag{5.48}$$

$$\frac{\partial}{\partial\rho}\left(\frac{3}{4}F_1 + 6F_2 + \frac{3}{2}T\right) = a\phi \tag{5.49}$$

$$\frac{\partial}{\partial\phi}\left(\frac{3}{4}F_1 + 6F_2 + \frac{3}{2}T\right) = a\rho \tag{5.50}$$

By similar reasoning to the above, we arrive at the viscosity constraints

$$\mu = a\tau\rho\phi \tag{5.51}$$

$$\lambda = -a^2\tau\rho\phi \tag{5.52}$$

and

$$F_1 = \frac{4}{9}\rho + \frac{2}{9}(a-3)\rho\phi \tag{5.53}$$

$$F_2 = \frac{2}{9}a\rho\phi - \frac{1}{18}\rho \tag{5.54}$$

$$T = \frac{1}{3}(1-a)\rho\phi \tag{5.55}$$

Applying the same procedure to the terms of order $O(v^0, B^1)$, we get

$$3P + 6U = 1 \tag{5.56}$$

$$\tau U\left[\frac{9}{2}\partial_i B_j - \frac{3}{2}\partial_j B_i - \frac{3}{2}\partial_k B_k \delta_{ij}\right] = \eta\partial_i B_j - \eta_1 \partial_j B_i - \eta_2 \partial_k B_k \delta_{ij} \tag{5.57}$$

Notice that this does not, in fact give us the correct resistivity tensor, which should be

$$\Lambda_{ij}^{(1)} = \eta\left(\partial_i B_j - \partial_j B_i\right)$$

ie. $\eta_1 = \eta$. However, if gradients in the resistivity are negligible, then when the expressions are substituted into the induction equation, the unphysical terms will vanish since $\nabla \cdot \mathbf{B} = 0$. It is possible to obtain the correct form for the resistive tensor (with the assumption that $\nabla \cdot \mathbf{B} = 0$) with a more general choice of particle states. However, for the choices which were investigated, it was found that the magnetic monopole charge density (which physically should vanish) obeyed a diffusion equation with a negative diffusion coefficient, thus creating numerical instabilities.

In addition, we have the constraints that

$$\frac{9}{2}\nabla U = a\nabla\phi + \frac{a\phi}{\rho}\nabla\rho \tag{5.58}$$

If this is to be obeyed exactly, then we must have

$$\frac{9}{2}\frac{\partial U}{\partial \rho} = a\frac{\phi}{\rho} \tag{5.59}$$

$$\frac{9}{2}\frac{\partial U}{\partial \phi} = a \tag{5.60}$$

Since the operators $\frac{\partial}{\partial\rho}$ and $\frac{\partial}{\partial\phi}$ should commute, then this would imply that

$$\frac{\partial}{\partial\phi}\left(\frac{\phi}{\rho}\right) = \frac{\partial 1}{\partial\rho}$$

which is false. However, recall that lattice Boltzmann methods are usually restricted to low Mach number flows, so that the variations in the density are small and we can write

$$\frac{9}{2}\nabla U = \frac{\nabla(a\rho\phi)}{\rho} \approx \frac{\nabla(a\rho\phi)}{\rho_0} \tag{5.61}$$

where ρ_0 is the mean density. Thus

$$\frac{9}{2}U = \frac{\eta}{\tau} = \frac{a\rho\phi}{\rho_0} + \text{constant} \tag{5.62}$$

Therefore, we have

$$P = \frac{1}{3}\left(1 - \frac{4\eta}{3\tau}\right) \tag{5.63}$$

$$U = \frac{2\eta}{9\tau} \tag{5.64}$$

Considering the terms of order $O(v^2, B^0)$ we get

$$\begin{aligned} C_0 + 6C_1 + 3G_1 + 6C_2 + 3G_2 &= 0 && (5.65)\\ 3C_1 + \frac{3}{2}G_1 + 12C_2 + 6G_2 &= \frac{1}{2}\rho && (5.66)\\ 6C_1 + 3G_1 + 24C_2 + 12G_2 &= \rho && (5.67)\\ \frac{3}{2}G_1 + 6G_2 &= \rho && (5.68) \end{aligned}$$

from the zeroth order contributions to the moments and

$$\begin{aligned} &3C_1 v_j \partial_i v_j + \frac{3}{4}G_1\left(v_j\partial_j v_i + v_j\partial_i v_j + v_i\partial_j v_j\right) + 48C_2 v_j\partial_i v_j \\ &\quad +12G_2\left(v_j\partial_j v_i + v_j\partial_i v_j + v_i\partial_j v_j\right) = \\ &\quad \frac{\mu}{\tau}v_j\partial_i v_j + \left(\frac{\mu}{\tau} + (a+1)\rho\phi\right)v_j\partial_j v_i + \left(\frac{\lambda}{\tau} + (a+1)^2\rho\phi\right)v_i\partial_j v_j \end{aligned} \tag{5.69}$$

$$\begin{aligned} &\frac{3}{2}v^2\partial_i C_1 + \left(\frac{3}{8}v^2\partial_i + \frac{3}{4}v_i v_j\partial_j\right)G_1 \\ &\quad +24v^2\partial_i C_2 + \left(6v^2\partial_i + 12v_i v_j\partial_j\right)G_2 = (2a+1)v_i v_j\partial_j(\rho\phi) + \frac{1}{2}av^2\partial_i(\rho\phi) \end{aligned} \tag{5.70}$$

from the first order contributions to the heat flux. These give us

$$3C_1 + \frac{3}{4}G_1 + 48C_2 + 12G_2 = \frac{\mu}{\tau} = a\rho\phi \tag{5.71}$$

$$\frac{3}{4}G_1 + 12G_2 = \frac{\mu}{\tau} + (a+1)\rho\phi = (2a+1)\rho\phi \tag{5.72}$$

Which upon solving:

$$\begin{aligned} C_0 &= \frac{1}{2}(3a+1)\rho\phi - \frac{5}{4}\rho && (5.73)\\ C_1 &= \frac{1}{9}(a+1)\rho\phi - \frac{2}{9}\rho && (5.74)\\ C_2 &= \frac{1}{72}\rho - \frac{1}{36}(a+1)\rho\phi && (5.75)\\ G_1 &= \frac{8}{9}\rho - \frac{4}{9}(2a+1)\rho\phi && (5.76)\\ G_2 &= \frac{1}{9}(2a+1)\rho\phi - \frac{1}{18}\rho && (5.77) \end{aligned}$$

The terms of order (v^1, B^1) have already been chosen to satisfy the constraints, as this part of the problem is essentially the same as that for the non-thermal model. The $O(v^0, B^2)$ terms give

$$\begin{aligned} D_0 + 6D_1 + 6D_2 + 6N + 12S + 6V_1 + 6V_2 &= 0 && (5.78)\\ 3D_1 + 12D_2 + 12S + 6V_1 + 15V_2 &= \frac{1}{2} && (5.79)\\ 6D_1 + 24D_2 + 12S + 6V_1 + 24V_2 &= 0 && (5.80)\\ -3V_1 + 12V_2 &= -1 && (5.81) \end{aligned}$$

$$\begin{aligned} &(3D_1 + 48D_2 + 12S)B_j\partial_i B_j + 3V_1\left(3B_j\partial_i B_j - B_j\partial_j B_i - B_i\partial_j B_j\right)\\ &+30V_2\left(B_j\partial_i B_j + B_j\partial_j B_i + B_i\partial_j B_j\right) = \left(\frac{\eta}{\tau} + (a+1)\phi\right)\left(B_j\partial_i B_j - B_j\partial_j B_i\right) \end{aligned} \quad (5.82)$$

so that

$$\begin{aligned} 3D_1 + 48D_2 + 12S + 9V_1 + 30V_2 &= \frac{\eta}{\tau} + (a+1)\phi && (5.83)\\ 3V_1 - 30V_2 &= \frac{\eta}{\tau} + (a+1)\phi && (5.84) \end{aligned}$$

The further constraint that

$$\begin{aligned} &B^2\partial_i\left(\frac{3}{2}D_1 + 24D_2 + 6S + \frac{9}{2}V_1 + 15V_2\right)\\ &+B_iB_j\partial_j\left(30V_2 - 3V_1\right) = \frac{aB^2}{\rho}\partial_i(\rho\phi) - \frac{B_i}{\rho}B_j\partial_j(\rho\phi) \end{aligned} \quad (5.85)$$

turns out to be inconsistent with the previous constraints. The main effect of the inability to satisfy this constraint is to introduce an anistropic thermal diffusion, with the diffusion enhanced in the direction orthogonal to the magnetic field. However, for large plasma β, where the Alfvén speed is small compared to the sound speed, this effect should not be important.

Writing $\eta' = \eta/\tau + (a+1)\phi$ for short hand, a solution for the unkowns is

$$\begin{aligned} D_0 &= -\frac{1+\eta'}{2} && (5.86)\\ D_1 &= 0 && (5.87)\\ D_2 &= \frac{\eta' - 1}{12} && (5.88)\\ N &= \frac{\eta'}{6} && (5.89)\\ S &= \frac{\eta' - 4}{18} && (5.90)\\ V_1 &= \frac{5 - 2\eta'}{9} && (5.91)\\ V_2 &= \frac{1 - \eta'}{18} && (5.92) \end{aligned}$$

The order $O(v^3, B^0)$ constraints are

$$\frac{9}{4}H_1 + \frac{9}{2}H_2 = 0 \tag{5.93}$$

$$\frac{9}{8}H_1 + 9H_2 = \frac{\rho}{2} \tag{5.94}$$

The order $O(v^3)$ contributions to the viscous tensor are small at low Mach number, so may be neglected. Thus we have

$$H_1 = -\frac{4}{27}\rho \tag{5.95}$$

$$H_2 = \frac{2}{27}\rho \tag{5.96}$$

Finally, the constraints of order $O(v^1, B^2)$ are

$$3J_1 + 6J_2 = 0 \tag{5.97}$$

$$\frac{3}{2}J_1 + 12J_2 = 1 \tag{5.98}$$

$$3K_1 + 6K_2 = 0 \tag{5.99}$$

$$\frac{3}{2}K_1 + 12K_2 = -1 \tag{5.100}$$

so that

$$J_1 = -\frac{2}{9} \tag{5.101}$$

$$J_2 = \frac{1}{9} \tag{5.102}$$

$$K_1 = \frac{2}{9} \tag{5.103}$$

$$K_2 = -\frac{1}{9} \tag{5.104}$$

5.2.4 Magnetosonic waves

In order to test our thermal MHD lattice Boltzmann model, we shall use it to model magnetosonic waves in a homogenous plasma. As with the Alfvén waves of section 3.2.1, the dispersion relation is derived by considering small, linearised perturbations about a homogenous, static equilibrium, thus:

$$\begin{aligned}
\frac{\partial \rho_1}{\partial t} + \rho_0 \nabla \cdot \mathbf{v}_1 &= 0 \\
\rho_0 \frac{\partial \mathbf{v}_1}{\partial t} &= -\nabla (p_1 + \mathbf{B}_0 \cdot \mathbf{B}_1) + \mathbf{B}_0 \cdot \nabla \mathbf{B}_1 \\
\frac{\partial \mathbf{B}_1}{\partial t} &= \mathbf{B}_0 \cdot \nabla \mathbf{v}_1 - \mathbf{B}_0 \nabla \cdot \mathbf{v}_1 \\
\rho_0 \frac{\partial \phi_1}{\partial t} &= -p_0 \nabla \cdot \mathbf{v}_1 \\
p_1 &= a(\rho_0 \phi_1 + \phi_0 \rho_1)
\end{aligned} \tag{5.105}$$

where the subscript 0 refers to the unperturbed field and the subscript 1 refers to the perturbation. The usual Fourier analysis in which the perturbations are assumed to be proportional to $e^{i(\mathbf{k}\cdot\mathbf{x}-\omega t)}$ reveals three types of wave. One is the incompressible Alfvén wave, the other two are compressible modes and obey the dispersion relation

$$\left(\frac{\omega}{k}\right)^2 = \frac{1}{2}\left(c_S^2 + v_A^2 \pm \sqrt{(c_S^2+v_A^2)^2 - 4c_S^2 v_A^2 \cos\theta}\right) \tag{5.106}$$

where $c_S = \sqrt{a(a+1)\phi_0}$ is the speed of sound, $v_A = B_0/\sqrt{\rho_0}$ is the Alfvén speed and θ is the angle between the wave vector $\mathbf{k}$ and the ambient magnetic field $\mathbf{B}_0$. The two solutions correspond to two different couplings of the Alfvén and acoustic modes and have quite different properties. The magnetic pressure plays a similar role to the kinetic pressure. In the fast magnetosonic wave, they fluctuate in phase, thereby increasing the speed of the compressional wave, whilst in the slow magnetosonic wave, they fluctuate in anti-phase, thus decreasing the speed. In fact, the variations in magnetic and kinetic pressure exactly balance in the slow magnetosonic mode when the wave vector is perpendicular to the ambient magnetic field, and since the magnetic tension also vanishes in this situation, the plasma is in static equilibrium. Thus the slow magnetosonic mode does not propagate perpendicular to the ambient magnetic field. Depending on whether $v_A > c_S$ or $v_A < c_S$, either the fast or the slow magnetosonic mode respectively is a modified Alfvén wave, and if $\mathbf{k}$ is parallel to $\mathbf{B}_0$, then the mode does not vibrate longitudinally and is degenerate with the incompressible Alfvén wave. If $v_A > c_S$, then, unlike the incompressible Alfvén wave, the compressible Alfvén wave can propagate perpendicular to the ambient magnetic field and if $v_A \gg c_S$, then this wave is just like a sound wave, but with the magnetic pressure replacing the role of the fluid pressure.

Figures 5.1- 5.6 show the results of various simulations of magnetosonic waves. In all cases the initial conditions were chosen so that the perturbed fields were proportional to $\sin kx$ and that either a pure fast or slow wave would travel in the positive x direction. The graphs show how the values of the perturbed fields at the point $x = 0$ varies with time. The values of the varies physical parameters were $\rho_0 = 1$, $\phi_0 = 0.3, 0.1$, $\mathbf{B} = (0,0), (0,0.3), (0.3,0.3), (1/3,1/3)$, $a = 1, 2/3$ and $\mathbf{k} = (\pi/50, 0)$. The numerical parameters were $\Delta x = 1$, $\Delta t = \tau = 0.01$, the small value of τ ensuring that dissipation effects are negligible. If dissipation (ie viscosity, resistivity, thermal diffusivity) is included, then the dispersion relation becomes very complicated, and so we have chosen to neglect them here. All the results show good agreement between the lattice Boltzmann model (□ symbols) and the analytic solution (solid lines).

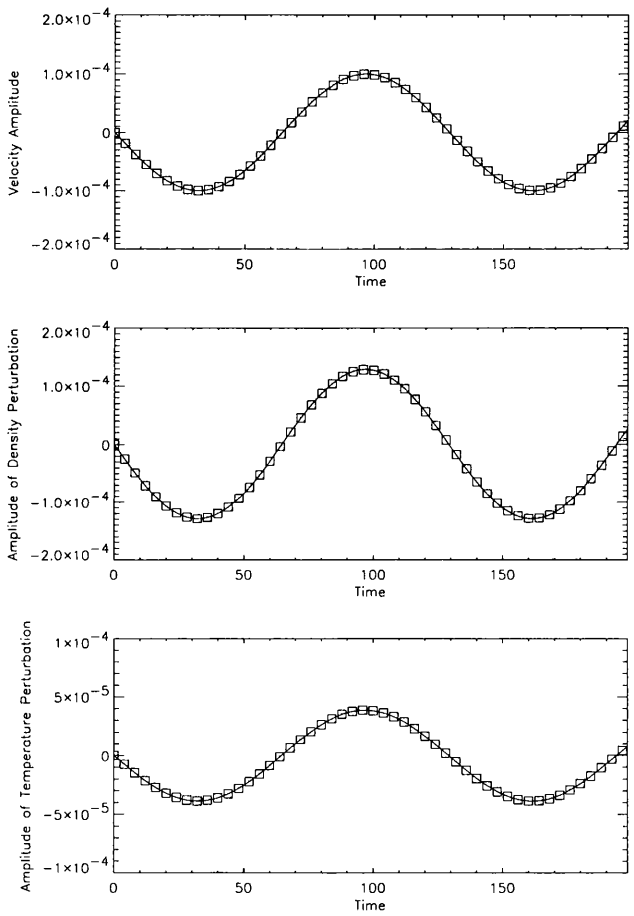

Figure 5.1: These graphs show the oscillations in the perturbed fields of a sound wave at a particular point in space. $\rho_0 = 1$, $B_0 = (0,0)$, $\phi_0 = 0.3$. The phase speed is 0.77. The analytic solution is shown by the solid line, the lattice Boltzmann results by the $\square$ symbol.

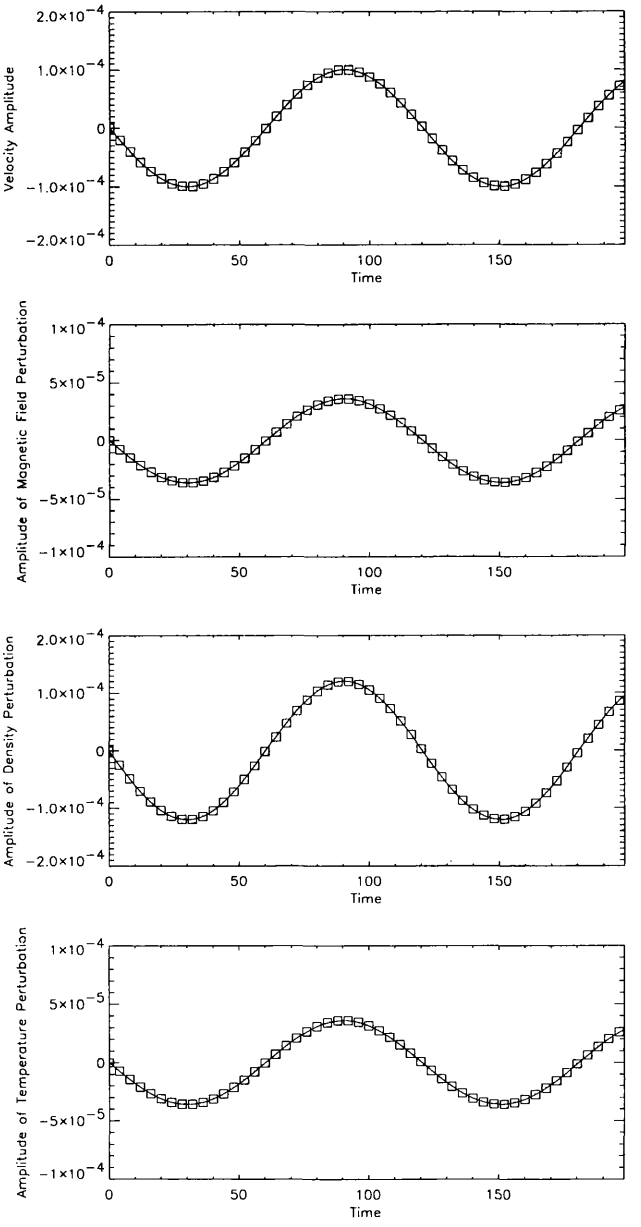

Figure 5.2: The oscillations of the perturbed fields in a fast magnetosonic wave at high β. $\rho_0 = 1$, $B_0 = (0, 0.3)$, $\phi_0 = 0.3$. The phase speed is 0.830

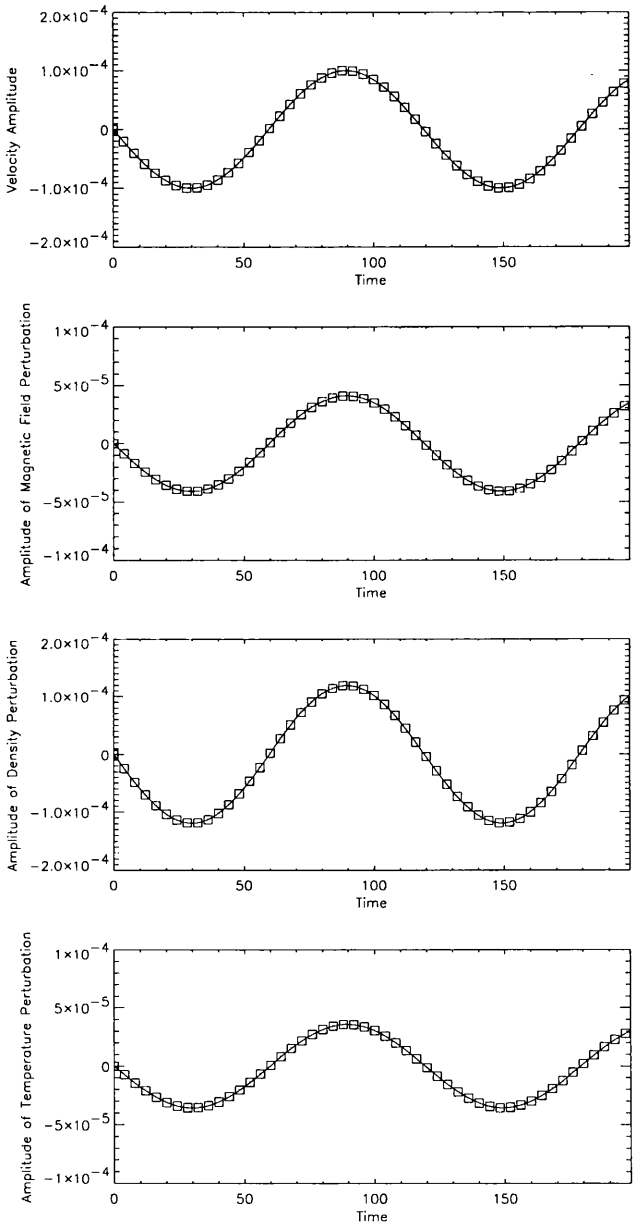

Figure 5.3: The oscillations of the perturbed fields in a fast magnetosonic wave at high β. $\rho_0 = 1$, $B_0 = (0.3, 0.3)$, $\phi_0 = 0.3$. The phase speed is 0.838, only slightly different from the simulations of figure 5.2. The similarity of these graphs with figures 5.1, 5.2 demonstrates that when the sound speed is large compared to the Alfvén speed, the fast magnetosonic wave propagates almost isotropically like a sound wave in an unmagnetised plasma.

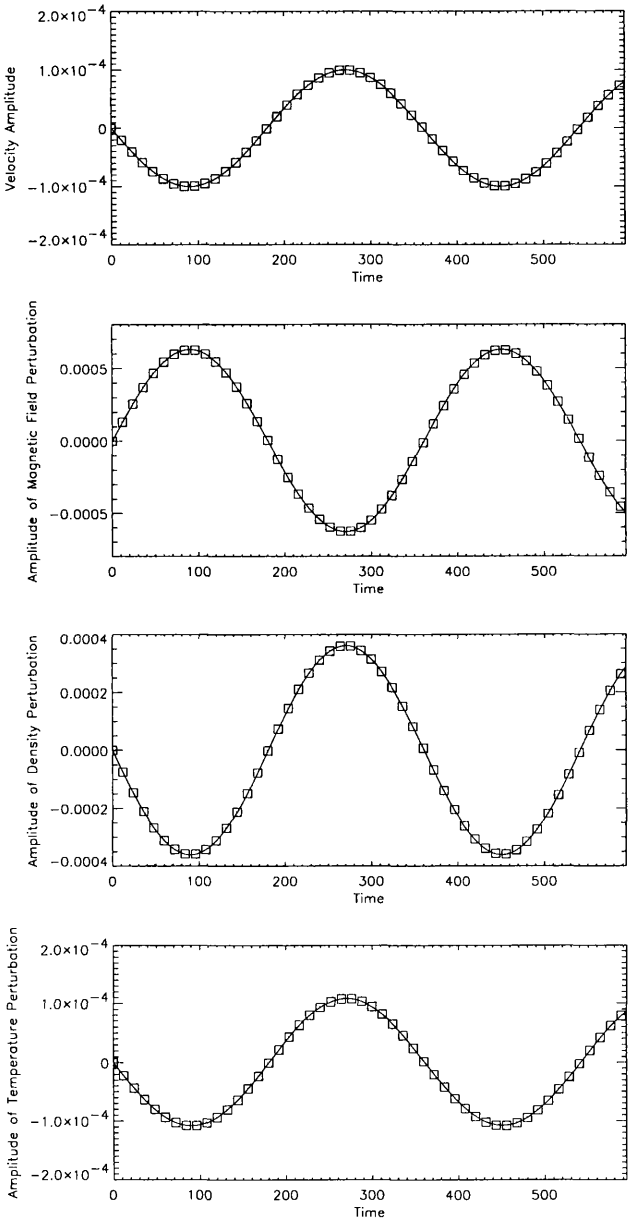

Figure 5.4: The oscillations of the perturbed fields in a slow magnetosonic wave at high β. The parameters are the same as the simulations in figure 5.3. The phase speed is 0.39.

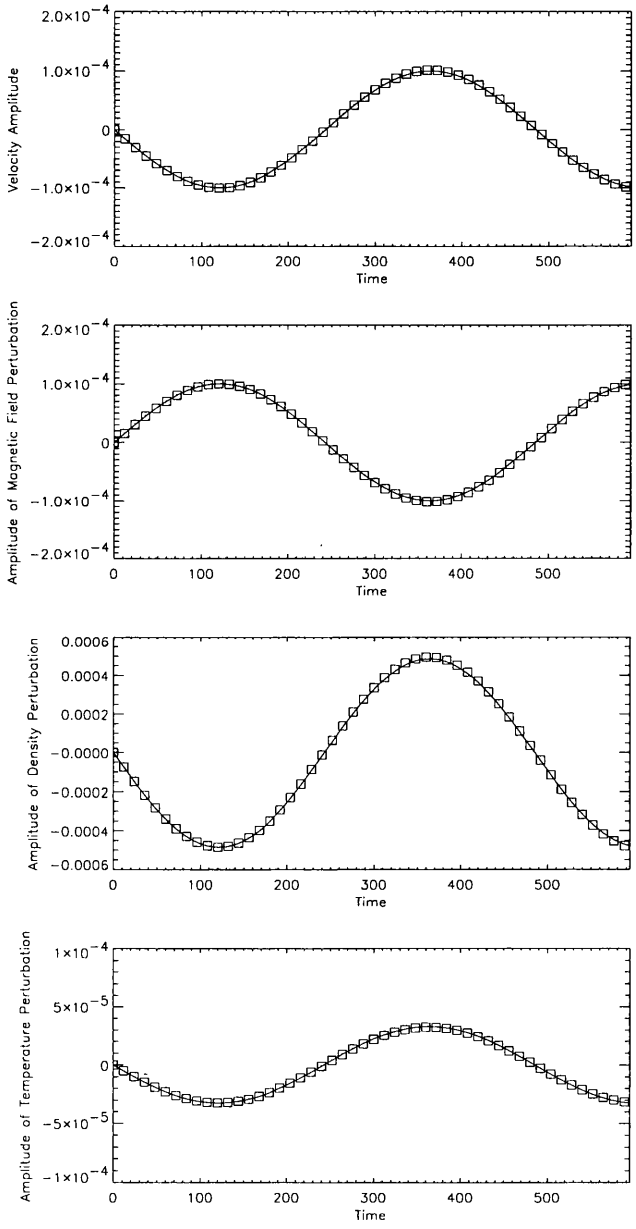

Figure 5.5: The oscillations of the perturbed fields in a fast magnetosonic wave at low β. $\rho_0 = 1$, $B_0 = (0.333, 0.333)$, $\phi_0 = 0.1$. The phase speed is 0.60.

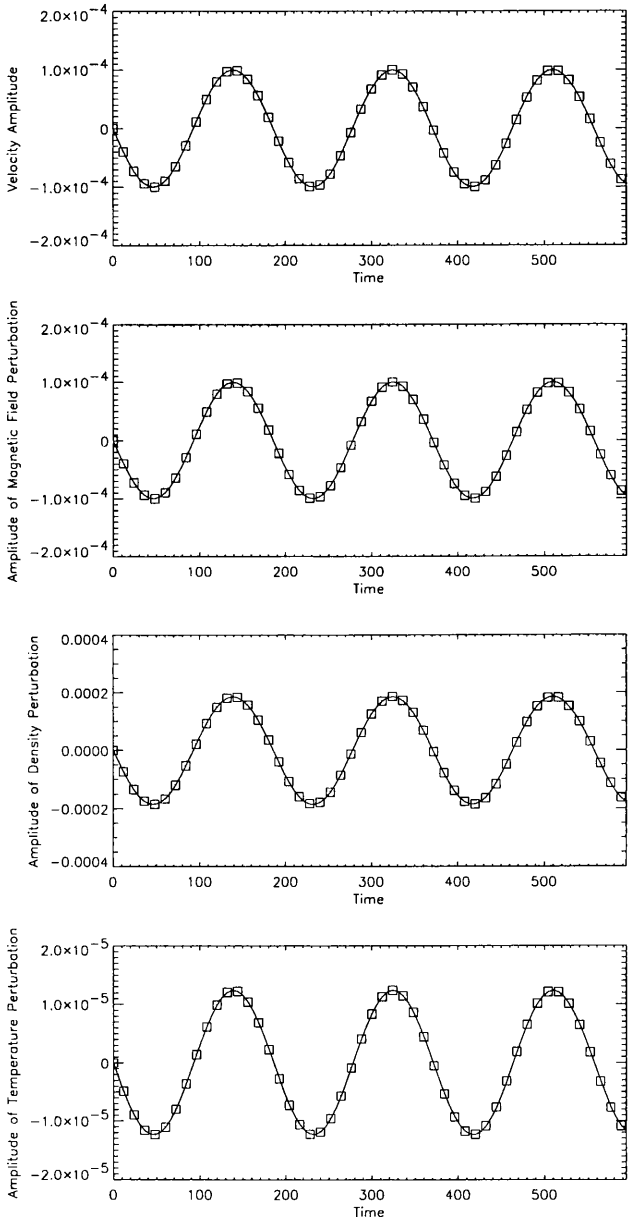

Figure 5.6: The oscillations of the perturbed fields in a slow magnetosonic wave at low β. $\rho_0 = 1$, $B_0 = (0.333, 0.333)$, $\phi_0 = 0.1$. The phase speed is 0.25.

5.3 Three Dimensional Lattice Boltzmann MHD

Having established that the lattice Boltzmann method can be applied to two dimensional MHD, it is worth asking whether the method can be generalised to three dimensions. As remarked in section 2.3.4, there are no three dimensional lattices which allow isotropic transport with a one speed model. The original three dimensional lattice gas model used a 4D face-centered, hypercubic lattice projected onto a 3D hypersurface [36]. Later work [37] showed that a multi-speed 3D lattice was more efficient and this is the approach we shall use here.

On this lattice the vectors are $(\pm 1, \pm 1, \pm 1)$ and permutations of $(\pm 1, 0, 0)$. As in the 2D model, the moving particle states are characterised by pairs of lattice vectors $\mathbf{e}_a, \mathbf{e}_b$, chosen so that $\mathbf{e}_a \cdot \mathbf{e}_b > 0$ and $a \neq b$, giving a total of 48 moving states. The moving particles are divided into two classes; class I particles have distribution function f_{ab} and $|\mathbf{e}_a| = 1$; class II particles have distribution function g_{ab} and $|\mathbf{e}_a| = \sqrt{3}$.

5.3.1 Microscopic dynamics

The updating rules are a direct generalisation of the single streaming two-dimensional model:

$$f_{ab}(\mathbf{x}, t) = f_{ab}(\mathbf{x} - e_a, t - 1) + \Omega_{1ab}(\mathbf{x} - e_a, t - 1) \tag{5.107}$$

$$g_{ab}(\mathbf{x}, t) = g_{ab}(\mathbf{x} - e_a, t - 1) + \Omega_{2ab}(\mathbf{x} - e_a, t - 1) \tag{5.108}$$

where

$$\Omega_{1ab} = -\frac{1}{\tau}(f_{ab} - f_{ab}^{(\mathrm{eq})}). \tag{5.109}$$

$$\Omega_{2ab} = -\frac{1}{\tau}(g_{ab} - g_{ab}^{(\mathrm{eq})}). \tag{5.110}$$

As usual, we choose f, g to be quadratic in the lattice vectors:

$$f_{ab}^{(\mathrm{eq})} = c^{(1)} + \mathbf{c}^{(2)} \cdot \mathbf{e}_a + \mathbf{c}^{(3)} \cdot \mathbf{e}_b + \mathbf{c}^{(4)} : \mathbf{e}_a\mathbf{e}_a + \mathbf{c}^{(5)} : \mathbf{e}_a\mathbf{e}_b + \mathbf{c}^{(6)} : \mathbf{e}_b\mathbf{e}_b \tag{5.111}$$

$$g_{ab}^{(\mathrm{eq})} = d^{(1)} + \mathbf{d}^{(2)} \cdot \mathbf{e}_a + \mathbf{d}^{(3)} \cdot \mathbf{e}_b + \mathbf{d}^{(4)} : \mathbf{e}_a\mathbf{e}_a + \mathbf{d}^{(5)} : \mathbf{e}_a\mathbf{e}_b + \mathbf{d}^{(6)} : \mathbf{e}_b\mathbf{e}_b \tag{5.112}$$

5.3.2 Macroscopic variables and conditions on the equilibrium distribution

The macroscopic variables are defined thus:

$$\rho = f_0 + \sum_{a,b} f_{ab} + \sum_{a,b} g_{ab} \tag{5.113}$$

$$\rho\mathbf{v} = \sum_{a,b} f_{ab}\mathbf{e}_a + \sum_{a,b} g_{ab}\mathbf{e}_a \tag{5.114}$$

$$\rho\mathbf{B} = \sum_{a,b} f_{ab}\left[r_1\mathbf{e}_a + q_1\mathbf{e}_b\right] + \sum_{a,b} g_{ab}\left[r_2\mathbf{e}_a + q_2\mathbf{e}_b\right] \tag{5.115}$$

$$\mathbf{\Pi} = \sum_{a,b} f_{ab}\mathbf{e}_a\mathbf{e}_a + \sum_{a,b} g_{ab}\mathbf{e}_a\mathbf{e}_a \tag{5.116}$$

$$\mathbf{\Lambda} = \sum_{a,b} f_{ab}\mathbf{B}^{\mathrm{I}}_{ab}\mathbf{e}_a + \sum_{a,b} g_{ab}\mathbf{B}^{\mathrm{II}}_{ab}\mathbf{e}_a \tag{5.117}$$

where $\mathbf{B}^{\mathrm{I}}_{ab} = r_1\mathbf{e}_a + q_1\mathbf{e}_b$ and $\mathbf{B}^{\mathrm{II}}_{ab} = r_2\mathbf{e}_a + q_2\mathbf{e}_b$.

Inserting the expressions 5.107, 5.108 into equations 5.113,..., 5.117 we get the following constraints on $c^{(1)}, \ldots, \mathbf{c}^{(6)}, d^{(1)}, \ldots, \mathbf{d}^{(6)}$:

$$\rho = f_0^{(\mathrm{eq})} + 24c^{(1)} + 8\mathrm{tr}\mathbf{c}^{(4)} + 8\mathrm{tr}\mathbf{c}^{(5)} + 24\mathrm{tr}\mathbf{c}^{(6)} + 24d^{(1)} + 24\mathrm{tr}\mathbf{d}^{(4)} + 8\mathrm{tr}\mathbf{d}^{(5)} + 8\mathrm{tr}\mathbf{d}^{(6)} \tag{5.118}$$

$$\rho\mathbf{v} = 8\mathbf{c}^{(2)} + 8\mathbf{c}^{(3)} + 24\mathbf{d}^{(2)} + 8\mathbf{d}^{(3)} \tag{5.119}$$

$$\rho\mathbf{B} = (8q_1 + 8r_1)\mathbf{c}^{(2)} + (24q_1 + 8r_1)\mathbf{c}^{(3)} + (8q_2 + 24r_2)\mathbf{d}^{(2)} + (8q_2 + 8r_1)\mathbf{d}^{(3)} \tag{5.120}$$

$$\begin{aligned}\mathbf{\Pi} = &\left[8c^{(1)} + 8\mathrm{tr}\mathbf{c}^{(6)} + 24d^{(1)} + 24\mathrm{tr}\mathbf{d}^{(4)} + 8\mathrm{tr}\mathbf{d}^{(5)} + \mathrm{tr}\mathbf{d}^{(6)}\right]\mathbf{I} \\ &+48\mathbf{d}^{(4)} + 16S(\mathbf{d}^{(5)}) + 8D(\mathbf{c}^{(4)}) + 8D(\mathbf{c}^{(5)}) - 48D(\mathbf{d}^{(4)}) - 16D(\mathbf{d}^{(5)})\end{aligned} \tag{5.121}$$

$$\begin{aligned}\mathbf{\Lambda} = &\left[\,(8q_1 + 8r_1)c^{(1)} + (8q_1 + 8r_1)\mathrm{tr}\mathbf{c}^{(6)} + (8q_2 + 24r_2)d^{(1)}\right. \\ &\left.+(8q_2 + 24r_2)\mathrm{tr}\mathbf{d}^{(4)} + 8r_2\mathrm{tr}\mathbf{d}^{(5)} + 8r_2\mathrm{tr}\mathbf{d}^{(6)}\,\right]\mathbf{I} \\ &+8q_1S(\mathbf{c}^{(5)}) + 16q_1\mathbf{c}^{(6)} + (16q_2 + 48r_2)\mathbf{d}^{(4)} + (8q_2 + 16r_2)S(\mathbf{d}^{(5)}) \\ &+ - 8q_1A(\mathbf{c}^{(5)}) - 8q_2A(\mathbf{d}^{(5)}) \\ &+8(q_1 + r_1)D(\mathbf{c}^{(4)}) + 8r_1D(\mathbf{c}^{(5)}) - 16q_1D(\mathbf{c}^{(6)}) \\ &-16(q_2 + 3r_2)D(\mathbf{d}^{(4)}) + 8(q_2 - r_2)D(\mathbf{d}^{(5)}) + 8(q_2 - r_2)D(\mathbf{d}^{(6)})\end{aligned} \tag{5.122}$$

where $S(M)$, $A(M)$ and $D(M)$ are the symmetric, anti-symmetric and leading diagonal parts of a matrix M respectively.

Following the same line of argument as section 2.4.2, we require that equations 2.65, 2.66 are obeyed. On inspection of the forms of $\mathbf{\Pi}^{(0)}$ and $\mathbf{\Lambda}^{(0)}$ it is clear that the 2nd rank tensors should be linear combinations of $(P + \frac{1}{2}\rho B^2)\mathbf{I}$, $\rho(\mathbf{vv} - \mathbf{BB})$, $\rho(\mathbf{Bv} - \mathbf{vB})$.

In order that there be no pressure like term in $\mathbf{\Lambda}$, we must have:

$$(8q_1 + 8r_1)c^{(1)} + (8q_2 + 24r_2)d^{(2)} = 0 \tag{5.123}$$

which can be satisfied if

$$q_1 = -r_1 \tag{5.124}$$

$$q_2 = -3r_2 \tag{5.125}$$

To eliminate the anisotropic components of $\mathbf{\Pi}, \mathbf{\Lambda}$:

$$8D(\mathbf{c}^{(4)}) + 8D(\mathbf{c}^{(5)}) - 48D(\mathbf{d}^{(4)}) - 16D(\mathbf{d}^{(5)}) = 0 \tag{5.126}$$

$$\begin{aligned} &8(q_1 + r_1)D(\mathbf{c}^{(4)}) + 8r_1 D(\mathbf{c}^{(5)}) - 16q_1 D(\mathbf{c}^{(6)}) \\ &-16(q_2 + 3r_2)D(\mathbf{d}^{(4)}) + 8(q_2 - r_2)D(\mathbf{d}^{(5)}) + 8(q_2 - r_2)D(\mathbf{d}^{(6)}) = 0 \end{aligned} \tag{5.127}$$

$\mathbf{\Lambda}$ should be anti-symmetric:

$$8q_1 S(\mathbf{c}^{(5)}) + 16q_1 \mathbf{c}^{(6)} + (16q_2 + 48r_2)\mathbf{d}^{(4)} + (8q_2 + 16r_2)S(\mathbf{d}^{(5)}) = 0 \tag{5.128}$$

$\mathbf{\Lambda}$ should contain no pressure like terms dependant on $\rho v^2, \rho B^2$:

$$(8q_1 + 8r_1)\mathbf{c}^{(6)} + (8q_2 + 24r_2)\mathbf{d}^{(4)} + 8r_2 S(\mathbf{d}^{(5)}) + 8r_2 \mathbf{d}^{(6)} = 0 \tag{5.129}$$

which, after inserting 5.124 and 5.125 becomes

$$S(\mathbf{d}^{(5)}) + \mathbf{d}^{(6)} = 0 \tag{5.130}$$

For the term $\rho(\mathbf{vv} - \mathbf{BB})$ in $\mathbf{\Pi}^{(0)}$ we must have:

$$48\mathbf{d}^{(4)} + 16S(\mathbf{d}^{(5)}) = \rho(\mathbf{vv} - \mathbf{BB}) \tag{5.131}$$

for $\mathbf{\Lambda} = \rho(\mathbf{Bv} - \mathbf{vB})$ we must have:

$$-8q_1 A(\mathbf{c}^{(5)}) - 8q_2 A(\mathbf{d}^{(5)}) = \rho(\mathbf{Bv} - \mathbf{vB}) \tag{5.132}$$

and for the pressure term in $\mathbf{\Pi}$

$$8c^{(1)} + 8\mathrm{tr}\mathbf{c}^{(6)} + 24d^{(1)} + 24\mathrm{tr}\mathbf{d}^{(4)} + 8\mathrm{tr}\mathbf{d}^{(5)} + \mathrm{tr}\mathbf{d}^{(6)} = P + \frac{1}{2}\rho B^2 \tag{5.133}$$

A particular solution of the above equations is

$$\mathbf{c}^{(4)} = 0 \tag{5.134}$$

$$S(\mathbf{c}^{(5)}) = \frac{\rho}{8}(\mathbf{vv} - \mathbf{BB}) \tag{5.135}$$

$$\mathbf{c}^{(6)} = -\frac{\rho}{16}(\mathbf{vv} - \mathbf{BB}) \tag{5.136}$$

$$\mathbf{d}^{(4)} = \frac{\rho}{48}(\mathbf{vv} - \mathbf{BB}) \tag{5.137}$$

$$S(\mathbf{d}^{(5)}) = 0 \tag{5.138}$$

$$\mathbf{d}^{(6)} = 0 \tag{5.139}$$

$$A(\mathbf{c}^{(5)}) = -\frac{\rho}{16q_1}(\mathbf{Bv} - \mathbf{vB}) \tag{5.140}$$

$$A(\mathbf{d}^{(5)}) = -\frac{\rho}{16q_2}(\mathbf{Bv} - \mathbf{vB}) \tag{5.141}$$

Inserting these expressions in equations 5.118 and 5.133 give us

$$f_0^{(\mathrm{eq})} + 24c^{(1)} + 24d^{(1)} = \rho \tag{5.142}$$

$$8c^{(1)} + 24d^{(1)} = c_s^2 P + \frac{1}{2}\rho B^2 \tag{5.143}$$

of which a particular solution is

$$f_0^{(\mathrm{eq})} = 0 \tag{5.144}$$

$$c^{(1)} = \frac{1}{16}\rho\left(1 - c_s^2 - \frac{1}{2}B^2\right) \tag{5.145}$$

$$d^{(1)} = \frac{1}{16}\rho\left(c_s^2 + \frac{1}{2}B^2 - \frac{1}{3}\right) \tag{5.146}$$

5.3.3 Transport Coefficients

Following the procedure established in section 2.4.3, the transport terms are given by:

$$\mathbf{\Pi}^{(1)} = \left(1 - \frac{1}{2\tau}\right)\left[\sum \mathbf{e}_a^{(\mathrm{I})}\mathbf{e}_a^{(\mathrm{I})} f_{ab}^{(1)} + \sum \mathbf{e}_a^{(\mathrm{II})}\mathbf{e}_a^{(\mathrm{II})} g_{ab}^{(1)}\right] \tag{5.147}$$

$$\mathbf{\Lambda}^{(1)} = \left(1 - \frac{1}{2\tau}\right)\left[\sum \mathbf{B}_{ab}^{\mathrm{I}}\mathbf{e}_a^{(\mathrm{I})} f_{ab}^{(1)} + \sum \mathbf{B}_{ab}^{\mathrm{II}}\mathbf{e}_a^{(\mathrm{II})} g_{ab}^{(1)}\right] \tag{5.148}$$

where

$$f_{ab}^{(1)} = -\tau\left[\frac{\partial}{\partial t} + \mathbf{e}_a^{(\mathrm{I})} \cdot \nabla\right] f_{ab}^{(0)}$$

$$g_{ab}^{(1)} = -\tau\left[\frac{\partial}{\partial t} + \mathbf{e}_a^{(\mathrm{II})} \cdot \nabla\right] g_{ab}^{(0)} \tag{5.149}$$

Evaluation of these expressions gives us

$$\nabla \cdot \mathbf{\Pi}^{(1)} = -\left(\tau - \frac{1}{2}\right)[\, \frac{\partial \nabla \cdot \mathbf{\Pi}^{(0)}}{\partial t} + 24\nabla^2 \mathbf{d}^{(2)} + 8\nabla^2 \mathbf{d}^{(3)} + 48\nabla\nabla \cdot \mathbf{d}^{(2)}$$
$$+16\nabla\nabla \cdot \mathbf{d}^{(3)} + \delta_{ijkl}\partial_j\partial_k(8\mathbf{c}_l^{(2)} - 48\mathbf{d}_l^{(2)} + 8\mathbf{c}_l^{(3)} - 16\mathbf{d}_l^{(2)}\,] \tag{5.150}$$

$$\nabla \cdot \mathbf{\Lambda}^{(1)} = -\left(\tau - \frac{1}{2}\right)[\, \frac{\partial \nabla \cdot \mathbf{\Lambda}^{(0)}}{\partial t} - 8r_1\nabla^2 \mathbf{c}^{(3)} - 16r_2\nabla^2 \mathbf{d}^{(3)} + 16r_2\nabla\nabla \cdot \mathbf{d}^{(3)}$$
$$+\delta_{ijkl}\partial_j\partial_k(8r_1\mathbf{c}_l^{(3)} - 16r_2\mathbf{d}_l^{(3)})\,] \tag{5.151}$$

where $\delta_{ijkl} = 1$ if $i = j = k = l$, and 0 otherwise.

These equations provide additional constraints on the vectors $\mathbf{c}^{(2)}, \mathbf{c}^{(3)}, \mathbf{d}^{(2)}, \mathbf{d}^{(3)}$. To eliminate anisotropic transport, we must have

$$\mathbf{c}^{(2)} + \mathbf{c}^{(3)} - 6\mathbf{d}^{(2)} - 8\mathbf{d}^{(3)} = 0 \tag{5.152}$$

$$r_1\mathbf{c}^{(3)} - r_2\mathbf{d}^{(2)} = 0 \tag{5.153}$$

Solving equations 5.152, 5.153 along with 5.119, 5.120 gives us

$$\mathbf{c}^{(2)} = -\frac{\rho\mathbf{v}}{16} - \frac{\rho\mathbf{B}}{16}\left(\frac{19}{3r_1} + \frac{7}{6r_2}\right) \tag{5.154}$$

$$\mathbf{c}^{(3)} = -\frac{\rho\mathbf{B}}{24r_1} \tag{5.155}$$

$$\mathbf{d}^{(2)} = \frac{\rho\mathbf{v}}{16} + \frac{\rho\mathbf{B}}{16}\left(\frac{7}{3r_1} + \frac{1}{2r_2}\right) \tag{5.156}$$

$$\mathbf{d}^{(3)} = -\frac{\rho\mathbf{B}}{48r_2} \tag{5.157}$$

Substitution of these expressions back into 5.150 reveals a relationship between r_1 and r_2 which is necessary to eliminate unphysical appearances of the magnetic field in the momentum equation. This is easily shown to be

$$r_1 = -6r_2 \tag{5.158}$$

Finally, the transport coefficients turn out to be

$$\nu = \frac{3}{2}\left(\tau - \frac{1}{2}\right) \tag{5.159}$$

$$\nu_b = (3 + c_s^2)\left(\tau - \frac{1}{2}\right) \tag{5.160}$$

$$\eta = \frac{2}{3}\left(\tau - \frac{1}{2}\right) \tag{5.161}$$

Chapter 6

Conclusions and Future Work

In this thesis, we have presented an investigation of the application of the lattice Boltzmann method to the modelling of magnetohydrodynamics. In chapter 1, we presented the basic theory of MHD, concentrating, in particular, on the underpinning kinetic theory, since the lattice Boltzmann method is essentially a kinetic model. In addition to disscussing the various applications of MHD, we also discussed briefly numerical methods for solving the PDEs, and the cellular automata and lattice gases from which the lattice Boltzmann method arose.

In chapter 2, we discussed the lattice Boltzmann method in detail, presenting the standard analysis by which the Navier-Stokes equations are derived from the microscopic rules, drawing close analogy with the physics presented in chapter 1. In particular, we presented the model of Martínez et al, which formed the basis of the numerical simulations in later chapters. Additionally, we proposed some improvements to the Martínez model, one of those being the abandonment of the bi-directional streaming, which, upon inspection, proved to be an unnecassary element of the original model and gave rise to certain undesirable features in the macroscopic equations. We also discussed a modification, originally applied by Cao et al to the hydrodynamic lattice Boltzmann model, which considered alternative finite difference discretisations of the lattice Boltzmann equation. This modification altered the form of the transport coefficients, and also improved the stability of the method. Finally, we performed a linear stability analysis of the method, deriving various bounds on the values of the macroscopic fields.

The results of some numerical simulations were presented in chapter 3 and 4. The simulations of chapter 3 were of well understood problems, namely flow down a channel, Alfvén waves and an example of magnetic reconnection - the coalescence of magnetic islands. These simulations were performed in order to test the effectiveness of the lattice Boltzmann method; the linear problems (channel flow and Alfvén waves) used the original Martínez model, the reconnection problem used the modified model.

The simulations of chapter 4 were of a simple model of an astrophysical phenomenon: the

vortex shedding by a magnetic flux tube erupting from the solar photosphere. The model was a generalisation of a problem in hydrodynamics which has been an object of intensive study. The results demonstrated the profound effect that a magnetic field has on the vortex shedding process and, like similar studies [59, 60], showed the advantages of using a non-uniform grid and applying alternative discretisations of the lattice Boltzmann equation.

In chapter 5 we generalised the lattice Boltzmann method to model thermal MHD and three dimensional MHD. We also presented some simulations of magnetosonic waves as a test of the thermal model. The results showed good agreement with the analytic solutions (where they were available) or with alternative numerical methods.

The results of this work demonstrate the viability of the lattice Boltzmann method as a tool for the numerical simulation of MHD, as it has already been established for various other applications. A number of issues remain to be addressed however before the full merits of the method can properly be assessed. For instance, the table shows a comparison of some lattice Boltzmann models for various systems and it can be seen that even a small increase in the complexity of the system can result in a substantial increase in the number of components required in the lattice Boltzmann distribution function. It is clearly desirable that the more complex LB models be simplified, and whether this can be done will be a topic of future investigation.

Physical System	Independent Variables	No. of states in LB model
2D isothermal hydrodynamics	ρ, v_x, v_y	7
2D thermohydrodynamics	ρ, ϕ, v_x, v_y	13
2D isothermal MHD	ρ, v_x, v_y, B_x, B_y	13
3D isothermal hydrodynamics	ρ, v_x, v_y, v_z	15
2D thermal MHD	$\rho, \phi, v_x, v_y, B_x, B_y$	43
3D isothermal MHD	$\rho, v_x, v_y, v_z, B_x, B_y, B_z$	48

Some other points came to light in the course of the research which have not been mentioned. For example, the stability constraint that $\Delta t \leq 2\tau$ proved to be quite restrictive when the Reynolds number was increased. This constraint can be removed by using an implicit collision operator in the discretised equation, ie. by calculating Ω_a at time $t + \Delta t$ rather than t. As noted by Cao et al [41], the macroscopic fields can be calculated using the moment equations, removing the necessity of inverting a tridiagonal matrix which usually accompanies implicit schemes. Whether choosing $\Delta t \gg \tau$ would lead to significant truncation errors is a matter requiring investigation. A related issue is the particular scheme used to discretise the lattice Boltzmann equation. The traditional method has various shortcomings due to the restrictions of the uniform mesh, and numerical instabilities at high Reynolds number. In addition to the original work of Cao et al [41], various other schemes have been investigated [59, 60, 64, 78, 79, 80, 81]. The Lax-Wendroff scheme used in this thesis has proved to be effective, but a thorough analysis of its truncation errors and comparison with other schemes would be useful.

The derivation of the thermal MHD model revealed some limitations in the ability of the lattice Boltzmann method to give rise to the correct macroscopic equations. As was discussed by Boghosian and Coveney [77], this is due to the form of the collision operator and the structure of the macroscopic equations and cannot be rectified by a different choice of microscopic states. Thus any means of circumventing these restrictions must focus on the collision operator. The simplest solution is to use a collision operator with multiple relaxation times, which McNamara and Alder [82] applied to the thermohydrodynamic model in order to allow an arbitrary choice of Prandtl number. This could, in principle be applied to the MHD model so that the magnetic Prandtl number can be chosen freely. Another possibility would be to use an equilbrium distribution dependant on the gradients of the macroscopic fields. This may be appropriate if we wish to eliminate certain unphysical effects which would appear if spatial variations in the resistivity are significant. It could also be used to guarantee a positive monopole diffusivity. Recall that in section 5.2.3 we found that although it was possible to obtain a correctly structured resistivity tensor (ie $\eta(\partial_i B_j - \partial_j B_i)$), $\nabla \cdot \mathbf{B}$ obeyed a diffusion equation with a negative diffusion coefficient causing numerical instabilities. Thus we settled for a resistivity tensor of the form $\eta \partial_i B_j + \eta_1 \partial_j B_i$, which would give the correct behaviour provided that spatial variations in the resistivity are small and would not introduce the numerical instabilities. The negative diffusion coefficient was due to the fact that the coefficient of the terms $\partial_j B_i$ and $\partial_k B_k \delta_{ij}$ were the same in the LB schemes we investigated. If, however, we introduce a term into the equilibrium distribution which is dependant on $\nabla \cdot \mathbf{B}$, then the new first order terms in the Chapman-Enskog expansion should exhibit diffusive effects, which could in principle cancel the negative monopole diffusivity which causes the numerical instability. Since these terms depend only on $\nabla \cdot \mathbf{B}$, which vanishes in reality, they should not introduce any unphysical effects into the macroscopic behaviour of the model.

There are several other possibilities of future work which arise from this thesis. For instance, although the simulations of magnetic island coalescence demostrated the correct qualitative behaviour of the system, the scaling laws obeyed in the reconnecting region showed a significant amount of scatter. This is probably due to the poor resolution of the current, and the results should improve on a finer grid. However, the dimensions of the current sheet are very small compared to the overall geometry of the system and therefore, a non-uniform grid would be essential if the current sheet should be resolved without a substantial increase in the computational cost of the simulations. The vortex shedding simulations of chapter 4 demonstrated clearly the advantages of a non-uniform grid when there are highly localised features in a flow, and it is desirable that the reconnection simulations be repeated in an analogous fashion.

A particular restriction of the present MHD model is that the magnetic Prandtl number η/ν is constrained to be a constant (namely 3). This is attributable to the simple fact that the collision operator employed a single relaxation time. Other lattice Boltzmann models, have solved this type of problem by using a matrix collision operator with multiple relaxation times [82] and there is no

apparent reason why this approach should not work in this case. Another restriction is the isotropy of the transport coefficients. In a real plasma, transport perpendicular to the magnetic field is suppressed. This is not very important in 2D MHD, which generally models motions perpendicular to a strong ambient magnetic field, with $B_z \gg B_x, B_y$, and so diffusive transport is indeed isotropic in this special case. However for 3D motions this is not so and a means of attaining anisotropic diffusion is therefore desirable. Preliminary investigations have indicated that the simple use of a multiple time scale collision operator would not solve this problem, and therefore a more sophisticated approach, possibly modifying the microscopic states, would be necessary.

Better representations of sub-grid scale turbulence are necessary. In a turbulent flow, the small scale motions are crucial for the transport and dissipation of the mean quantities. However, no model will ever be able to resolve such fine scales in any realistic flows. In chapter 4, we dealt with this problem by assuming that the turbulent transport behaved like the molecular transport and simply replaced the molecular viscosity and resistivity by a constant eddy viscosity and resistivity. Of course there is no reason to suppose that the eddy viscosity and resistivity should be constant (or even isotropic) and more sophisticated models exist to calculate these parameters. One example in hydrodynamics is the $k - \epsilon$ model [5], which introduces the dynamical variables k, the turbulent kinetic energy (TKE) and ϵ, the rate of viscous dissipation of TKE into heat, which obey transport equations similar to the other quantities. The turbulent transport coefficients are then calculated from k and ϵ using dimensional arguments, the non-dimensional quantities being estimated from experiments. The possibility of extending the lattice Boltzmann method to incorporate such models has been investigated [83], the basic idea being that the equilibrium distribution and collisional relaxation times should be adjusted so that the viscous part of the stress tensor should equal the Reynolds stresses. The development of similar techniques in the MHD model are certainly possible.

Appendix A

Code listing

What follows is an example of the FORTRAN code for the lattice Boltzmann MHD program. The subroutines `setup` and `update` need to be modified to account for differing initial and boundary conditions.

```
C=====================================================================
program lattbolt

include 'lattice.inc'
integer incr, i, j, a
C Diagnostice variable, looking for periodicities
C real osc(0:50000)

C Some diagnostic variables in the reconnecting current sheet
integer im1, im2, im3, ndiag
double precision bm1, bm2, vm1, vm2, vm3

call setup

C NB This is just a one off!
C open(41,file='end.dat',status='old',form='unformatted')
C read(41) incr, f
C close(41)

C The main output file
open(8,file='lbmhd.dat',status='unknown',form='unformatted')
```

```
C A diagnostic file
open(10,file='diag.dat',status='unknown',form='unformatted')

C Write out some lattice and time information
write(8) m, n, tmax, tout

C Find a suitable number of diagnostic points to print out
ndiag = tmax / 1000

do incr=0, tmax

  if(mod(incr,100).eq.0) then
   write(6,*) 'Iteration ',incr
   call flush(6)
  endif
C    open(61,file='iteration',status='unknown')
C    write(61,*) incr
C    call flush(61)
C    close(61)

C Printout f if necessary
   if(mod(incr,tout).eq.0) then
      write(6,*) 'Writing out iteration', incr
      write(8) f
      call flush(8)
   endif


C Write out the test variable, which checks for periodicities
C    if( incr .lt. 50000 ) then
C osc(incr) = f(1,2,2)
C    endif

   call update

C Do the diagnostics
```

```
if(mod(incr,ndiag).eq.0) then
   call diagnostics(im1, bm1, vm1, im2, bm2, vm2, im3, vm3)
   write(10) im1, bm1, vm1, im2, bm2, vm2, im3, vm3
endif

C Check for negative f
C (the columns i=1,m-1 are specified by boundary conditions)
   do i=1, m-2
   do j=0, n-1
   do a=0, 12
     if( f(a,i,j).lt.-.1d0 ) then
        write(8) f
        call flush(8)
        close(8)
        write(6,*) 'f ',a,' negative at ',i,j
        stop
     endif
   enddo
   enddo
   enddo

enddo

close(8)

C Diagnostic file, to look for periodicities in the flow
C open(9,file='oscill.dat',status='unknown',form='unformatted')
C write(9) osc
C call flush(9)
C close(9)

open(81,file='end.dat',status='unknown',form='unformatted')
write(81) tmax, f
close(81)

end
```

```
C-------------------------------------------------------
subroutine diagnostics(im1, bm1, vm1, im2, bm2, vm2, im3, vm3)
integer im1, im2, im3
double precision bm1, vm1, bm2, vm2, vm3

C Calculate various diagnostic quantities in magnetic island
C coalescence

include 'lattice.inc'

integer i, m2, n2
double precision rho, vx, vy, bx, by


C Find the local maxima Bx, vy along the line x = 0, nearest y = 2 Pi
bm1 = 0.d0
bx = 0.d0
vm2 = 0.d0
m2 = m/2
i = n/2

do while( i.lt.n.and.abs(bx).ge.bm1)
  call macros(m2,i,rho,vx,vy,bx,by)
  if( abs(bx).ge.bm1 ) then
    bm1 = abs(bx)
    vm1 = abs(vy)
  endif
  i = i + 1
enddo
im1 = i

vy = 0.d0
i = n/2
do while( i.lt.n.and.abs(vy).ge.vm2)
  call macros(m2,i,rho,vx,vy,bx,by)
  if( abs(vy).ge.vm2 ) then
```

```
    bm2 = abs(bx)
    vm2 = abs(vy)
  endif
  i = i + 1
enddo
im2 = i


C Find the extremal vx, along the line y = 2 pi
vm3 = 0.d0
n2 = n/2
do i = 0, m-1
   call macros(i, n2, rho, vx, vy, bx, by)
   if( abs(vx) .ge. vm3 ) then
      vm3 = abs(vx)
      im3 = i
   endif
enddo

end

C=======================================================================

double precision function equilibrium(rho, vx, vy, bx, by, a, s)

C=======================================================================
C Calculates the lattice Boltzmann 2D-MHD equilibrium distribution function,
C given the macroscopic fields rho, (vx, vy), (bx, by) for the particle state
C given by (a, s).
C
C Rest particles are specified by s = 0.
C
C Ref: Martineze et al, Phys Plasmas, 6, 1994
C=======================================================================

include 'lattice.inc'
```

```
double precision rho, vx, vy, bx, by
integer a, b, s, ss
double precision eav, esv, eab, esb, bbb, v2, b2

C-------------------------
C Rest or moving particles?
C-------------------------

if( s.eq.0 ) then

   equilibrium = rho * (1. - alpha - vx**2 - vy**2)

else

C NB s = 1 or -1
   b = mod(6 + a + s, 6)

C------------------
C Some dot products
C------------------
   eav = ex(a) * vx + ey(a) * vy
   esv = ex(b) * vx + ey(b) * vy
   eab = ex(a) * bx + ey(a) * by
   esb = ex(b) * bx + ey(b) * by
   ss = (1 - s)/2
   bbb = microbx(a,ss) * bx + microby(a,ss) * by
   v2 = vx**2 + vy**2
   b2 = bx**2 + by**2

C    equilibrium = (rho/12.d0) * (alpha
C     . + 2.d0 * ( eav + bbb
C     .     - 2.d0 * (esv**2 - esb**2)
C     .     + 2.d0 * (eav*esv - eab*esb)
C     .     + q * (eav * esb - eab * esv)
C     .     + v2 - .5d0 * b2))

   equilibrium = (rho * (alpha
```

```
     . + 2.d0 * ( eav
     .     - 2.d0 * (esv**2)
     .     + 2.d0 * (eav*esv)
     .     + v2))
     .          + 2.d0 * (bbb + 2.d0 * esb * (esb - eab)
     .               + q * (eav * esb - eab * esv)
     .               -.5d0 * b2) ) / 12.d0

endif

return
end

C=====================================================================
subroutine macros(i, j, rho, vx, vy, bx, by)

C=====================================================================
C Calculates the macroscopic fields at the grid point (i,j) and puts
C the result in rho, (vx, vy), (bx, by)
C=====================================================================

include 'lattice.inc'

integer i, j
double precision rho, vx, vy, bx, by
double precision ff
integer a, a1, a7

rho = f(0,i,j)
vx = 0.d0
vy = 0.d0
bx = 0.d0
by = 0.d0

do a=0, 5

   a1 = a + 1
```

```
      a7 = a + 7
      ff = f(a1,i,j) + f(a7,i,j)

      rho = rho + ff

      vx = vx + ff * ex(a)
      vy = vy + ff * ey(a)

      bx = bx + f(a1,i,j) * microbx(a,0)
     . + f(a7,i,j) * microbx(a,1)
      by = by + f(a1,i,j) * microby(a,0)
     . + f(a7,i,j) * microby(a,1)

enddo

vx = vx / rho
vy = vy / rho

C bx = bx / rho
C by = by / rho

end

C=====================================================================
subroutine setup

C=====================================================================
C Initialises the global paramaters in the lattice Boltzmann MHD model
C=====================================================================

include 'lattice.inc'

C Array indices
integer a, b, s
integer i, j

C Current sheet half-width, domain length, wave number for
```

```
C perturbations, island size
double precision width, length, knum, isl

C Grid spacing
C double precision dxi, deta

C Coordinates
double precision x(0:m-1,0:n-1), y(0:m-1,0:n-1)

C Macroscopic fields
double precision rho, vx, vy, bx, by, u0, b0

C Temporary variables
double precision denom, sn, cs, cs2y, csh, chi, chip, fac
integer ind

C Function declaration
double precision equilibrium

C Microscopic velocities, relative to the (xi,eta) coordinate system
double precision e1, e2, de1, de2

C The magnetosonic speed
ms2 = sqrt(cs2 + .01d0)

do a=0, 5
   ex(a) = cos(pi * a / 3.d0)
   ey(a) = sin(pi * a / 3.d0)
enddo
do a=0, 5
   do s=0, 1
      b = mod(7 + a - 2 * s, 6)
      microbx(a,s) = (2.d0*ex(b) - ex(a))/sqrt(3.d0)
      microby(a,s) = (2.d0*ey(b) - ey(a))/sqrt(3.d0)
   enddo
enddo
```

```
C alpha = 4.d0/9.d0
C cs2 = 2.d0/9.d0
q = 2.d0 / sqrt(3.d0)

C------------
C Parameters to be read in from a file
C------------
open(4,file='lattice.in',status='old')
rewind(4)

C Time parameters
read(4,*) tmax, tout, tau, dt
dtovertau = dt / tau

C Are we continuing from a previous run
read(4,*) cont

C Domain size
read(4,*) xiinf, length, isl
knum = 2.d0 * pi / length
width = .25d0 * length / pi

C Ambient flow speed
read(4,*) u0, b0

close(4)

if(cont) then

   write(6,*) 'Reading in intial data'
   call flush(6)

C Read in the intial data from a file
   open(81,file='end2.dat',status='unknown',form='unformatted')
   read(81) f
   close(81)
endif
```

```
C-------------------------------------------------------------
C Setup the initial conditions, for magnetic island coalescence
C-------------------------------------------------------------
C dxi = 2.d0 * xiinf / (m-1)
C dxi = 2.d0 * xiinf * width / (m-1)
C deta = length / n
dxi = 2.d0 * xiinf / (m-1)
deta = 4.d0 * pi / n

do i=0, m-1
do j=0, n-1

C Calculate the (x,y) coordinates
C (for IDL display routines that depend on Cartesian grids)
C    x(i,j) = width * sinh(dxi * i - xiinf)
   x(i,j) = (dxi * i - xiinf)
   y(i,j) = deta * j

C Calculate the velocity field
C    vx = -u0 * cos(knum * y(i,j)) * sinh(x(i,j)/width)
C     .             / cosh(x(i,j)/width)**2
C    vy = u0 * sin(knum * y(i,j)) *
C     .             (1-sinh(x(i,j)/width)**2)
C     .             / cosh(x(i,j)/width)**3

if(.not. cont) then

   ind = 2
   sn = sin(.5*y(i,j))
   cs = cos(.5*y(i,j))
   cs2y = cos(y(i,j))
   csh = 1.0001d0 + isl * (1-cs2y)
   chi = log(csh + sqrt(csh**2-1.d0))
   chip = 2.d0*isl*sin(y(i,j)) / sinh(chi)
C    fac = -(x(i,j)/chi)**ind
C write(6,*) 'ok'
```

```
      fac = u0*exp(-abs(sn)-(x(i,j)/chi)**ind/ind)
      vx = x(i,j) * (cs * (abs(sn)-1.d0) -
     .                        (x(i,j)/chi)**ind
     .                        * chip/chi * sn) * fac
      vy = (1.d0-(x(i,j)/chi)**ind) * sn * fac


C and the magnetic field

C     bx = 0.d0
C     by = b0 * tanh(x(i,j)/width)

      denom = cosh(x(i,j)) + isl*cos(y(i,j))
      bx = b0*isl*sin(y(i,j)) / denom
      by = b0 * sinh(x(i,j)) / denom

C ... and the density field, (assuming that the total pressure field
C is uniform ie rho( cs^2 + 1/2 B^2) = const)
C     rho = (cs2)
C      .          / (cs2 + .5 * (bx**2+by**2))

C Assign a pressure field which balances the Lorentz force
C     rho = (b0**2 * cosh(x(i,j)/width)/denom + cs2-.5*b0**2)
C      .        / (cs2 + .5 * (bx**2+by**2))
      rho = (b0**2 * cosh(x(i,j))/denom
     .           - .5 * (bx**2+by**2) - b0**2)/cs2 + 1.d0
C     rho = 1.d0 - .5d0 * (bx**2+by**2)/cs2
C     rho = 1.d0

C Initialise the distribution function to its equilibrium value
      f(0,i,j) = equilibrium(rho,vx,vy,bx,by,0,0)
      do a=0,5
         f(a+1,i,j) =
     .           equilibrium(rho,vx,vy,bx,by,a,1)
         f(a+7,i,j) =
     .           equilibrium(rho,vx,vy,bx,by,a,-1)
      enddo
```

```
C End the "not cont" conditional
endif


C-------------------------------------------------------
C Set up the weights for the disretisation
C-------------------------------------------------------
   do a=0, 5
C Calculate the components of (ex,ey) in (xi, eta) coordinates
C       e1 = ex(a) / (width * cosh(dxi*j-xiinf))
      e1 = ex(a)
      e2 = ey(a)

C ...and their derivatives
      de1 = -0*pi * e1
      de2 = e1*0
      if(abs(e1*dt/dxi).gt..7d0
     .            .or.abs(e2*dt/deta).gt..7d0) then
         write(6,*) abs(e1*dt/dxi), abs(e2*dt/deta)
         stop
      endif
C ...and the weights (Lax-Wendroff discretisation)
      w1(a,i,j) = .5d0 * (e1*dt/dxi
     .                    + (e1*dt/dxi)**2)
      w2(a,i,j) = 1.d0 - dtovertau
     .            - (e1*dt/dxi)**2 - (e2*dt/deta)**2
      w3(a,i,j) = .5d0 * (-e1*dt/dxi
     .                    + (e1*dt/dxi)**2)
      w4(a,i,j) = .5d0 * (e2*dt/deta
     .                   + (e2*dt/deta)**2)
               w5(a,i,j) = .5d0 * (-e2*dt/deta
     .                   + (e2*dt/deta)**2)

C ...upwind discretisation
C       w2(a,i,j) = 1.d0 - dtovertau
C       if(e1.gt.0.d0) then
```

```
C w1(a,i,j) = e1*dt/dxi
C         w3(a,i,j) = 0.d0
C w2(a,i,j) = w2(a,i,j) - e1*dt/dxi
C       else
C w1(a,i,j) = 0.d0
C         w3(a,i,j) = -e1*dt/dxi
C w2(a,i,j) = w2(a,i,j) + e1*dt/dxi
C       endif
C       if(e2.gt.0.d0) then
C         w4(a,i,j) = e2*dt/deta
C         w5(a,i,j) = 0.d0
C         w2(a,i,j) = w2(a,i,j) - e2*dt/deta
C       else
C         w4(a,i,j) = 0.d0
C         w5(a,i,j) = -e2*dt/deta
C         w2(a,i,j) = w2(a,i,j) + e2*dt/deta
C       endif

   enddo

enddo
enddo

C Write out the Cartesian coordinates
open(7,file='points',status='unknown',form='unformatted')
write(7) x, y
close(7)


end

C=======================================================================
subroutine update

C=======================================================================
C Updates the lattice Boltzmann 2D-MHD distribution function, using a
C Lax-Wendroff approximation for the streaming process
```

```
C==============================================================================

include 'lattice.inc'

C Some array indices
integer i,im,ip,j,jm,jp,a,a1,a7,aa

C Some columns
C double precision ff(0:12,0:n-1),fff(0:12,0:n-1),
C     . F1(0:12,0:N-1)

C A Temporary array
double precision ff(0:12,0:m-1,0:n-1)

C Macroscopic fields
double precision rho, vx, vy, bx, by,
     . rho0, vx0, vy0, bx0, by0,
     . rho1, vx1, vy1, bx1, by1,
     . rho2, vx2, vy2, bx2, by2

C Function declarations
double precision equilibrium

C-------------------------------
C Note that the code is inevitably specific to the particular boundary
C conditions for the problem. Here, we shall assume that there are boundaries
C along the first and last columns (ie x = 0, x = xmax) and that the domain
C is periodic in the y direction.
C-------------------------------

C-------------------------------
C This is specific to flow current sheet instabilities
C-------------------------------

C--------------
C Set the distribution function to be its equilibrium value at the
C far field flow.
```

```
C--------------

C do j=0, n-1
C
C Give a value for fff, just to keep the main loop consistent
C   do a=0, 12
C      fff(a,j) = f(a,0,j)
C   enddo
C
C enddo


C-------------
C The first, last columns are 'close to infinity', and so don't change
C-------------

C STORE THE FIRST COLUMN
C DO J= 0, N-1
C DO A= 0, 12
C   F1(A,J) = F(A,1,J)
C ENDDO
C ENDDO

C Do an extrapolate and bounce for the boundary conditions
C do j=0, n-1
C do a=0, 12
C The extrapolation
C   ff(a,0,j) = 2.d0*f(a,1,j) - f(a,2,j)
c   ff(a,m-1,j) = 2.d0*f(a,m-2,j) - f(a,m-3,j)
c enddo
c enddo
c
c do j=0, n-1
c do a=0, 5
C The bounce
c   f(1+a,0,j) = f(7+mod(a+3,6),0,j)
c   f(7+a,0,j) = f(1+mod(a+3,6),0,j)
```

```
c   f(1+a,m-1,j) = f(7+mod(a+3,6),m-1,j)
c   f(7+a,m-1,j) = f(1+mod(a+3,6),m-1,j)
c enddo
c enddo

C Apply the boundary condition:
C f  = feq - tau e . grad feq
c do j=0, n-1
c   call macros(0, j, rho0, vx0, vy0, bx0, by0)
c   call macros(0, j, rho1, vx1, vy1, bx1, by1)
c   call macros(0, j, rho2, vx2, vy2, bx2, by2)
c
c   f(0,0,j) = equilibrium(rho0,vx0,vy0,bx0,by0,0,0)
c   do a=0, 5
c    f(1+a,0,j) = (1.d0+1.5*tau*ex(a)/dxi)
c     .               * equilibrium(rho0,vx0,vy0,bx0,by0,a,1)
c     .               -2.d0 * tau * ex(a) / dxi
c     .               * equilibrium(rho1,vx1,vy1,bx1,by1,a,1)
c     .               +.5d0*tau*ex(a)/dxi
c     .               * equilibrium(rho2,vx2,vy2,bx2,by2,a,1)
c    f(7+a,0,j) = (1.d0+1.5*tau*ex(a)/dxi)
c     .               * equilibrium(rho0,vx0,vy0,bx0,by0,a,-1)
c     .               -2.d0 * tau * ex(a) / dxi
c     .               * equilibrium(rho1,vx1,vy1,bx1,by1,a,-1)
c     .               +.5d0*tau*ex(a)/dxi
c     .               * equilibrium(rho2,vx2,vy2,bx2,by2,a,-1)
c   enddo
c
c   call macros(m-1, j, rho0, vx0, vy0, bx0, by0)
c   call macros(m-2, j, rho1, vx1, vy1, bx1, by1)
c   call macros(m-3, j, rho2, vx2, vy2, bx2, by2)
c
c   f(0,m-1,j) = equilibrium(rho0,vx0,vy0,bx0,by0,0,0)
c   do a=0, 5
c    f(1+a,m-1,j) = (1.d0-1.5*tau*ex(a)/dxi)
c     .               * equilibrium(rho0,vx0,vy0,bx0,by0,a,1)
c     .               +2.d0 * tau * ex(a) / dxi
```

```
c     .               * equilibrium(rho1,vx1,vy1,bx1,by1,a,1)
c     .               -.5d0*tau*ex(a)/dxi
c     .               * equilibrium(rho2,vx2,vy2,bx2,by2,a,1)
c    f(7+a,m-1,j) = (1.d0-1.5*tau*ex(a)/dxi)
c     .               * equilibrium(rho0,vx0,vy0,bx0,by0,a,-1)
c     .               +2.d0 * tau * ex(a) / dxi
c     .               * equilibrium(rho1,vx1,vy1,bx1,by1,a,-1)
c     .               -.5d0*tau*ex(a)/dxi
c     .               * equilibrium(rho2,vx2,vy2,bx2,by2,a,-1)
c   enddo
c
c enddo

C Try periodic boundaries either end, but reflecting the magnetic field
C vector.
do j=0, n-1

      call macros(0, j, rho, vx, vy, bx, by)
c       vx = 0.d0
c       vy = 0.d0
c       bx = 0.d0
c       by = -b0

      ff(0,0,j) = f(0,0,j) +
     .    (equilibrium(rho,vx,vy,bx,by,0,0) - f(0,0,j))
     . * dtovertau

      jp = mod(j+1,n)
      jm = mod(n+j-1,n)

      do a=0, 5
         a1 = a + 1
         a7 = a + 7

         ff(a1,0,j) = equilibrium(rho,vx,vy,bx,by,a,1)
     .                                          * dtovertau
     .                  + w1(a,0,j) * f(a7,m-1,j)
```

```
     .                  + w2(a,0,j) * f(a1,0,j)
     .                  + w3(a,0,j) * f(a1,1,j)
     .                  + w4(a,0,j) * f(a1,0,jm)
     .                  + w5(a,0,j) * f(a1,0,jp)

        ff(a7,0,j) = equilibrium(rho,vx,vy,bx,by,a,-1)
     .                                          * dtovertau
     .                  + w1(a,0,j) * f(a1,m-1,j)
     .                  + w2(a,0,j) * f(a7,0,j)
     .                  + w3(a,0,j) * f(a7,1,j)
     .                  + w4(a,0,j) * f(a7,0,jm)
     .                  + w5(a,0,j) * f(a7,0,jp)
      enddo

C and the last column
      call macros(m-1, j, rho, vx, vy, bx, by)
c       vx = 0.d0
c       vy = 0.d0
c       bx = 0.d0
c       by = b0

      ff(0,m-1,j) = f(0,m-1,j) +
     .    (equilibrium(rho,vx,vy,bx,by,0,0) - f(0,m-1,j))
     . * dtovertau

      jp = mod(j+1,n)
      jm = mod(n+j-1,n)

      do a=0, 5
         a1 = a + 1
         a7 = a + 7

         ff(a1,m-1,j) = equilibrium(rho,vx,vy,bx,by,a,1)
     .                                          * dtovertau
     .                  + w1(a,0,j) * f(a1,m-2,j)
     .                  + w2(a,0,j) * f(a1,m-1,j)
     .                  + w3(a,0,j) * f(a7,0,j)
```

```
     .                    + w4(a,0,j) * f(a1,m-1,jm)
     .                    + w5(a,0,j) * f(a1,m-1,jp)

         ff(a7,m-1,j) = equilibrium(rho,vx,vy,bx,by,a,-1)
     .                                          * dtovertau
     .                    + w1(a,0,j) * f(a7,m-2,j)
     .                    + w2(a,0,j) * f(a7,m-1,j)
     .                    + w3(a,0,j) * f(a1,0,j)
     .                    + w4(a,0,j) * f(a7,m-1,jm)
     .                    + w5(a,0,j) * f(a7,m-1,jp)
      enddo

enddo


C Do a column at a time
do i = 1, m-2
C***********************************************
C DO I = 0, M-1
   im = mod(m+i-1,m)
   ip = mod(i+1,m)

C The i-th column
   do j = 0, n-1
      call macros(i, j, rho, vx, vy, bx, by)

      ff(0,i,j) = f(0,i,j) +
     .    (equilibrium(rho,vx,vy,bx,by,0,0) - f(0,i,j))
     . * dtovertau

      jp = mod(j+1,n)
      jm = mod(n+j-1,n)

      do a=0, 5
         a1 = a + 1
         a7 = a + 7
```

```
          ff(a1,i,j) = equilibrium(rho,vx,vy,bx,by,a,1)
     .                                              * dtovertau
     .                    + w1(a,i,j) * f(a1,im,j)
     .                    + w2(a,i,j) * f(a1,i,j)
     .                    + w3(a,i,j) * f(a1,ip,j)
     .                    + w4(a,i,j) * f(a1,i,jm)
     .                    + w5(a,i,j) * f(a1,i,jp)

          ff(a7,i,j) = equilibrium(rho,vx,vy,bx,by,a,-1)
     .                                              * dtovertau
     .                    + w1(a,i,j) * f(a7,im,j)
     .                    + w2(a,i,j) * f(a7,i,j)
     .                    + w3(a,i,j) * f(a7,ip,j)
     .                    + w4(a,i,j) * f(a7,i,jm)
     .                    + w5(a,i,j) * f(a7,i,jp)
      enddo


C***********************************
C FF(0,J) = EQUILIBRIUM(RHO,VX,VY,BX,BY,0,0)
C DO A=0, 5
C   FF(A+1,J) = EQUILIBRIUM(RHO,VX,VY,BX,BY,A,1)
C   FF(A+7,J) = EQUILIBRIUM(RHO,VX,VY,BX,BY,A,-1)
C ENDDO
C***********************************

   enddo



C Update column i-1
C    do j=0, n-1
C       do a=0, 12
C          f(a,im,j) = fff(a,j)
C          fff(a,j) = ff(a,j)
C       enddo
C    enddo
```

```
enddo

C Update the lattice
c do i=1, m-2
DO I=0, M-1
do j=0, n-1
do a=0, 12
   f(a,i,j) = ff(a,i,j)
enddo
enddo
enddo

return
end


C================================================================================
C Include file common block declarations for the lattice Boltzmann MHD program
C================================================================================

C Pi
double precision pi
parameter(pi = 3.14159265358979311599796346854 4d0)

C-------------------------------------------------
C Parameters associated with the microscopic rules
C
C alpha - the 'alpha' parameter in the equilibrium distribution
C   which sets the speed of sound
C cs2 - the speed of sound squared
C ms2 - the magnetosonic speed
C ex, ey - the microscopic velocity vectors
C microbx, microby - the microscopic magnetic field vectors
C q - a coefficient in the distribution function (= 2/sqrt(3))
C-------------------------------------------------

double precision alpha, cs2, ms2, q
```

```
common /waves/ ms2
double precision ex(0:5), ey(0:5)
double precision microbx(0:5,0:1), microby(0:5,0:1)
common /micros/ ex, ey, microbx, microby, q
parameter(alpha = .555555555555555555d0)
parameter(cs2 = .2777777777777777777d0)

C-------------------------------------------------------
C m,n - The size of the grid
C f - the equilibrium distribution
C     Note that f(0) - Rest particles
C with a=0,..,5 f(1+a), state given by (a,a+1)
C       f(7+a), state given by (a,a-1)
c-------------------------------------------------------

integer m, n
parameter(m = 81, n = 1024)
C Flow past a cylinder m=181, n=241
C Tearing mode m=61, n=161
C Island coalescence m = 101, n = 200
double precision f(0:12, 0:m-1, 0:n-1)
common /distribution/ f

C-------------------------------------------------------
C dt - the time step
C tau - the collisional relaxation time
C dtovertau - dt / tau
C tmax - the simulation time
C-------------------------------------------------------
double precision dt, tau, dtovertau
integer tmax, tout
common /times/ dt, tau, dtovertau, tmax, tout

C-------------------------------------------------------
C cont - true if initial conditions are to be read in from
C  a file
C-------------------------------------------------------
```

```
logical cont
common /cont/ cont

C-------------------------------------------------------
C Grid spacing
C-------------------------------------------------------
double precision dxi, deta
common /grid/ dxi, deta

C-------------------------------------------------------
C Weights used for the discretisation
C-------------------------------------------------------
double precision w1(0:5,0:m-1,0:n-1), w2(0:5,0:m-1,0:n-1),
     .           w3(0:5,0:m-1,0:n-1), w4(0:5,0:m-1,0:n-1),
     .           w5(0:5,0:m-1,0:n-1)
common /weights/ w1, w2, w3, w4, w5

C-------------------------------------------------------
C Domain size
C-------------------------------------------------------
double precision xiinf
common /domain/ xiinf

C-------------------------------------------------------
C Flow parameters
C-------------------------------------------------------
C double precision b0
C common /flow/ b0
```

Bibliography

[1] D. O. Martínez, S. Chen, and W. H. Matthaeus. Lattice Boltzmann magnetohydrodynamics. *Physics of Plasmas*, 6:1850–1867, 1994.

[2] T. J. M. Boyd and J. J. Sanderson. *Plasma Dynamics.* Nelson, London, 1969.

[3] Paul Lorrain, Dale P. Corson, and François Lorrain. *Electromagnetic Fields and Waves.* W. H. Freeman and Company, 1988.

[4] R. O. Dendy, editor. *Plasma Physics: an Introductory Course.* Cambridge University Press, Cambridge, 1993.

[5] C. A. J. Fletcher. *Computational Techniques for Fluid Dynamics.* Springer, 1991.

[6] T. Toffoli. *Cellular Automata Machines: a New Environment for Modelling.* MIT Press, Cambridge, Mass. and London, 1987.

[7] E. F. Codd. *Cellular Automata.* Academic Press, New York and London, 1968.

[8] S. Wolfram, editor. *Theory and Applications of Cellular Automata.* World Scientific, Singapore, 1986.

[9] J. Demongeot, E. Goles, and M. Tchuente, editors. *Dynamical Systems and Cellular Automata.* Academic, London, 1985.

[10] J. von Neumann. *Theory of Self-Reproducing Automata.* Illinois University Press, 1966.

[11] J. von Neumann. *Collected Works / John von Neumann.* Pergamon Press, Oxford, 1961-1963.

[12] E. Rietman. *Creating Artificial Life: Self-Organization.* Windcrest / McGraw-Hill, Blue Ridge Summit, PA, 1993.

[13] K. Sigmund. *Games of Life: Explorations in Ecology, Evolution and Behaviour.* Oxford University Press, Oxford and New York, 1993.

[14] Elwyn Berlekamp, John Conway, and Richard Guy. *Winning ways for your mathematical plays*, volume 2. Academic Press, 1982.

[15] Martin Gardner. The fantastic combinations of John Conway's new solitaire games of life. *Scientific American*, 223:120–123, 1970.

[16] J. Hardy, O. de Pazzis, and Yves Pomeau. Molecular dynamics of a classical lattice gas: Transport properties and time correlation functions. *Physical Review A*, 13:1949–1960, 1976.

[17] Uriel Frisch, Brosl Hasslacher, and Yves Pomeau. Lattice-gas automata for the Navier-Stokes equation. *Physcial Review Letters*, 56:1505–1508, 1986.

[18] D. Montgomery and G. Doolen. Magnetohydrodynamic cellular automata. *Physics Letters A*, 120:229–231, 1987.

[19] D. Montgomery and G. Doolen. *Complex Systems*, 1:831, 1987.

[20] Hudong Chen and William H. Matthaeus. New cellular automaton model for magentohydrodynamics. *Physical Review Letters*, 58:1845–1848, 1987.

[21] H. Chen, W. H. Matthaeus, and L. W. Klein. An analytic theory and formulation of a local magnetohydrodynamic lattice gas model. *Physics of Fluids*, 31:1439–1455, 1988.

[22] Shiyi Chen, Hudong Chen, Daniel Martínez, and William Matthaeus. Lattice Boltzmann model for simulation of magnetohydrodynamics. *Physical Review Letters*, 67:3776–3779, 1991.

[23] W. Elsasser. *Physical Review*, 79:183, 1950.

[24] Stephen Wolfram. Cellular automaton fluids 1: Basic theory. *Journal of Statistical Physics*, 45:471–526, 1986.

[25] S. Succi, R. Benzi, and F. Higuera. The lattice Boltzmann-equation - a new tool for computational fluid- dynamics. *Physica D*, 47:219–230, 1991.

[26] Hudong Chen, Shiyi Chen, and William H. Matthaeus. Recovery of the Navier-Stokes equations using a lattice gas Boltzmann method. *Physical Review A*, 45:R5339–R5342, 1992.

[27] G. McNamara and G. Zannetti. Use of the Boltzmann-equation to simulate lattice-gas automata. *Physical Review Letters*, 61:2332–2335, 1988.

[28] U. Frisch. Relation between the lattice Boltzmann-equation and the Navier-Stokes equations. *Physica D*, 47:231–232, 1991.

[29] M. Vergassola, R. Benzi, and S. Succi. On the hydrodynamic behavior of the lattice Boltzmann-equation. *Europhysics Letters*, 13:411–416, 1990.

[30] Y. H. Qian, D. d'Humieres, and P. Lallemand. Lattice BGK models for the Navier-Stokes equation. *Europhysics Letters*, 17:479–484, 1992.

[31] S. Succi, R. Benzi, and F. Massaioli. A review of the lattice Boltzmann method. *International J. Modern Phys. C-Physics Computers*, 4:409–415, 1993.

[32] S. Succi. Lattice Boltzmann equation: Failure or success? *Physica A*, 240:221–228, 1997.

[33] U. Frisch, D. d'Humieres, B. Hasslacher, P. Lallemand, Y. Pomeau, and J.-P. Rivet. *Complex Systems*, 1:649, 1987.

[34] F. J. Alexander, S. Chen, and J. D. Sterling. Lattice Boltzmann thermohydrodynamics. *Physical Review E*, 47:R2249–R2252, 1993.

[35] Y. H. Qian and S. A. Orszag. Lattice BGK models for the Navier-Stokes equation: Nonlinear deviation in compressible regimes. *Europhysics Letters*, 21:255–259, 1993.

[36] D. d'Humieres, P. Lallemand, and U. Frisch. Lattice gas models for 3D hydrodynamics. *Europhysics Letters*, 2:291–297, 1986.

[37] Shiyi Chen, Zheng Wang, Xiaowen Shan, and Gary D. Doolen. Lattice Boltzmann computational fluid dynamics in three dimensions. *Journal of Statistical Physics*, 68:379–400, 1992.

[38] S. Y. Chen, H. D. Chen, G. D. Doolen, S. Gutman, and M. X. Lee. A lattice gas model for thermohydrodynamics. *Journal of Statistical Physics*, 62:1121–1151, 1991.

[39] S. Succi, M. Vergassola, and R. Benzi. Lattice Boltzmann scheme for 2-dimensional magnetohydrodynamics. *Phys. Review A*, 43:4521–4524, 1991.

[40] J. D. Sterling and S. Y. Chen. Stability analysis of lattice Boltzmann methods. *J. Computational Phys.*, 123:196–206, 1996.

[41] Nianzheng Cao, Shiyi Chen, Shi Jin, and Daniel Martínez. Physical symmetry and lattice symmetry in the lattice Boltzmann method. *Physical Review E*, 55:R21–R24, 1997.

[42] S. Y. Chen, D. Martinez, and R. W. Mei. On boundary-conditions in lattice Boltzmann methods. *Phys. Fluids*, 8:2527–2536, 1996.

[43] G. R. McNamara, A. L. Garcia, and B. J. Alder. Stabilization of thermal lattice Boltzmann models. *J. Statistical Phys.*, 81:395–408, 1995.

[44] R. Moreau. *Magnetohydrodynamics*. Kluwer Academic Publishers, 1990.

[45] A. R. Paterson. *A First Course in Fluid Dynamics*. Cambridge University Press, 1983.

[46] Dieter Biskamp. *Nonlinear Magnetohydrodynamics*. Cambridge University Press, 1993.

[47] P. L. Pritchett and C. C. Wu. Coalescence of magnetic islands. *Physics of Fluids*, 22:2140–2146, 1979.

[48] J. M Finn and P. K. Kaw. Coalescence instability of magnetic islands. *Physics of Fluids*, 20:72–78, 1977.

[49] D. Biskamp and H. Welter. Coalescence of magnetic islands. *Physical Review Letters*, 44:1069–1071, 1980.

[50] D. Biskamp. Effect of secondary tearing instability on the coalescence of magnetic islands. *Physics Letters A*, 87:357–360, 1982.

[51] P. A. Sweet. The production of high energy particles in solar flares. *Nuovo Cimento Suppl.*, 8:188–96, 1970.

[52] E. N. Parker. The solar flare phenomenon and the theory of reconnection and annihilation of magnetic fields. *Astrophysical Journal*, 8:177–211, 1963.

[53] K. D. Leka, L. van Driel-Gesztelyi, and R. C. Canfield. Evidence for twisted emerging flux in NOAA AR 7260. In K. S. Balasubramaniam and George W. Simon, editors, *Solar Active Region Evolution: Comparing Models with Observations*, volume 68, pages 145–148, 1994.

[54] Louis Strous. *Dynamics in Solar Active Regions: Patterns in Magnetic-Flux Emergence.* PhD thesis, University of Utrecht, Utrecht, Netherlands, 1994.

[55] G. K. Batchelor. *An Introduction to Fluid Dynamics.* Cambridge University Press, 1970.

[56] F. J. Higuera and S. Succi. Simulating the flow around a circular-cylinder with a lattice Boltzmann-equation. *Europhysics Letters*, 8:517–521, 1989.

[57] L. Wagner. Pressure in lattice Boltzmann simulations of flow around a cylinder. *Phys. Fluids*, 6:3516–3518, 1994.

[58] L. Wagner and F. Hayot. Lattice Boltzmann simulations of flow past a cylindrical obstacle. *J. Statistical Phys.*, 81:63–70, 1995.

[59] Xiaoyi He and Gary D. Doolen. Lattice Boltzmann method on curvilinear coordinates system: flow around a circular cylinder. *Journal of Computational Physics*, 134:306–315, 1997.

[60] Xiaoyi He and Gary D. Doolen. Lattice Boltzmann method on a curvilinear coordinate system: Vortex shedding behind a circular cylinder. *Physical Review E*, 56:434–440, 1997.

[61] Louis H. Strous, Göran Scharmer, Theodore D. Tarbell, Alan M. Title, and Cornelis Zwaan. Phenomena in an emerging activer region i. horizontal dynamics. *Astronomy and Astrophysics*, 306:947–959, 96.

[62] U. Frisch. *Turbulence: the legacy of A. N. Kolmogorov.* Cambridge University Press, 1995.

[63] H. Tennekes and J. L. Lumley. *A First Course in Turbulence.* MIT Press, 1972.

[64] Xiaoyi He, Li-Shi Luo, and Micah Dembo. Some progress in lattice Boltzmann method: Part i. nonuniform mesh grids. *Journal of Computational Physics*, 129:357–363, 1996.

[65] P. Lavallee, J. P. Boon, and A. Noullez. Boundaries in lattice gas flows. *Physica D*, 47:233–240, 1991.

[66] M. A. Gallivan, D. R. Noble, J. G. Georgiadis, and R. O. Buckius. An evaluation of the bounce-back boundary condition for lattice Boltzmann simulations. *International Journal for Numerical Methods in Fluids*, 25:249–263, 1997.

[67] P. A. Skordos. Initial and boundary-conditions for the lattice Boltzmann method. *Phys. Review E*, 48:4823–4842, 1993.

[68] D. P. Ziegler. Boundary-conditions for lattice Boltzmann simulations. *J. Statistical Phys.*, 71:1171–1177, 1993.

[69] D. R. Noble, S. Y. Chen, J. G. Georgiadis, and R. O. Buckius. A consistent hydrodynamic boundary-condition for the lattice Boltzmann method. *Phys. Fluids*, 7:203–209, 1995.

[70] D. R. Noble, J. G. Georgiadis, and R. O. Buckius. Direct assessment of lattice Boltzmann hydrodynamics and boundary- conditions for recirculating-flows. *J. Statistical Phys.*, 81:17–33, 1995.

[71] T. Inamuro, M. Yoshino, and F. Ogino. Non-slip boundary-condition for lattice Boltzmann simulations. *Phys. Fluids*, 7:2928–2930, 1995.

[72] T. Inamuro, M. Yoshino, and F. Ogino. A non-slip boundary-condition for lattice Boltzmann simulations (vol 7, pg 2928, 1995). *Phys. Fluids*, 8:1124–1124, 1996.

[73] R. S. Maier, R. S. Bernard, and D. W. Grunau. Boundary-conditions for the lattice Boltzmann method. *Phys. Fluids*, 8:1788–1801, 1996.

[74] I. Ginzbourg and D. d'Humieres. Local 2nd-order boundary methods for lattice Boltzmann models. *J. Statistical Phys.*, 84:927–971, 1996.

[75] X. Y. He, Q. S. Zou, L. S. Luo, and M. Dembo. Analytic solutions of simple flows and analysis of nonslip boundary conditions for the lattice Boltzmann BGK model. *Journal of Statistical Physics*, 87:115–136, 1997.

[76] E. R. Priest. *Solar Magnetohydrodynamics.* D. Reidel Publishing Company, 1982.

[77] Bruce M. Boghosian and Peter V. Coveney. Inverse Chapman-Enskog derivation of the thermohydrodynamic lattice-BGK model for the ideal gas. *International journal of modern physics C*, 9:1231–1245, 1998.

[78] J. Tolke, M. Krafczyk, M. Shulz, E. Rank, and R. Berrios. Implicit discretization and nonuniform mesh refinement approaches for FD discretizations of LBGK models. *International Journal of Modern Physics C*, 9:1143–1157, 1998.

[79] I. V. Karlin, S. Succi, and S. Orszag. Lattice Boltzmann method for irregular grids. *Physical Review Letters*, 82:5245–5248, 1999.

[80] G. W. Peng, H. W. Xi, C. Duncan, and S. H. Chou. Lattice Boltzmann method on irregular meshes. *Physical Review E*, 58:R4124–R4127, 1998.

[81] R. W. Mei and W. Shyy. On the finite difference-based lattice Boltzmann method in curvilinear coordinates. *Journal of Computational Physics*, 143:426–448, 1998.

[82] G. McNamara and B. Alder. Analysis of the lattice Boltzmann treatment of hydrodynamics. *Physica A*, 194:218–228, 1993.

[83] C. M. Teixeira. Incorporating turbulence models into the lattice-Boltzmann method. *International Journal of Modern Physics C*, 9:1159–1175, 1998.